Quantum optical experiments towards atom-photon entanglement

Dissertation at the Department of Physics
of the
Ludwig-Maximilians-Universität München

Markus Weber

München, March 31, 2005

Gutachter: Prof. Dr. Harald Weinfurter
Prof. Dr. Khaled Karrai

Tag der mündlichen Prüfung: 17. Juni 2005

für Merle und Caspar

Acknowledgements

I would like to thank you all:

Jürgen Volz, Prof. Harald Weinfurter, Prof. Christian Kurtsiefer, Daniel Schlenk, Wenjamin Rosenfeld, Dr. Markus Greiner, Karen Saucke, Johannes Vrana, Nikolei Kiesel, Prof. Mohamed Bourennane, Patrick Zarda, Oliver Schulz, Tobias Schmitt-Manderbach, Christian Schmid, Manfred Eibl, Dr. Markus Oberparleiter, Chunlang Wang, Henning Weier, Nadja Regner, Gerhard Huber, Anton Scheich, Prof. T. W. Hänsch, Prof. Sophie Kröger, Prof. Theo Neger, Prof. Laurentius Windholz, Dr. Richard Kamendje, Prof. Dieter Zimmermann, Olaf Mandel, Prof. Jakob Reichel, Gabriele Gschwendtner, Nicole Schmid, Prof. Immanuel Bloch, Artur Widera.

Abstract

In 1935 *Einstein, Podolsky and Rosen (EPR)* used the assumption of local realism to conclude in a Gedankenexperiment with two entangled particles that quantum mechanics is not complete. For this reason *EPR* motivated an extension of quantum mechanics by so-called local hidden variables. Based on this idea in 1964 *Bell* constructed a mathematical inequality whereby experimental tests could distinguish between quantum mechanics and local-realistic theories. Many experiments have since been done that are consistent with quantum mechanics, disproving the concept of local realism. But all these tests suffered from loopholes allowing a local-realistic explanation of the experimental observations by exploiting either the low detector efficiency or the fact that the detected particles were not observed space-like separated. In this context, of special interest is entanglement between different quantum objects like atoms and photons, because it allows one to entangle distant atoms by the interference of photons. The resulting space-like separation together with the almost perfect detection efficiency of the atoms allows a first loophole-free test of Bell's inequality.

The primary goal of the present thesis is the experimental realization of entanglement between a single localized atom and a single spontaneously emitted photon at a wavelength suitable for the transport over long distances. In the experiment a single optically trapped ^{87}Rb atom is excited to a state which has two selected decay channels. In the following spontaneous decay a photon is emitted coherently with equal probability into both decay channels. This accounts for perfect correlations between the polarization state of the emitted photon and the Zeeman state of the atom after spontaneous decay. Because these decay channels are spectrally and in all other degrees of freedom indistinguishable, the spin state of the atom is entangled with the polarization state of the photon. To verify entanglement, appropriate correlation measurements in complementary bases of the photon polarization and the internal quantum state of the atom are performed. It is shown, that the generated atom-photon state yields an entanglement fidelity of 0.82.

The experimental results of this work mark an important step towards the generation of entanglement between space-like separated atoms for a first loophole-free test of Bell's inequality. Furthermore entanglement between a single atom and a single photon is an important tool for new quantum communication and information applications, e.g. the remote state preparation of a single atom over large distances.

Zusammenfassung

Im Jahr 1935 veröffentlichten *Einstein, Podolsky und Rosen (EPR)* ein Gedankenexperiment, in dem mit Hilfe zweier verschränkter Teilchen und der Annahme, dass jede physikalische Theorie lokal sein muss, gezeigt wurde, dass die Quantenmechanik eine unvollständige Theorie ist. *EPR* motivierten damit die Erweiterung der Quantenmechanik durch sogenannte lokale verborgene Parameter. Basierend auf dieser Idee konstruierte *Bell* 1964 eine mathematische Ungleichung, anhand derer erstmals mit Hilfe von experimentellen Tests zwischen der Quantentheorie und lokalen realistischen Theorien unterschieden werden konnte. Seither wurden viele Experimente durchgeführt, die die Quantentheorie bestätigten und das Konzept der lokalen verborgenen Parameter widerlegten. Aber all diese experimentellen Tests litten unter sogenannten Schlupflöchern, die eine lokal-realistische Erklärung der experimentellen Beobachtungen zuließen. Entweder die verwendeten Detektoren hatten eine zu niedrige Detektionseffizienz, oder die detektierten Teilchen wurden nicht raumartig getrennt beobachtet. In diesem Zusammenhang ist die Verschränkung zwischen unterschiedlichen Quantenobjekten wie Atomen und Photonen von besonderem Interesse, da hiermit zwei weit voneinander entfernte Atome durch Interferenz von Photonen robust verschränkt werden können. Die daraus resultierende raumartige Trennung ermöglicht zusammen mit der beinahe perfekten Detektionseffizienz der Atome einen ersten schlupflochfreien Test der Bell'schen Ungleichung.

Das vorrangige Ziel dieser Arbeit ist die experimentelle Realisierung von Verschränkung zwischen einem einzelnen lokalisierten Atom und einem einzelnen spontan emittierten Photon, mit einer Wellenlänge die sich gut zum Transport über große Entfernungen eignet. In dem vorliegenden Experiment wird ein einzelnes, optisch gefangenes, ^{87}Rb Atom in einen Zustand angeregt, der zwei ausgezeichnete Zerfallskanäle hat. Beim nachfolgenden Spontanzerfall wird ein Photon mit gleicher Wahrscheinlichkeit kohärent in beide Kanäle emittiert. Dies bedingt eine perfekte Korrelation zwischen der Polarisation des emittierten Photons und dem Zeemanzustand des Atoms nach dem Spontanzerfall. Da diese Kanäle spektral und in allen anderen Freiheitsgraden ununterscheidbar sind, kommt es zur Verschränkung des Polarisationsfreiheitsgrads des Photons mit dem Spinfreiheitsgrad des Atoms. Zum Nachweis der Verschränkung werden geeignete Korrelationsmessungen zwischen dem internen Zustand des Atoms und dem Polarisationszustand des Photons in komplementären Messbasen vorgenommen. Es wird gezeigt, dass der generierte Atom-Photon Zustand mit einer Güte von 82 Prozent verschränkt ist.

Die in dieser Arbeit gewonnenen experimentellen Ergebnisse markieren einen wichtigen Schritt in Richtung Verschränkung zweier raumartig getrennter Atome für einen ersten schlupflochfreien Test der Bell'schen Ungleichung. Darüberhinaus ist die Verschränkung zwischen einem einzelnen Atom und einem einzelnen Photon ein wichtiges Werkzeug zur Realisierung von neuen Anwendungen auf dem Gebiet der Quantenkommunikation und Quanteninformationsverarbeitung, wie zum Beispiel der Zustandspräparation eines einzelnen Atoms über große Entfernungen.

Contents

1 Introduction

Since the early days of quantum theory *entanglement* - first introduced by Schrödinger in his famous paper on *"Die gegenwärtige Situtation in der Quantenmechanik* [1] - has been a considerable subject of debate because it highlighted the counter-intuitive nonlocal aspect of quantum mechanics. In particular, Einstein, Podolsky and Rosen (EPR) [2] presented an argument to show that there are situations in which the general probabilistic scheme of quantum theory seems not to describe the physical reality. In this famous *Gedankenexperiment* EPR used the assumption of local realism to conclude by means of two entangled particles that quantum mechanics is incomplete. For this reason *EPR* motivated an extension of quantum mechanics by so-called local hidden variables. Based on this idea in 1964 John Bell constructed mathematical inequalities which allow to distinguish between quantum mechanics and local-realistic theories [3]. Many experiments have since been done [4, 5, 6, 7, 8] that are consistent with quantum mechanics, disproving the concept of local realism.

But all these tests suffered from at least one of two primary loopholes. The first is called the locality loophole [9, 10], in which the correlations of apparently separate events could result from unknown subluminal signals propagating between two different regions of the measurement apparatus. An experiment was performed with entangled photons [7] enforcing strict relativistic separation between the measurements. But this experiment suffered from low detection efficiencies allowing the possibility that the subensemble of detected events agrees with quantum mechanics even though the entire ensemble satisfies the predictions of Bell's inequalities for local-realistic theories. This loophole is referred to as detection loophole [11, 12] and was addressed in an experiment with two trapped ions [8], where the quantum state detection of the atoms was performed with almost perfect efficiency. Because the ion separation was only a few μm this experiment could not eliminate the locality loophole. A possibility to close both loopholes in the same experiment is the preparation of space-like separated entangled atoms [13, 14]. The key-element of this proposal is the faithful generation of two highly entangled states between a single localized atom and a single spontaneously emitted photon (at a wavelength suitable for low-loss transport over large distances). The photons coming from each of the atoms travel then to an intermediate location where a partial Bell-state measurement is performed leaving the two distant atoms in an entangled state [15, 14]. Because the atoms can be detected with an efficiency up to 100 percent [8] this finally should allow a first loophole-free test of Bell's inequality [13, 14].

Nowadays there is also a large interest in the generation and engineering of quantum entanglement for the implementation of quantum communication and information [16,

17]. Until now entanglement was observed mainly between quantum objects of similar type like single photons [6, 18, 7], single atoms [19, 20, 21, 22] and recently between optically thick atomic ensembles [23, 24]. But all distributed quantum computation and scalable quantum communication protocols [17] require to coherently transfer quantum information between photonic- and matter- based quantum systems. The importance of this process is due to the fact that matter-based quantum systems provide excellent long-term quantum memory storage, whereas long-distance communication of quantum information will be accomplished by coherent propagation of light, e.g. in the form of single photons. The faithful mapping of quantum information between a stable quantum memory and a reliable quantum information channel would allow, for example, quantum communication over long distances and quantum teleportation of matter. But, because quantum states cannot in general be copied, quantum information could be distributed in these applications by entangling the quantum memory with the communication channel. In this sense entanglement between atoms and photons is necessary because it combines the ability to store quantum information with an effective communication channel [25, 13, 26, 27, 14].

Atom-photon entanglement has been implicit in many previous experimental systems, from early measurements of Bell inequality violations in atomic cascade systems [4, 6] to fluorescence studies in trapped atomic ions [28, 29] and atomic beam experiments [30]. Furthermore, on the basis of entanglement between matter and light, different experimental groups combined in the last few years the data storage properties of atoms with coherence properties of light. E.g., in the microwave domain, coherent quantum control has been obtained between single Rydberg atoms and single photons [31, 32, 33]. Recently, Matsukevich *et al.* [34] reported the experimental realization of coherent quantum state transfer from a matter qubit onto a photonic qubit using entanglement between a single photon and a single collective excitation distributed over many atoms in two distinct optically thick atomic samples. However, atom-photon entanglement has not been directly observed until quite recently [35], as the individual atoms and photons have not been under sufficient control.

The primary goal of the present work is the experimental realization of entanglement between a single localized atom and a single spontaneously emitted photon (at a wavelength suitable for long-distance transport in optical fibers and air) for a future loophole-free test of Bell's inequality. This task can be managed using optically trapped neutral alkali atoms like Rubidium or Cesium which radiate photons in the NIR of the electromagnetic spectrum.

To generate atom-photon entanglement in this experiment, a single ^{87}Rb atom (stored in an optical dipole trap) is excited to a state which has two decay channels. In the following spontaneous emission the atom decays either to the $|\uparrow\rangle$ ground state while emitting a $|\sigma^+\rangle$-polarized photon or to the $|\downarrow\rangle$ state while emitting a $|\sigma^-\rangle$-polarized photon. Provided these decay channels are indistinguishable a coherent superposition of the two possibilities is formed and the spin state of the atom is entangled with the polarization state of the emitted photon. Thus, the resulting atom-photon pair is in the

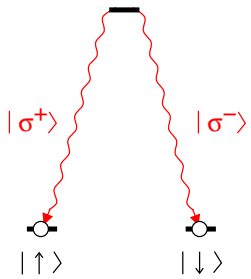

Figure 1.1: Atomic dipole transition to generate atom-photon entanglement.

maximally entangled quantum state

$$|\Psi^+\rangle = \frac{1}{\sqrt{2}}(|\uparrow\rangle|\sigma^+\rangle + |\downarrow\rangle|\sigma^-\rangle). \tag{1.1}$$

To verify entanglement of the generated atom-photon state one has to disprove the possibility that the two-particle quantum system can be a statistical mixture of separable states. This task is closely connected to a violation of Bell's inequality and requires correlated local state measurements of the atom and the photon in complementary bases. The polarization state of the photon can be measured simply by a combination of a polarization filter and a single photon detector. However, the spin state of a single atom is not trivial to measure and therefore one of the challenges of this experiment.

In the context of the present work we set up an optical dipole trap which allows one to localize and manipulate a single ^{87}Rb atom. The internal quantum state of the atom is analyzed by means of a Stimulated-Raman-Adiabatic-Passage (STIRAP) technique, where the polarization of the STIRAP light field defines the atomic measurement basis. To proof atom-photon entanglement the internal quantum state of the atom is measured conditioned on the detection of the polarization state of the photon. We observe strong atom-photon correlations in complementary measurement bases verifying entanglement between the atom and the photon.

Overview

In the second chapter I will introduce in general the property of entanglement between two spin-1/2 particles and in particular spin-entanglement between a single atom and a single photon. The third chapter deals with trapping single atoms in a far-off-resonance optical dipole potential. After the theory of optical dipole potentials is discussed, the trap setup is presented and the observation of single atom resonance fluorescence is reported. A detailed investigation of the resonance fluorescence spectrum is performed which allows to determine the mean kinetic energy of the stored atom. In the fourth chapter, the photon statistics of the emission from a single four-level atom is analyzed. The measured photon-pair correlation functions are discussed and compared with theoretical models. The fifth chapter describes in detail the atomic state detection scheme.

The theory of coherent-population-trapping (CPT) and Stimulated-Raman-Adiabatic-Passage (STIRAP) is discussed and experiments are presented which show the coherent analysis of Zeeman superposition states of a single atom. In the sixth chapter I will report on the observation of entanglement between a single optically trapped ^{87}Rb atom and a spontaneously emitted single photon. Finally in the seventh chapter the experimental achievements are discussed and future applications of atom-photon entanglement are highlighted.

2 Theory of atom-photon entanglement

2.1 Introduction

In the context of this chapter I will introduce the concept of entanglement between the spin state of a single atom and the polarization state of a single photon. I will begin by very briefly recapitulating some basic features of quantum mechanics which later on will become relevant for the understanding of the experimental investigation of atom-photon entanglement in chapter 6. Then I will establish in general the property of "entanglement" between two quantum systems and important applications in the field of quantum communication. Finally I will present the basic idea of my thesis how to generate and analyze a spin-entangled atom-photon state.

2.2 Basics of quantum mechanics

2.2.1 The superposition principle

One of the most important concepts in quantum mechanics is the *superposition* principle. Quantum states denoted by $|\Psi\rangle$ can exist in a superposition, i.e. a linear combination, of two possible orthogonal basis states $|\uparrow\rangle$ and $|\downarrow\rangle$

$$|\Psi\rangle = a|\uparrow\rangle + b|\downarrow\rangle, \tag{2.1}$$

where a and b are complex numbers and $|a|^2 + |b|^2 = 1$. Examples of states in a two dimensional Hilbert space are the polarization states $|\sigma^+\rangle$ and $|\sigma^-\rangle$ of a single photon or the states $|m_L = -1/2\rangle$ and $|m_L = +1/2\rangle$ of the magnetic moment of a single atom with the angular momemtum $L = 1/2$. The state $|\Psi\rangle$ can be written in a useful geometric representation as:

$$|\Psi\rangle = \cos\left(\frac{\theta}{2}\right)|\uparrow\rangle + e^{i\phi}\sin\left(\frac{\theta}{2}\right)|\downarrow\rangle, \tag{2.2}$$

where θ and ϕ define a point on the three-dimensional Bloch sphere (see Fig. 2.1).

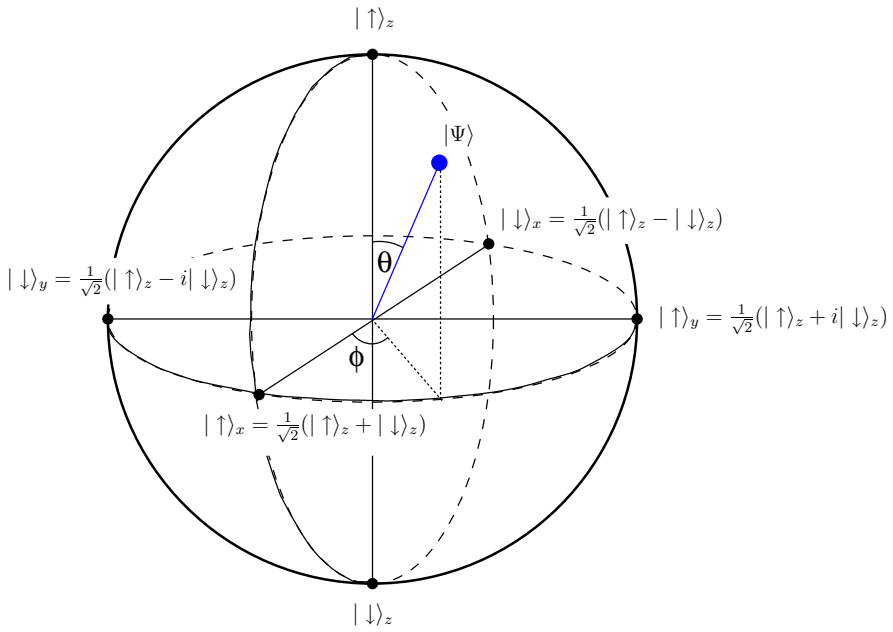

Figure 2.1: An arbitrary spin-1/2 state $|\Psi\rangle$ and the three complementary bases x,y,z in the Bloch sphere representation.

2.2.2 Quantum measurements

A measurement in quantum mechanics is inherently *indeterministic*. If we ask (measure) whether $|\Psi\rangle$ is in the state $|\uparrow\rangle$, we obtain this result with probability $|\langle\uparrow|\Psi\rangle|^2 = |a|^2$. After the measurement, the state is projected to $|\uparrow\rangle$. In this ideal *Von Neumann measurement*, it is not possible to measure an unknown quantum state without disturbance.

2.2.3 Complementary observables

Two well known complementary observables are position and momentum of a single particle. These two observables cannot be measured with arbitrary accuracy in an experiment at the same time [36]. In general, let $\hat{A}$ and $\hat{B}$ denote two non-commuting Hermitian operators (observables) of a quantum system of dimension N, $\hat{A}$ and $\hat{B}$ are said to be complementary, or mutually unbiased, if their eigenvalues are non-degenerate and the inner product between any two normalized eigenvectors $|\Psi_A\rangle$ of $\hat{A}$ and $|\Psi_B\rangle$ of $\hat{B}$, always has the same magnitude. For the case of a two-dimensional Hilbert space, there are three complementary observables $\hat{\sigma}_x$, $\hat{\sigma}_y$ and $\hat{\sigma}_z$, which are called Pauli spin-operators. These operators can be represented by 2×2 Hermitian matrices defined by

$$\sigma_x = \begin{pmatrix} 0 & 1 \\ 1 & 0 \end{pmatrix} \quad \sigma_y = \begin{pmatrix} 0 & -i \\ i & 0 \end{pmatrix} \quad \sigma_z = \begin{pmatrix} 1 & 0 \\ 0 & -1 \end{pmatrix} \tag{2.3}$$

The eigenvalues of σ_x, σ_y and σ_z are $\lambda = \pm 1$ and the corresponding eigenvectors are given by

$$|\uparrow\rangle_x = \frac{1}{\sqrt{2}}(|\uparrow\rangle_z + |\downarrow\rangle_z) \tag{2.4}$$

$$|\downarrow\rangle_x = \frac{1}{\sqrt{2}}(|\uparrow\rangle_z - |\downarrow\rangle_z) \tag{2.5}$$

$$|\uparrow\rangle_y = \frac{1}{\sqrt{2}}(|\uparrow\rangle_z + i|\downarrow\rangle_z) \tag{2.6}$$

$$|\downarrow\rangle_y = \frac{1}{\sqrt{2}}(|\uparrow\rangle_z - i|\downarrow\rangle_z) \tag{2.7}$$

and $|\uparrow\rangle_z$ and $|\downarrow\rangle_z$, respectively. Fig. 2.1 shows these three complementary basis vectors on the Bloch sphere.

The inner product $\langle .|.\rangle$ between any two basis states belonging to different bases is $1/\sqrt{2}$. This property guarantees that if a quantum system is prepared in one basis, the outcome of a measurement in any complementary basis is totally random.

2.3 Entanglement

Since the early days of quantum mechanics entanglement - first introduced by Schrödinger in his famous paper on *"Die gegenwärtige Situtation in der Quantenmechanik* [1] - has been a considerable subject of debate because it highlighted the counter-intuitive non-local aspect of quantum mechanics. In particular, Einstein, Podolsky and Rosen (EPR) [2] presented an argument to show that there are situations in which the general probabilistic scheme of quantum theory seems not to describe the physical reality properly. In this famous *Gedankenexperiment* EPR used the assumption of local realism to conclude by means of two entangled particles that quantum mechanics is incomplete. Here I will introduce the essential features of entanglement between two spin-1/2 particles following Bohm [37].

Let us consider a quantum state $|\Psi_{AB}\rangle$ of two spin-1/2 particles A and B. Up to some time $t = 0$, these particles are taken to be in a bound state of zero angular momentum. Then we turn off the binding potential (e.g., we disintegrate the bound system in two parts), but introduce no angular momentum into the system and do not disturb the spins in any way. The seperate parts of the system are now free but due do conservation of angular momentum the two particles are entangled and the state is given by

$$|\Psi_{AB}\rangle = \frac{1}{\sqrt{2}}(|\uparrow_A\rangle|\downarrow_B\rangle - |\downarrow_A\rangle|\uparrow_B\rangle). \tag{2.8}$$

This state has four important properties:

1. it can not be expressed as a tensor product $|\Psi_A\rangle \otimes |\Psi_B\rangle$ of two single particle states.

2. it is rotationally invariant.

3. the expectation value of the spin of a single particle is zero.

4. the spin states of both particles are anti-correlated in any analysis direction.

The probability to simultaneously "measure" the spin of particle A on the equator of the Bloch-sphere at the angle ϕ_A and particle B at the angle ϕ_B, respectively, is

$$P_{AB}(\phi_A, \phi_B) = \langle \Psi_{AB} | \hat{\pi}^A_{\phi_A} \hat{\pi}^B_{\phi_B} | \Psi_{AB} \rangle, \tag{2.9}$$

where the projection operators $\hat{\pi}^A_{\phi_A}$ and $\hat{\pi}^B_{\phi_B}$ corresponding to particles A and B are given by

$$\hat{\pi}^i_{\phi_i} = \frac{1}{2}(\hat{I}^i + \hat{\sigma}^i_x \cos\phi_i + \hat{\sigma}^i_y \sin\phi_i), \quad i = A, B. \tag{2.10}$$

After some calculations, we find

$$P_{AB}(\phi_A, \phi_B) = \frac{1}{4}[1 - \cos(\phi_A - \phi_B)] = \frac{1}{2}\sin^2\left(\frac{\phi_A - \phi_B}{2}\right). \tag{2.11}$$

If we now ask for the conditional probability to find particle A along ϕ_A if particle B was measured along ϕ_B we get

$$P(\phi_A|\phi_B) = \sin^2\left(\frac{\phi_A - \phi_B}{2}\right). \tag{2.12}$$

This quantity is shown in Fig. 2.2 as a function of the analysis direction ϕ_B if particle A was measured as $|\uparrow\rangle$ in σ_x or σ_y. If the analysis direction of both particles is the same ($\phi_A = \phi_B$), the conditional probability of detection is zero, because the spins are always anticorrelated. But for $\phi_A = \phi_B + \pi$ the conditional probability is equal to one. This property holds true for any initial choice of the analyzer direction ϕ_A and is invariant under the exchange of the two particles $P(\phi_A|\phi_B) = P(\phi_B|\phi_A)$. The described two-particle correlations are independent of the choice of the measurement basis. This is the main signature of the entangled singlet state $|\Psi_{AB}\rangle$.

For an arbitrary quantum system consisting of two spin-1/2 particles A and B the four entangled states

$$|\Psi^+\rangle = \frac{1}{\sqrt{2}}(|\uparrow_A\rangle|\downarrow_B\rangle + |\downarrow_A\rangle|\uparrow_B\rangle) \tag{2.13}$$

$$|\Psi^-\rangle = \frac{1}{\sqrt{2}}(|\uparrow_A\rangle|\downarrow_B\rangle - |\downarrow_A\rangle|\uparrow_B\rangle) \tag{2.14}$$

$$|\Phi^+\rangle = \frac{1}{\sqrt{2}}(|\uparrow_A\rangle|\uparrow_B\rangle + |\downarrow_A\rangle|\downarrow_B\rangle) \tag{2.15}$$

$$|\Phi^-\rangle = \frac{1}{\sqrt{2}}(|\uparrow_A\rangle|\uparrow_B\rangle - |\downarrow_A\rangle|\downarrow_B\rangle) \tag{2.16}$$

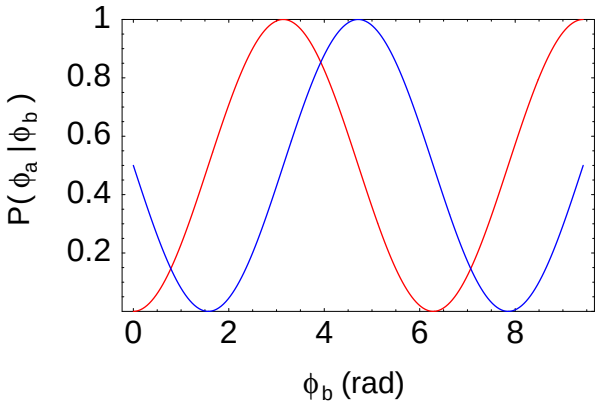

Figure 2.2: Expected spin correlations of an entangled state $|\Psi_{AB}\rangle$ for complementary measurement bases of particle A as the analyzer-direction of particle B is varied by an angle ϕ_B . (Red line) particle A is measured along $\phi_A = 0$ corresponding to $|\uparrow\rangle_x$. (Blue line) particle A is analyzed along $\phi_A = \pi/2$ corresponding to $|\uparrow\rangle_y$.

form an orthonormal basis of the 2×2 dimensional Hilbert space. These states are called Bell states and violate a Bell inequality (see subsection 2.3.2) by the maximum value predicted by quantum mechanics. Furthermore the Bell states have the important property that each state can be transformed into any other of the four Bell states by unitary single particle rotations.

2.3.1 The EPR "paradox"

Every spin-entangled state has the property that none of the two spins has a defined value. Therefore it is impossible to predict the outcome of a spin measurement on one particle with certainty. But if we perform a measurement on one spin, instantaneously the outcome of a spin measurement on the other particle is known. This holds true even if the spins are separated by an arbitrary distance. These counterintuitive features of entangled quantum systems were used by Einstein, Podolsky and Rosen (EPR) [2] to argue that the quantum mechanical description of the physical reality can not be considered complete. EPR understand a theory to be complete if every element of the **physical reality** is represented in the physical theory in the sense that:

"If, without in any way disturbing a system, we can predict with certainty (i.e. with probability equal to unity) the value of a physical quantity, then there exists an element of physical reality corresponding to this quantity."

The first part of the reality criterion requires that the prediction can be made without

disturbing the object in question. It is, for instance, possible to predict the value of the mass of the next pion crossing a bubble chamber without interacting with it. In every case in which the prediction can be made in this way, the EPR reality criterion assigns to the object an *element of reality*, i.e., something real that does not necessarily coincide with the observed property but generates it deterministically when a measurement is made.

Furthermore EPR require that any physical theory has to be local. In other words the **locality postulate** is based on the reasonable belief that the strength of interaction between objects depends inversily on their separation. If an electron is observed in a laboratory, another electron 10 or 10^{10} m away acquires no new property. To summarize, the idea of locality can be formulated as follows:

"Given two separated objects A and B, the modifications of A due to anything that may happen to B can be made arbitrarily small for any measurable physical quantity, by increasing their separation."

In 1951 David Bohm restated and simplified the EPR argument on the basis of the spin-entangled state $|\Psi_{AB}\rangle$ from (2.8) as follows [37]:

1. Pick an arbitrary analysis basis, e.g. the z-basis and measure the spin of particle A. Then the result will be either $\uparrow$ or $\downarrow$, say $\uparrow$.

2. Knowing that the spin of particle A is "up", we know with certainty that the result of a spin-measurement of B will be "down". But if we then measure particle B in the x-basis we will find that particle B has a definite spin (either $\uparrow_x$ or $\downarrow_x$), i.e., we know the value of σ_x.

3. Therefore, we know both the z and x components of the spin of particle B, which is a violation of complementarity.

In the words of EPR this implies a very unsatisfactory state of affairs: "Thus, it is possible to assign two different state vectors to the same reality." One way out of this problem is to argue that in a single experiment one can measure particle B only in one basis and not in two bases at the same time. The knowledge of a fictitious measurement result does not replace the measurement process itself. From this point of view the EPR assumption about elements of reality becomes useless: it can only lead to the conclusion that *"an element of reality is associated with a concretely performed act of measurement"*. This argument was used by Bohr [38] in a reply to EPR, whereas EPR used the inability of quantum mechanics to make definite predictions for the outcome of a certain measurement to postulate the existence of "hidden" variables which are not known and perhaps not measurable. It was hoped that an inclusion of these hidden variables (LHV) would restore the completness and determinism to the quantum theory.

2.3.2 Bell's inequality

In 1964, John Bell [3] constructed an inequality for observables of spin correlation experiments, for which predictions of hidden variable theories based on Einstein's locality principle do not agree with the statistical predictions of quantum mechanics. Here I will sketch the simplest derivation of Bell's inequality as given by Bell in 1970 [39].

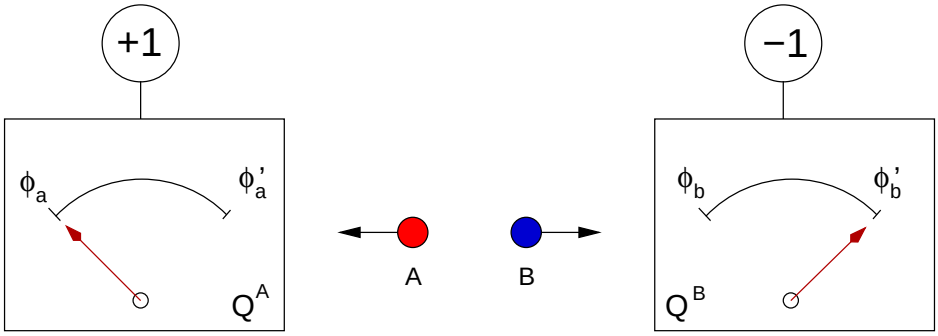

Figure 2.3: Experimental apparatuses measuring one of the dichotomic observables $Q^A(\phi_A)$, $Q^A(\phi'_A)$, $Q^B(\phi_B)$, $Q^B(\phi'_B)$ on the incoming physical systems A and B, respectively. The results (+1 and -1) of the last measurement are shown on the upper screens.

It is assumed that in an EPR experiment dichotomic observables $Q^A(\phi_A) = \pm 1$ and $Q^B(\phi_B) = \pm 1$ are measured on the two particles A and B, respectively, moving in opposite directions, as in Fig. 2.3. These observables depend on instrumental parameters ϕ_A and ϕ_B (polarizers' axes, directions of magnetic fields, etc.) that can be varied. In practice, only two observables [$Q^A(\phi_A)$ and $Q^A(\phi'_A)$] are of interest for particle A, and two [$Q^B(\phi_B)$ and $Q^B(\phi'_B)$] for particle B. In general, it is expected that $Q^A(\phi_A)$ and $Q^A(\phi'_A)$ are incompatible and hence cannot be measured at the same time, and that the same holds for $Q^B(\phi_B)$ and $Q^B(\phi'_B)$.

It is assumed that hidden variables belonging to A and B fix the outcome of all possible measurements. These hidden variables are collectively represented by λ, assumed to vary in a set Λ with a probability density $\rho(\lambda)$. The normalization condition

$$\int_\Lambda d\lambda \rho(\lambda) = 1 \tag{2.17}$$

holds. Thus one can write

$$Q^A(\phi_A, \lambda) = \pm 1; \quad Q^A(\phi'_A, \lambda) = \pm 1; \quad Q^B(\phi_B, \lambda) = \pm 1; \quad Q^B(\phi'_B, \lambda) = \pm 1 \tag{2.18}$$

meaning that, given λ, every one of the four dichotomic observables assumes a well-defined value. The correlation function $E(\phi_A, \phi_B)$ is defined as the average product of two dichotomic observables. In the hidden-variable approach it can be written

$$E(\phi_A, \phi_B) = \int_\Lambda d\lambda \rho(\lambda) Q^A(\phi_A, \lambda) Q^B(\phi_B, \lambda). \tag{2.19}$$

This is a local expression, in the sense that neither Q^A depends on ϕ_B nor Q^B on ϕ_A.

It is easy to show that [39]

$$\begin{aligned} &|E(\phi_A,\phi_B)-E(\phi_A,\phi'_B)+E(\phi'_A,\phi_B)+E(\phi'_A,\phi'_B)| \\ \leq \int_\Lambda d\lambda\{&|Q^A(\phi_A,\lambda)||Q^B(\phi_B,\lambda)-Q^B(\phi'_B,\lambda)|+|Q^A(\phi'_A,\lambda)||Q^B(\phi_B,\lambda)-Q^B(\phi'_B,\lambda)|\} \\ &= \int_\Lambda d\lambda\{|Q^B(\phi_B,\lambda)-Q^B(\phi'_B,\lambda)|+|Q^B(\phi_B,\lambda)-Q^B(\phi'_B,\lambda)|\} \end{aligned}$$

since $|Q^A(\phi_A,\lambda)|=|Q^A(\phi'_A,\lambda)|=1$. But the moduli $Q^B(\phi_B,\lambda)$ and $Q^B(\phi'_B,\lambda)$ are also equal to 1, so

$$|Q^B(\phi_B,\lambda)-Q^B(\phi'_B,\lambda)|+|Q^B(\phi_B,\lambda)+Q^B(\phi'_B,\lambda)|=2 \tag{2.20}$$

From (2.17) and (2.20) one obtains the inequality

$$S(\phi_A,\phi_B,\phi'_A,\phi'_B)=|E(\phi_A,\phi_B)-E(\phi_A,\phi'_B)|+|E(\phi'_A,\phi_B)+E(\phi'_A,\phi'_B)|\leq 2. \tag{2.21}$$

This is Bell's inequality in the CHSH form [40], which is more general than its original form [3].

The present proof is based on a general form of realism because the hidden variable λ is thought to belong objectively to the real physical systems A and B. It is also based on locality for three reasons: (1) the dichotomic observables Q^A and Q^B do not depend on the parameters ϕ_A and ϕ_B of the experimental apparatus; (2) the probability density $\rho(\lambda)$ does not depend on ϕ_A and ϕ_B; (3) the set Λ of possible λ values does not depend on ϕ_A and ϕ_B. The time arrow assumption is also implicit in the dependance of $\rho(\lambda)$ on ϕ. In principle, the choices of the values of the instrumental parameters could be made when the particles A and B are in flight from the source to the analyzers.

But now, supposed two particles are in the entangled singlet state $|\Psi_{AB}\rangle$. Quantum mechanically, the measurement of the dichotomic variables Q^A and Q^B is represented by the spin operators $\vec{\sigma}_A\vec{a}$ and $\vec{\sigma}_B\vec{b}$. The corresponding quantum mechanical correlations entering Bell's inequality are given by the expectation value for the product of spin-measurements on particle A and B along the directions $\vec{a}$ and $\vec{b}$:

$$\begin{aligned} E_{QM}(\vec{a},\vec{b}) &= \langle\Psi_{AB}|\vec{\sigma}_A\vec{a}\otimes\vec{\sigma}_B\vec{b}|\Psi_{AB}\rangle \\ &= \frac{1}{2}(\langle\uparrow|\vec{\sigma}_A\vec{a}|\uparrow\rangle\langle\downarrow|\vec{\sigma}_B\vec{b}|\downarrow\rangle-\langle\uparrow|\vec{\sigma}_A\vec{a}|\downarrow\rangle\langle\downarrow|\vec{\sigma}_B\vec{b}|\uparrow\rangle \\ &\quad -\langle\downarrow|\vec{\sigma}_A\vec{a}|\uparrow\rangle\langle\uparrow|\vec{\sigma}_B\vec{b}|\downarrow\rangle+\langle\downarrow|\vec{\sigma}_A\vec{a}|\downarrow\rangle\langle\uparrow|\vec{\sigma}_B\vec{b}|\uparrow\rangle) \\ &= -\vec{a}\vec{b}=\cos(\phi_A-\phi_B) \end{aligned}$$

Choosing the directions $\phi_A=0$, $\phi'_A=\pi/2$, $\phi_B=\pi/4$ and $\phi'_B=3\pi/4$ of the spin analyzers, one finds a maximal violation of inequality (2.21), namely

$$S_{QM}(0,\pi/2,\pi/4,3\pi/4)=2\sqrt{2}>2. \tag{2.22}$$

Thus, for the spin entangled singlet state, the quantum mechanical correlations between the measurement results of two distant observers are stronger than any possible correlation predicted by LHV theories.

The great achievement of John Bell was, that he derived a formal expression which allows to distinguish experimentally between local-realistic theories and quantum theory. In real experiments it is hard to violate Bell's inequality without the additional assumption of *fair sampling*. Pearle [11], for example, noted that a subensemble of detected events can agree with quantum mechanics even though the entire ensemble satisfies the predictions of Bell's inequality for local-realistic theories.

Clauser-Horne inequality

In 1974 Clauser and Horne derived an inequality, which can be tested in real experiments with an essential weaker assumption [41]. Supposed during a period of time, while the adjustable parameters of the apparatus have the values ϕ_A and ϕ_B, the source emits, say, N two-particle systems of interest. For this period, denote by $N_A(\phi_A)$ and $N_B(\phi_B)$ the number of counts at detectors A and B, respectively, and by $N_{AB}(\phi_A, \phi_B)$ the number of simultaneous counts from the two detectors (coincident events). If N is sufficiently large, then the ensemble probabilities of these results are

$$\begin{aligned} P_A(\phi_A) &= N_A(\phi_A)/N, \\ P_B(\phi_B) &= N_B(\phi_B)/N, \\ P_{AB}(\phi_A, \phi_B) &= N_{AB}(\phi_A)/N. \end{aligned} \tag{2.23}$$

After some algebra they obtain

$$S(\phi_A, \phi_B, \phi'_A, \phi'_B) = \frac{P_{AB}(\phi_A, \phi_B) - P_{AB}(\phi_A, \phi'_B) + P_{AB}(\phi'_A, \phi_B) + P_{AB}(\phi'_A, \phi'_B)}{P_A(\phi'_A) + P_B(\phi_B)} \leq 1. \tag{2.24}$$

In this inequality the probabilities can be replaced simply by count rates because the normalization to the real number of emitted pairs N cancels.

Loopholes

To exclude any local realistic theory in a Bell-type experiment one generally assumes: (1) the detection probability of a pair of particles which has passed the analyzers is independent of the analyzer settings [40]; (2) the detected subset is a sample of the whole emitted pairs; (3) a distant apparatus does not influence a space-like and time-limited measurement due to any relativistic effect. If any of these assumptions is dropped a hard proof that local-realistic theories can not describe our physical reality is impossible. Most prominently the *detection loophole* (2) and the *locality loophole* (3) are used by critics to argue that no experiment disproves the concept of local realism.

In 1972 Freedman and Clauser [4] published an experiment which was designed for a first test of Bell's inequality. A cascade transition in ^{40}Ca was used to generate polarization entangled photon pairs. Ten years later Aspect *et al.* [5, 6] modified the Ca experiments by Clauser in a way that they used a non-resonant two-photon process for the excitation instead of a Deuterium arc lamp. Furthermore this experiment took great care to use non-absorptive state analyzers and to switch fast between different measurement bases in order to fulfill the requirements assumed by John Bell in his original work. Aspect *et al.* retrieved experimental data violating the CHSH-inequality by 2.697 ± 0.015. A new era of Bell experiments was opened by the application of the nonlinear optical effect of parametric down-conversion to generate entangled photon pairs [18]. A sequence of different experiments have been performed which culminated in two Bell experiments [7, 42] highlighting the strict relativistic separation between measurements. But both experiments suffered from low detection efficiencies allowing the possibility that the subensemble of detected events agrees with quantum mechanics even though the entire ensemble satisfies the predictions of Bell's inequalities for local-realistic theories. This loophole is referred to as detection loophole and was addressed in an experiment with two trapped ions [8], whereby the quantum state detection of the atoms was performed with almost perfect efficiency. But the ion separation was not large enough to eliminate the locality loophole.

2.3.3 Quantifying entanglement

The quantification of entanglement is a long standing problem in quantum information theory. Any good measure of entanglement should satisfy certain conditions. An important condition is that entanglement cannot increase by local operations and classical communications (for more detail see [43]). The question which amount of entanglement is contained in an arbitrary two-particle quantum state represented by a density matrix ρ is connected closely to the general question "how close are two quantum states". One measure of distance between quantum states is the *fidelity* F.

For an unknown quantum system consisting of two spin-1/2 particles the state is represented by a 4×4 density matrix ρ. The entanglement fidelity with respect to a particular maximally entangled pure state $|\Psi_{AB}\rangle$ is given by [44]

$$F(|\Psi_{AB}\rangle, \rho) = \langle\Psi_{AB}|\rho|\Psi_{AB}\rangle = \frac{1}{2}(\langle\downarrow\uparrow|\rho|\downarrow\uparrow\rangle + \langle\uparrow\downarrow|\rho|\uparrow\downarrow\rangle + \langle\downarrow\uparrow|\rho|\uparrow\downarrow\rangle + \langle\uparrow\downarrow|\rho|\downarrow\uparrow\rangle), \quad (2.25)$$

the overlap between $|\Psi\rangle$ and ρ. The first two terms in this expression are the measured conditional probabilities of detecting $|\downarrow\rangle_A|\uparrow\rangle_B$ and $|\uparrow\rangle_A|\downarrow\rangle_B$. The last two terms can be determined by repeating the experiment while rotating each spin through a polar angle of $\pi/2$ in the Bloch sphere before measurement. The rotated quantum state is then given by $\tilde{\rho}$. Without a complete state tomography of ρ the entanglement fidelity F can

not be determined accurately. But one can derive a lower bound of F, expressed only in terms of diagonal density matrix elements in the original and rotated basis [35]:

$$F \geq \frac{1}{2}(\langle\downarrow\uparrow|\rho|\downarrow\uparrow\rangle + \langle\uparrow\downarrow|\rho|\uparrow\downarrow\rangle - 2\sqrt{\langle\downarrow\downarrow|\rho|\downarrow\downarrow\rangle\langle\uparrow\uparrow|\rho|\uparrow\uparrow\rangle} + \langle\downarrow\uparrow|\tilde{\rho}|\downarrow\uparrow\rangle + \langle\uparrow\downarrow|\tilde{\rho}|\uparrow\downarrow\rangle \\ -\langle\downarrow\downarrow|\tilde{\rho}|\downarrow\downarrow\rangle - \langle\uparrow\uparrow|\tilde{\rho}|\uparrow\uparrow\rangle) \quad (2.26)$$

Another possibility to determine the entanglement fidelity of an unknown quantum state ρ is to do the following. Suppose, a source emits two spin-1/2 particles in the entangled pure state $|\Psi_{AB}\rangle$. But due to experimental imperfections in the state detection of spin A and B, the state $|\Psi_{AB}\rangle$ can be measured with the probability $0 \leq p \leq 1$. For the rest of the unperfect state we expect white noise, corresponding to the maximally mixed state $\frac{1}{4}\hat{I}$. Technically speaking, the imperfect detection is modeled by an ideal preparation accompanied/followed by a noisy channel, which transforms the maximally entangled initial state $\rho = |\Psi_{AB}\rangle\langle\Psi_{AB}|$ as

$$\rho \rightarrow \rho = p|\Psi_{AB}\rangle\langle\Psi_{AB}| + \frac{(1-p)}{4}\hat{I}, \quad (2.27)$$

where $\hat{I}$ is the identity operator. If we plug this expression into the definition of the entanglement fidelity F in Eq. 2.25, we obtain

$$F = p + \frac{(1-p)}{4} \quad (2.28)$$

For a mixed state denoted by a density matrix ρ, the correlations entering a Bell inequality are given by

$$E(\vec{a},\vec{b}) = Tr\{\rho\vec{\sigma}_A\vec{a} \otimes \vec{\sigma}_B\vec{b}\} = \sum_{i,k}^{4}\langle u_i|\rho|u_k\rangle\langle u_k|\vec{\sigma}_A\vec{a} \otimes \vec{\sigma}_B\vec{b}|u_i\rangle, \quad (2.29)$$

where $|u_i\rangle$ denotes the two particle spin-1/2 basis states $|\uparrow\uparrow\rangle$, $|\uparrow\downarrow\rangle$, $|\downarrow\uparrow\rangle$ and $|\downarrow\downarrow\rangle$. On the basis of the mixed state density matrix (2.27) and (2.29) it is possible to derive the minimal amount of entanglement necessary to violate a Bell inequality. One obtains $p \geq 0.707$ corresponding to a minimum entanglement fidelity of $F = 0.78$. For fidelities $F > 0.5$, the underlying quantum state is entangled [44].

2.3.4 Applications of entanglement

Until the early 1990s the general physical interest concerning entanglement was focused on fundamental tests of quantum mechanics. But in 1991 A. Ekert [45] realized that the specific correlations of entangled spin-1/2 particles and Bell's theorem can be used to distribute secret keys. Two years later Bennet, Brassard, Crepeau, Josza, Peres and Wootters [46] proposed to transfer the quantum state of a particle to another particle at

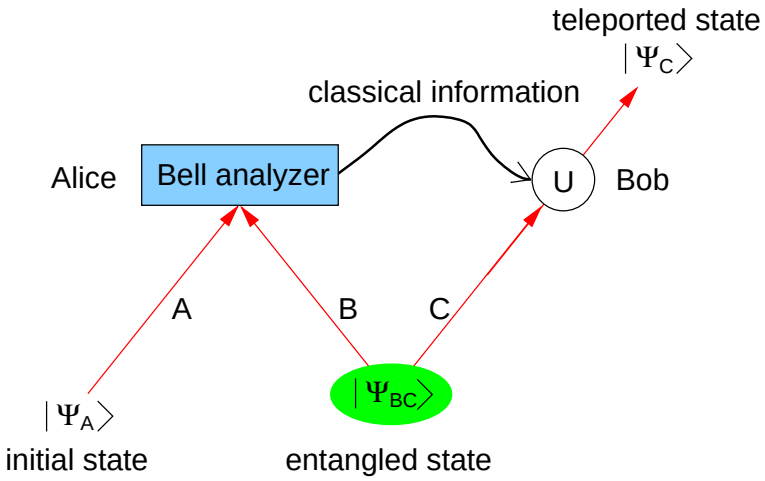

Figure 2.4: Principle of quantum teleportation using two-particle entanglement. Alice performs a Bell state measurement on the initial particle and particle B. After she has sent the measurement result as classical information to Bob, he performes a unitary transformation (U) on particle C depending on Alice' measurement result to reconstruct the initial state.

a distant location employing entanglement as a resource, and it was realized by Zukowski *et al.* [15] that two particles can be entangled by a projection measurement on entangled Bell-states although they never interacted in the past. In the last decade the physical interest about entanglement focused also on applications for computational tasks. On the next pages I will give a short review on quantum teleportation and entanglement swapping because entanglement between a single atom and a single photon can be used to map quantum information between light- and matter-based quantum systems and for entangling space-like separated atoms for a loophole-free test of Bell's inequality.

Quantum Teleportation

The idea of of quantum teleportation [46] is that Alice has a spin-1/2 particle in a certain quantum state $|\Psi_A\rangle = a|\uparrow_A\rangle + b|\downarrow_A\rangle$. She wishes to transfer this quantum state to Bob, but she cannot deliver the particle directly to him because their only connection is via a classical channel. According to the projection postulate of quantum mechanics we know that any quantum measurement performed by Alice on her particle will destroy the quantum state at hand without revealing all the necessary information for Bob to reconstruct the quantum state. So how can she provide Bob with the quantum state? The answer is to use an ancillary pair of entangled particles B and C in the singlet state

$$|\Psi^-_{BC}\rangle = \frac{1}{\sqrt{2}}(|\uparrow_B\rangle|\downarrow_C\rangle - |\downarrow_B\rangle|\uparrow_C\rangle) \tag{2.30}$$

shared by Alice and Bob.

Although initially particles A and B are not entangled, their joint state can always be expressed as a superposition of four maximally entangled Bell states, given by (2.13), since these states form a complete orthonormal basis. The total state of the three particles can be written as:

$$\begin{aligned}|\Psi_{ABC}\rangle = |\Psi_A\rangle \otimes |\Psi_{BC}\rangle = \frac{1}{2} \quad [\quad & |\Psi^-_{AB}\rangle \otimes (-a|\uparrow_C\rangle - b|\downarrow_C\rangle) \\ + \quad & |\Psi^+_{AB}\rangle \otimes (-a|\uparrow_C\rangle + b|\downarrow_C\rangle) \\ + \quad & |\Phi^-_{AB}\rangle \otimes (+a|\downarrow_C\rangle + b|\uparrow_C\rangle) \\ + \quad & |\Phi^+_{AB}\rangle \otimes (+a|\downarrow_C\rangle - b|\uparrow_C\rangle)]. \end{aligned} \tag{2.31}$$

Alice now performs a Bell state measurement (BSM) on particles A and B, that is, she projects her two particles onto one of the four Bell states. As a result of the measurement Bob's particle will be found in a state that is directly related to the initial state. For example, if the result of Alice's Bell state measurement is $|\Phi^-_{AB}\rangle$ then particle C in the hands of Bob is in the state $a|\downarrow_C\rangle + b|\uparrow_C\rangle$. All that Alice has to do is to inform Bob via a classical communication channel on her measurement result and Bob can perform the appropriate unitary transformation (U) on particle C in order to obtain the initial state of particle A.

Entanglement Swapping

Entanglement can be realized by having two entangled particles emerge from a common source, or by allowing two particles to interact with each other. Yet, another possibility to obtain entanglement is to make use of a projection of the state of two particles onto an entangled state. This projection measurement does not necessarily require a direct interaction between the two particles. When each of the two particles is entangled with another particle, an appropriate measurement, for example, a Bell-state measurement, of the partner particles will automatically collapse the state of the remaining two particles into an entangled state. This striking application of the projection postulate is referred to as *entanglement swapping* [15] or teleportation of entanglement.

Consider two EPR sources, simultaneously emitting a pair of entangled particles (Fig.2.5) each. We assume that the entangled particles are in the state

$$|\Psi_{ABCD}\rangle = \frac{1}{2}(|\uparrow_A\rangle|\downarrow_B\rangle - |\downarrow_A\rangle|\uparrow_B\rangle) \otimes (|\uparrow_C\rangle|\downarrow_D\rangle - |\downarrow_C\rangle|\uparrow_D\rangle). \tag{2.32}$$

If one now performs a joint Bell-state measurement on particles B and C, the particles A and D are projected onto a Bell state. This is a consequence of the fact that the state of (2.32) can be written as

$$\begin{aligned}|\Psi_{ABCD}\rangle = \frac{1}{2} \quad (\quad & |\Psi^+_{AD}\rangle|\Psi^+_{BC}\rangle - |\Psi^-_{AD}\rangle|\Psi^-_{BC}\rangle \\ - \quad & |\Phi^+_{AD}\rangle|\Phi^+_{BC}\rangle + |\Phi^-_{AD}\rangle|\Phi^-_{BC}\rangle). \end{aligned} \tag{2.33}$$

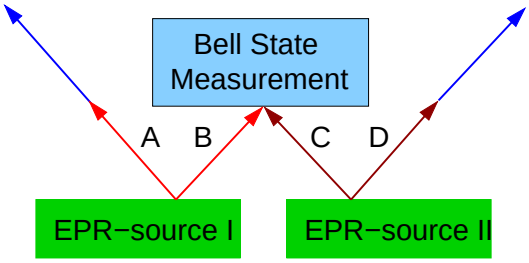

Figure 2.5: Principle of entanglement swapping. Two sources produce two pairs of entangled particles, pair A-B and pair C-D. One particle from each pair (particles B and C) is subjected to a Bell-state measurement. This results in a projection of particles A and D onto an entangled state.

In all cases particles A and D emerge entangled, despite the fact that they never interacted in the past.

2.4 Atom-photon entanglement

When a single atom is prepared in an excited state $|e\rangle$ it can spontaneously decay to the ground level $|g\rangle$ and emit a single photon. Due to conservation of angular momentum in spontaneous emission the polarization of the emitted photon is correlated with the final quantum state $|g\rangle$ of the atom. For a simple two-level atom, after spontaneous emission, the system is in a tensor product state of the atom and the photon. But for multiple decay channels to different ground states the resuling state of atom and photon is entangled.

The physical process of spontaneous emission can not be explained by a semiclassical treatment of the light field but only by a quantum field approach (this can be found in [47]). I do not intend to give a sophisticated treatment of spontaneous emission, but I rather give a phenomenological approach, which will be sufficient to understand atom-photon entanglement in the context of the present work.

2.4.1 Weisskopf-Wigner theory of spontaneous emission

Let us consider a single atom at time $t = 0$ in the excited state $|e\rangle$ and the field modes in the vacuum state $|0\rangle$. In the *"dressed state picture"* the state of the system is then given by $|e, 0\rangle = |e\rangle \otimes |0\rangle$, the product of the atomic state $|e\rangle$ and the vacuum state $|0\rangle$ of the electromagnetic field. Due to coupling of the atom to vacuum fluctuations of the electromagnetic field (this can be found in [48]) the atom will decay with a characteristic time constant τ, called the natural lifetime, to the ground state $|g\rangle$ and emit a single photon into the field mode k. For $t \to \infty$ the sytem atom+photon will be in the state $|g, 1\rangle$.

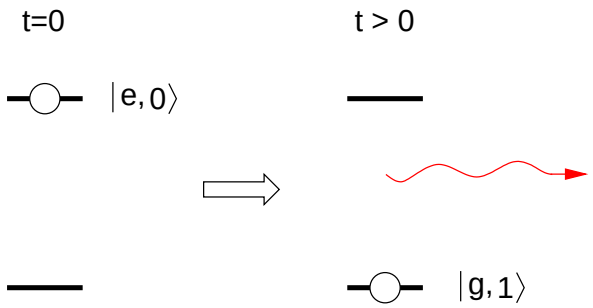

Figure 2.6: Spontaneous emission of a photon. At time $t = 0$ the atom is in the excited state $|e\rangle$. After spontaneous emission the atom passes to the ground state $|g, 1\rangle$, and the electromagnetic field mode is occupied with one photon.

The time evolution of the system is governed by the time-dependent Schrödinger equation

$$|\dot{\Psi}(t)\rangle = -\frac{i}{\hbar} H |\Psi(t)\rangle, \tag{2.34}$$

where H denotes the Hamiltonian describing the interaction of a single two-level atom with a multi-mode radiation field. In the rotating-wave approximation the simplified Hamiltonian H is given by

$$H = \sum_k \hbar\omega_k \hat{a}_k^\dagger \hat{a}_k + \frac{1}{2}\hbar\omega_{eg}\hat{\sigma}_z + \hbar \sum_k g_k(\hat{\sigma}_+ \hat{a}_k + \hat{a}_k^\dagger \hat{\sigma}_-). \tag{2.35}$$

This Hamiltonian consists of three parts. The first term in Eq. (2.35) describes the energy of the free radiation field in terms of the creation and destruction operators $\hat{a}_k^\dagger$ and $\hat{a}_k$, respectively. The second term $\hbar\omega_{eg}\hat{\sigma}_z/2$ desrcibes the energy of the free atom, whereby $\hat{\sigma}_z$ is given by $|e\rangle\langle e| - |g\rangle\langle g|$. The third term finally characterizes the interaction energy of the radiation field with the two-level atom. In detail $\hat{\sigma}_+$ and $\hat{\sigma}_-$ are operators which take the atom from the lower state to the upper state and vice versa. Hence, $\hat{a}_k^\dagger \hat{\sigma}_-$ describes the process in which the atom makes a transition from the upper to the lower level and a photon in the mode k is created, whereas $\hat{\sigma}_+ \hat{a}_k$ describes the opposite process in which the atom is excited from the lower to the upper level and a photon is annihilated.

In the Weisskopf-Wigner approximation the eigenstate vector is given by (see [49], pp. 206)

$$|\Psi(t)\rangle = e^{-\Gamma t/2}|e, 0\rangle + |g\rangle \sum_k W_k e^{-ikr_0} \left[\frac{1 - e^{i\Delta t - \Gamma t/2}}{i\Gamma/2 + \Delta}\right] |1_k\rangle. \tag{2.36}$$

Here, the form of the probability amplitude of the state $|e, 0\rangle$ signals that an atom in the excited state $|e\rangle$ in vacuum decays exponentially with the lifetime $\tau = 1/\Gamma$ and emits a photon of angular frequency ω_k. The probability amplitude of the state $|1_k\rangle$ describes

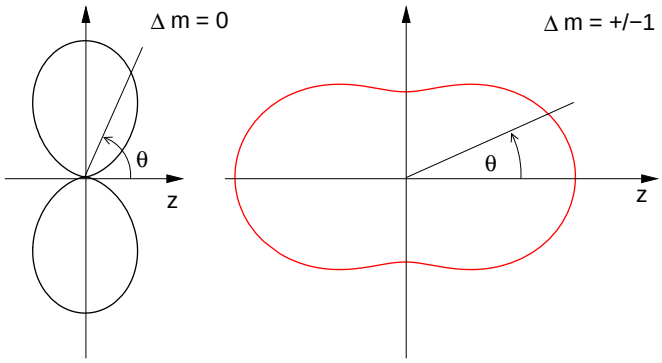

Figure 2.7: Emission characteristics of light emitted from dipole transitions with $\Delta m = 0, \pm 1$.

the temporal occupation of the modes k of the radiation field, where W_k denotes the overlap between the atomic states $|g\rangle$ and $|e\rangle$ in the field mode k, and $\Delta = \omega_k - \omega_{eg}$ the detuning in respect to the atomic transition frequency ω_{eg}. For times long compared to the radiative decay the first term in (2.36) is negligible and the state of the system is given by a linear superposition of single-photon states with different wave vectors.

2.4.2 Properties of the emitted photon

Because atomic states are eigenstates of the total angular momentum, the modes of the electromagnetic field after spontaneous emission are also eigenstates of angular momentum. Therefore the polarization state of a photon spontaneously emitted from an atomic dipole depends upon the change in angular momentum Δm of the atom along the dipole axis, and the direction of the emission. For $\Delta m = 0, \pm 1$, the polarization state of a spontaneously emitted photon is

$$|\Pi_0\rangle = \sin\theta \quad |\pi\rangle \qquad \text{for} \quad \Delta m = 0 \tag{2.37}$$

$$|\Pi_{\pm 1}\rangle = \sqrt{1+\cos^2\theta}/\sqrt{2} \quad |\sigma^{\pm}\rangle \qquad \text{for} \quad \Delta m = \pm 1, \tag{2.38}$$

where θ is the spherical polar angle with respect to the dipole (quantization) axis, and $|\pi\rangle$ and $|\sigma^{\pm}\rangle$ denote the polarization state of the photon. Note that along a viewing axis parallel to the dipole ($\theta = 0$) only $|\sigma^{\pm}\rangle$-polarized radiation is emitted.

2.4.3 Spontaneous emission as a source of atom-photon entanglement

Until now we considered a single atom in free space which spontaneously emits a photon from a two-level transition. According to Weisskopf and Wigner the state of the system atom+photon is a simple tensor product state of the form $|g\rangle|\Pi_{\Delta m}\rangle$, where the atom is

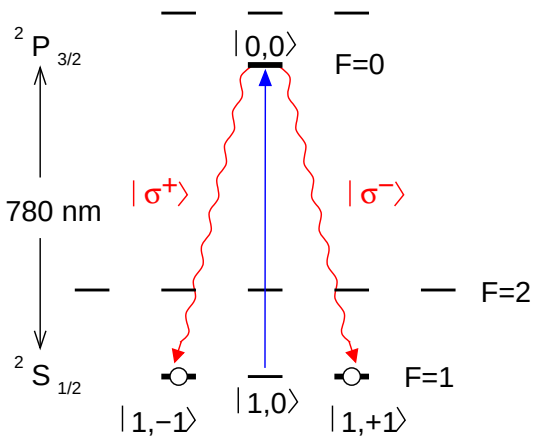

Figure 2.8: Atomic level structure in ^{87}Rb used to generate atom-photon entanglement. Provided the emission frequencies for σ^+, σ^- and π polarized transitions are indistinguishable within the natural linewidth of the transition, the polarization of a spontaneously emitted photon will be entangled with the spin state of the atom.

in the ground state $|g\rangle$ and the photon in the state $|\Pi_{\Delta m}\rangle$. For multiple decay channels of spontaneous emission to different ground states of atomic angular momentum F, the resulting (unnormalized) state of photon and atom is

$$|\Psi\rangle = \sum_{\Delta m} C_{\Delta m}|F_{\Delta m}\rangle|\Pi_{\Delta m}\rangle, \tag{2.39}$$

where $C_{\Delta m}$ are atomic Clebsch-Gordon coefficients for the possible decay channels and $|F_{\Delta m}\rangle$ denote the respective atomic ground states. The state in (2.39) can not be represented as a tensor product, only as a linear superposition of different product states. Therefore the spin degree of freedom of the atom and the polarization of the photon are entangled.

In the current experiment we excite a single ^{87}Rb atom to the $^2P_{3/2}, |F = 0, m_F = 0\rangle$ state by a short optical π-pulse. In the following spontaneous emission the atom decays either to the $|1, -1\rangle$ ground state while emitting a $|\sigma^+\rangle$-polarized photon, or to the $|1, 0\rangle$ state while emitting a $|\pi\rangle$-polarized photon, or to the $|1, +1\rangle$ ground state and emits a $|\sigma^-\rangle$-polarized photon. Provided these decay channels are spectrally indistinguishable, a coherent superposition of the three possibilities is formed and the magnetic quantum number m_F of the atom is entangled with the polarization of the emitted photon resulting in the atom-photon state

$$|\Psi\rangle = \frac{1}{\sqrt{2}}\left[\sqrt{(1+\cos^2\theta)/2}\left(|1,-1\rangle|\sigma^+\rangle + |1,+1\rangle|\sigma^-\rangle\right) + \sin\theta|1,0\rangle|\pi\rangle\right], \tag{2.40}$$

where the first index in the atomic basis state $|F, m_F\rangle$ denotes the total angular momentum F and the second index indicates the respective magnetic quantum number

m_F.

If we now put a single photon detector in the far-field region of the atom and detect the spontaneously emitted photon along the quantization axis z - defined by the optical axis of the detection optics - then the $|\pi\rangle$-polarized light is not detected (see Fig. 2.7). Thus the resulting atom-photon state is maximally entangled:

$$|\Psi^+\rangle = \frac{1}{\sqrt{2}}(|1,-1\rangle|\sigma^+\rangle + |1,+1\rangle|\sigma^-\rangle). \tag{2.41}$$

2.4.4 Experimental proof of atom-photon entanglement

To verify atom-photon entanglement in an experiment, one has to disprove the alternative description of the system being in a statistical mixture of seperable states. Experimentally one has to determine the diagonal density matrix elements in at least two complementary measurement bases (see sect. 2.3.3). The choice of the measurement basis can be realized in two ways. First, the atomic and photonic spin-state is rotated by an active unitary transformation into the new measurement basis. Second, the atomic and photonic spin-state stay unchanged, but the spin-analyzer is rotated by a respective passive transformation. For photons, the state-measurement can be realized relatively simple by a rotable birefringent waveplate followed by a polarizer. For atomic spin-states $|\uparrow\rangle_z = |1,-1\rangle$ and $|\downarrow\rangle_z = |1,+1\rangle$ active rotations can be realized by suitable optical Raman laser pulses that perform the transformation:

$$|\uparrow\rangle_z + e^{i\phi}|\downarrow\rangle_z \;\rightarrow\; |\uparrow\rangle_z \tag{2.42}$$
$$|\uparrow\rangle_z - e^{i\phi}|\downarrow\rangle_z \;\rightarrow\; |\downarrow\rangle_z, \tag{2.43}$$

where ϕ is the relative geometric phase between the basis states $|\uparrow\rangle_z$ and $|\downarrow\rangle_z$.

In the present experiment the atomic state detection is realized by a suitable Stimulated-Raman-Adiabatic-Passage (STIRAP) laser pulse which transfers, e.g. the superposition state $|\uparrow\rangle_z + e^{i\phi}|\downarrow\rangle_z$ to the hyperfine ground state $F = 2$, whereas the orthogonal superposition state $|\uparrow\rangle_z - e^{i\phi}|\downarrow\rangle_z$ does not couple to the laser field and remains "dark". By scattering light from a preceding laser pulse which couples only to $F = 2$ both states can be identified with nearly perfect efficiency (see chapter 5).

2.5 Summary

In this chapter I gave a short theoretical review about the properties of entangled states. A discussion about fundamental tests of quantum mechanics on the basis of Bell's inequalities is presented and applications of entanglement in quantum information and communication is discussed. Finally the spontaneous decay of single atoms is introduced as a source for the generation of entangled atom-photon states.

3 Single atom dipole trap

3.1 Introduction

To investigate the nonclassical correlation properties of an entangled atom-photon pair experimentally it is necessary to isolate a single atom and to detect the atom and the spontaneously emitted photon with high efficiency. For this reason it is convenient to localize the atom in a region of a few optical wavelengths. This experimental requirement can be accomplished with various kinds of traps, but due to the intrinsic properties of the generation process of atom-photon entanglement there exist important constraints on the trapping mechanism: (1) All magnetic substates of the atomic ground state have to experience the same binding potential; (2) The energy splitting of the atomic qubit states has to be less than the natural linewidth of the transition in order to fulfill the requirement of spectral indistinguishability; (3) The trap must preserve the internal state of the atom.

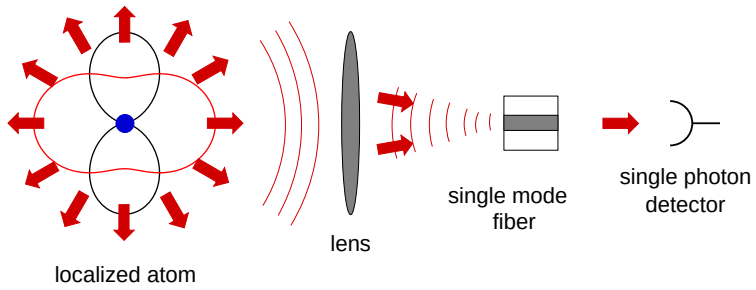

Figure 3.1: Schematic setup for the detection of light emitted from a single atom.

Furthermore, the present experiment should be designed such, that it should allow in a next step the faithful generation of entanglement between space-like separated atoms by the interference of photons emitted from the atoms. A possible way to do that is to use single ions stored in electrodynamical traps [35] that are separated by large distances. But, because most ions radiate photons from atomic transitions in the visible and ultraviolet range of the electromagnetic spectrum the transport of emitted photons over large distances is complicated by high transmission losses in optical fibers and air. This problem can be avoided by the use of single trapped ^{87}Rb atoms which radiate light in the near-infrared (NIR). Different kinds of traps for neutral atoms have been realized

in the last 20 years, but not all trapping mechanisms are applicable for the investigation of atom-photon and atom-atom entanglement. *Magnetic traps* [50, 51] are based on the state-dependent force of the magnetic dipole moment in an inhomogenous field. Hence, this kind of trap is unsuitable for trapping atomic spin states with different sign. In addition, magnetic traps do not preserve the spectral indistinguishability of the possible photonic emission paths due to different Zeeman-splitting of the magnetic substates $m_F = -1$ and $m_F = +1$. The trapping mechanism of *Magneto-optical traps* (MOT) [52, 53] relies on near resonant scattering of light destroying any atomic coherence on a timescale of the excited state lifetime. Optical dipole traps - first proposed by Letokhov in 1968 [54, 55] - rely on the electric dipole interaction with far-detuned light at which the optical excitation can be kept extremely low. In optical dipole traps atomic coherence times up to several seconds are possible [56], and under appropriate conditions the trapping mechanism is independent of the particular magnetic sub-level of the electronic ground state. Therefore a localized single ^{87}Rb atom in a far-off-resonance optical dipole trap satisfies all necessary requirements for the investigation of atom-photon and atom-atom entanglement.

In the context of this thesis our group has set up a microscopic optical dipole trap, which allows to trap single Rubidium atoms one by one with a typical trap life- and coherence time of several seconds. In order to understand the operating mode of our trap I will first indroduce the basic theoretical concepts of atom trapping in optical dipole potentials. Then I will describe the experimental setup of our dipole trap and measurements which prove the subpoissonian occupation statistics. Finally the mean kinetic energy of a single atom was determined via the spectral analysis of the emitted fluorescence light.

3.2 Theory of optical dipole traps for neutral atoms

Following Grimm et al. [57] I will introduce the basic concepts of atom trapping in optical dipole potentials that result from the interaction with *far-detuned* light. In this case of particular interest, the optical excitation is very low and the radiation force due to photon scattering is negligible as compared to the dipole force. In Sec. 3.2.1, I consider the atom as a simple classical or quantum-mechanical oscillator to derive the main equations for the optical dipole interaction. Then the case of real multi-level atoms is considered, which allows to calculate the dipole potential of the $^2S_{1/2}$ ground and $^2P_{3/2}$ excited state in ^{87}Rb. Atom trapping in dipole potentials requires cooling to load the trap and eventually also to counteract heating in the dipole trap. I therefore briefly review two laser cooling methods and their specific features with respect to our experiment. Then I discuss sources of heating, and derive explicit expressions for the heating rate in the case of thermal equilibrium in a dipole trap. Finally I will present a simple model which allows to understand the atom number limitation in a small volume

dipole trap due to light-induced two-body collisions. This effect opens the possibility to trap only single atoms and simplifies the experimental investigation of an entangled atom-photon state.

3.2.1 Optical dipole potentials

Oscillator model

The optical dipole force arises from the dispersive interaction of the induced atomic dipole moment with the intensity gradient of the light field [54]. Because of its conservative character, the force can be derived from a potential, the minima of which can be used for atom trapping. The absorptive part of the dipole interaction in far-detuned light leads to residual photon scattering of the trapping light, which sets limits to the performance of dipole traps. In the following I will derive the basic equations for the dipole potential and the scattering rate by considering the atom as a simple oscillator subject to the classical radiation field.

When an atom is irradiated by laser light, the electric field $\mathbf{E}$ induces an atomic dipole moment $\mathbf{p}$ that oscillates at the driving frequency ω. In the usual complex notation $\mathbf{E}(\mathbf{r},t) = \hat{\mathbf{e}}\hat{E}(\mathbf{r})e^{i\omega t} + \hat{\mathbf{e}}\hat{E}^*(\mathbf{r})e^{-i\omega t}$ and $\mathbf{p}(\mathbf{r},t) = \hat{\mathbf{e}}\hat{p}(\mathbf{r})e^{i\omega t} + \hat{\mathbf{e}}\hat{p}^*(\mathbf{r})e^{-i\omega t}$, where $\hat{\mathbf{e}}$ is the unit polarization vector, the amplitude $\hat{p}$ of the dipole moment is simply related to the field amplitude $\hat{E}$ by

$$\hat{p} = \alpha(\omega)\hat{E}. \tag{3.1}$$

Here α is the *complex polarizability*, which depends on the driving frequency ω.

The interaction potential of the induced dipole moment $\mathbf{p}$ in the driving field $\mathbf{E}$ is given by

$$U_{dip} = -\frac{1}{2}\langle \mathbf{pE} \rangle = -\frac{1}{2\epsilon_0 c}\mathrm{Re}(\alpha)I \tag{3.2}$$

where $<>$ denote the time average over the rapid oscillating terms. The laser field intensity is

$$I = \frac{1}{2}\epsilon_0 c|\hat{E}|^2, \tag{3.3}$$

and the factor $1/2$ takes into account that the dipole moment is an induced, not a permanent one. The potential energy of the atom in the field is thus proportional to the intensity I and to the real part of the polarizability, which describes the in-phase component of the dipole oscillation being responsible for the dispersive properties of the interaction. The *dipole force* results from the gradient of the interaction potential

$$\mathbf{F}_{dip}(\mathbf{r}) = -\nabla V_{dip}(\mathbf{r}) = \frac{1}{2\epsilon_0 c}\mathrm{Re}(\alpha)\nabla I(\mathbf{r}). \tag{3.4}$$

It is thus a conservative force, proportional to the intensity gradient of the driving field.

The power absorbed by the oscillator from the driving field (and re-emitted as dipole radiation) is given by

$$P_{abs} = \langle \dot{\mathbf{p}}\mathbf{E} \rangle = \frac{\omega}{\epsilon_0 c} \mathrm{Im}(\alpha) I(\mathbf{r}). \tag{3.5}$$

The absorption results from the imaginary part of the polarizability, which describes the out-of-phase component of the dipole oscillation. Considering the light as a stream of photons $\hbar\omega$, the absorption can be interpreted in terms of photon scattering in cycles of absorption and subsequent spontaneous reemission processes. The corresponding *scatteringrate* is

$$\Gamma_{Sc}(\mathbf{r}) = \frac{P_{abs}}{\hbar\omega} = \frac{1}{\hbar\epsilon_0 c} \mathrm{Im}(\alpha) I(\mathbf{r}). \tag{3.6}$$

We have now expressed the two main quantities of interest for dipole traps, the *interaction potential* and the *scattered radiation power*, in terms of the position dependent intensity $I(\mathbf{r})$ and the polarizibility $\alpha(\omega)$. These expressions are valid for any polarizable neutral particle in an oscillating electric field. This can be an atom in a near-resonant or far off-resonant laser field, or even a molecule in an optical or microwave field.

In order to calculate its polarizability α, I first consider the atom in Lorenz's model as a classical oscillator (see, e.g. [58]). In this simple and very useful picture, an electron (mass m_e, elementary charge e) is considered to be bound elastically to the core with an oscillation eigenfrequency ω_0 corresponding to the optical transition frequency. Damping results from the dipole radiation of the oscillating electron according to Larmor's well-known formula for the power radiated by an accelerated charge.

It is straightforward to calculate the polarizability by integration of the equation of motion

$$\ddot{x} + \Gamma_\omega \, \dot{x} + \omega_0^2 x = -\frac{eE(t)}{m_e} \tag{3.7}$$

for the driven oscillation of the electron with the result

$$\alpha = \frac{e^2}{m_e} \frac{1}{\omega_0^2 - \omega^2 - i\omega\Gamma_\omega}. \tag{3.8}$$

Here

$$\Gamma_\omega = \frac{e^2\omega^2}{6\pi\epsilon_0 m_e c^2} \tag{3.9}$$

is the classical damping rate due to the radiative energy loss. Introducing the on-resonance damping rate $\Gamma \equiv \Gamma_{\omega_0} = (\frac{\omega_0}{\omega})^2 \Gamma_\omega$, one can put Eq. 3.8 into the form

$$\alpha(\omega) = 6\pi\epsilon_0 c^2 \frac{\Gamma/\omega_0^2}{\omega_0^2 - \omega^2 - i(\omega^3/\omega_0^2)\Gamma}. \tag{3.10}$$

In a *semiclassical approach* the atomic polarizability can be calculated by considering the atom as a two-level quantum system interacting with a classical radiation field. When saturation effects can be neglected, the semiclassical calculation yields the same result as

the classical calculation with only one modification, the damping rate Γ (corresponding the spontaneous decay rate of the excited state) is determined by the dipole matrix element $\langle e|\mu|g\rangle$ between the ground state $|g\rangle$ and the excited state $|e\rangle$ by

$$\Gamma = \frac{\omega_0^3}{3\pi\epsilon_0\hbar c^2}|\langle e|\mu|g\rangle|^2. \tag{3.11}$$

For many atoms with a strong dipole-allowed transition starting from its ground state, the classical formula Eq. 3.9 nevertheless provides a good approximation to the spontaneous decay rate. For the D lines of the alkali atoms Na, K, Rb, and Cs, the classical result agrees with the true decay rate to within a few percent.

An important difference between the quantum-mechanical and the classical oscillator is the possible occurence of saturation. At very high intensities of the driving field, the excited state gets strongly populated and the classical result (Eq. 3.10) is no longer valid. For dipole trapping, however one is essentially interested in the far-detuned case with very low saturation and thus very low scatttering rates ($\Gamma_{Sc} \ll \Gamma$). Thus the expression in Eq. 3.10 for the atomic polarizability can be used as an excellent approximation for the quantum-mechanical oscillator and the explicit expressions for the dipole potential U_{dip} and the scattering rate Γ_{Sc} can be derived.

$$U_{dip}(\mathbf{r}) = -\frac{3\pi c^2}{2\omega_0^3}\left(\frac{\Gamma}{\omega_0-\omega}+\frac{\Gamma}{\omega_0+\omega}\right) I(\mathbf{r}) \tag{3.12}$$

$$\Gamma_{Sc}(\mathbf{r}) = \frac{3\pi c^2}{2\hbar\omega_0^3}\left(\frac{\omega}{\omega_0}\right)^3\left(\frac{\Gamma}{\omega_0-\omega}+\frac{\Gamma}{\omega_0+\omega}\right)^2 I(\mathbf{r}) \tag{3.13}$$

These general expressions are valid for any driving frequency ω and show two resonant contributions: Besides the usually considered resonance at $\omega = \omega_0$, there is also the so-called counter-rotating term resonant at $\omega = -\omega_0$.

In most experiments, the laser is tuned relatively close to the resonance ω_0 such that the detuning $\Delta = \omega - \omega_0$ fulfills $|\Delta| \ll \omega_0$. In this case, the counter-rotating term can be neglected in the well-known *rotating wave approximation* and the general expressions for the dipole potential and the scattering rate simplify to

$$U_{dip}(\mathbf{r}) = \frac{3\pi c^2}{2\omega_0^3}\left(\frac{\Gamma}{\Delta}\right) I(\mathbf{r}), \tag{3.14}$$

$$\Gamma_{Sc}(\mathbf{r}) = \frac{3\pi c^2}{2\hbar\omega_0^3}\left(\frac{\Gamma}{\Delta}\right)^2 I(\mathbf{r}). \tag{3.15}$$

The basic physics of dipole trapping in far-detuned laser fields can be understood on the basis of these two equations. Obviously, a simple relation exists between the scattering rate and the dipole potential,

$$\hbar\Gamma_{Sc} = \frac{\Gamma}{\Delta}U_{dip}. \tag{3.16}$$

Equation 3.14 and 3.15 show two essential points for dipole trapping. First: below an atomic resonance ("red" detuned, $\Delta < 0$) the dipole potential is negative and the interaction thus attracts atoms into the light field. Potential minima are therefore found at positions with maximum intensity. Above resonance ("blue" detuned, $\Delta > 0$) the dipole interaction repels atoms out of the field, and potential minima correspond to minima of the intensity. Second: the dipole potential scales as I/Δ, whereas the scattering rate scales as I/Δ^2. Therefore, optical dipole traps usually use large detunings and high intensities to keep the scattering rate as low as possible for a certain potential depth.

Dressed state picture

In terms of the oscillator model, multi-level atoms can be described by state-dependent atomic polarizabilies. An alternative description of dipole potentials is given by the *dressed state picture* [47] where the atom is considered together with a quantized light field. In its ground state the atom has zero internal energy and the field energy is $n\hbar\omega$ depending on the number of photons. When the atom is put into an excited state by absorbing a photon, the sum of its internal energy $\hbar\omega_0$ and the field energy $(n-1)\hbar\omega$ becomes $E_j = \hbar\omega_0 + (n-1)\hbar\omega = -\hbar\Delta_{ij} + n\hbar\omega$.

For an atom interacting with laser light, the interaction Hamiltonian is $H_{int} = -\hat{\mu}\mathbf{E}$ with $\hat{\mu} = -e\mathbf{r}$ representing the electric dipole operator. The effect of far-detuned laser light on the atomic levels can be treated as a time-independent perturbation in the second order of the electric field. Applying this perturbation theory for nondegenerate states, the interaction Hamiltonian H_{int} leads to an energy shift of the i-th state with the unperturbed energy E_i, that is given by

$$\Delta E_i = \sum_{j \neq i} \frac{|\langle j|H_{int}|i\rangle|^2}{E_i - E_j}. \tag{3.17}$$

For a *two-level atom*, this equation simplifies to

$$\Delta E = \pm \frac{|\langle e|\mu|g\rangle|^2}{\Delta}|E|^2 = \pm \frac{3\pi c^2}{2\omega_0^3}\frac{\Gamma}{\Delta}I \tag{3.18}$$

with the plus and the minus sign for the excited and ground state, respectively. This optically induced energy shift (known as *Light Shift* or *AC-Stark shift*) of the ground-state exactly corresponds to the dipole potential for the two-level atom in Eq. 3.14.

Semiclassical treatment of multi-level atoms

When calculating the *light shift* on the basis of the semiclassical treatement for a multi-level atom in a specific electronic ground state $|i\rangle$ all dipole allowed transitions to the excited states $|f\rangle$ have to be taken into account. Time-dependent perturbation theory

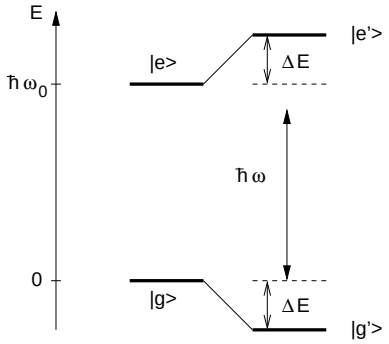

Figure 3.2: Light shifts for a two-level atom. Red-detuned light ($\Delta < 0$) shifts the ground state $|g\rangle$ down and the excited state $|e\rangle$ up by the energy ΔE.

yields an expression for the energy shift of the atomic levels $|i\rangle$ - characterized by their eigenenergies E_i - due to interaction with a time-dependent classical electric field with angular frequency ω, which is given by [59]

$$\Delta E_i(\omega) = \frac{-|\hat{E}|^2}{4\hbar} \sum_{f \neq i} |\langle i|e\mathbf{r}|f\rangle|^2 \left(\frac{1}{\omega_{if} - \omega} + \frac{1}{\omega_{if} + \omega} \right), \tag{3.19}$$

where the sum covers all atomic states $|f\rangle$ except for the initial state $|i\rangle$, and $\omega_{if} = \omega_f - \omega_i$ denotes the atomic transition frequencies.

The transition matrix elements $\langle i|e\mathbf{r}|f\rangle$ in general depend on the quantum numbers of the initial state $|i\rangle$ respresented by n, J, F, m_F and n', J', F, m'_F for the final states $|f\rangle$ and upon the laser polarization ($\epsilon = 0, \pm 1$ for π and $\sigma^{\pm}$ transitions respectively). Using the Wigner-Eckart theorem [60], the matrix elements $\langle i|e\mathbf{r}|f\rangle$ can be expressed as a product of a real *Clebsch-Gordan coefficient* $\langle F, m_F|F', 1, m'_F, \epsilon\rangle$ and a reduced matrix element $\langle F||e\mathbf{r}||F'\rangle$:

$$\langle i|e\mathbf{r}|f\rangle = \langle F||e\mathbf{r}||F'\rangle \langle F, m_F|F', 1, m'_F, \epsilon\rangle. \tag{3.20}$$

This reduced matrix element can be further simplified by factoring out the F and F' dependence into a Wigner $6j$ symbol, leaving a *fully reduced matrix element* $\langle J||e\mathbf{r}||J'\rangle$ that depends only on the electronic orbital wavefunctions:

$$\langle F||e\mathbf{r}||F'\rangle = \langle J||e\mathbf{r}||J'\rangle (-1)^{F'+J+I+1} \sqrt{(2F'+1)(2J+1)} \begin{pmatrix} J & J' & 1 \\ F' & F & I \end{pmatrix}_{6j}. \tag{3.21}$$

The remaining fully reduced matrix element $\langle J||e\mathbf{r}||J'\rangle$ can be calculated from the lifetime of the transition $J \rightarrow J'$ via the expression [61]

$$\frac{1}{\tau_{JJ'}} = \frac{\omega_{if}^3}{3\pi\epsilon_0\hbar c^3} \frac{2J+1}{2J'+1} |\langle J||e\mathbf{r}||J'\rangle|^2. \tag{3.22}$$

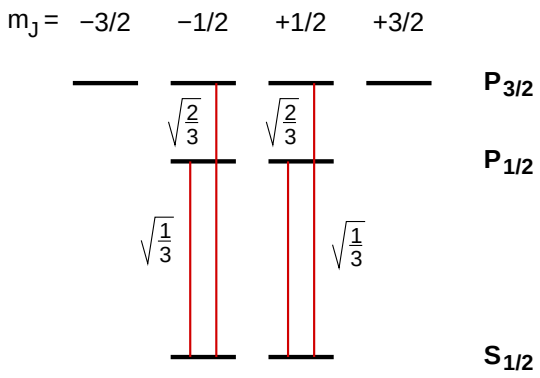

Figure 3.3: Reduced level scheme in ^{87}Rb. Dipole matrix elements for π-polarized light are shown as multiples of $\langle J||e\mathbf{r}||J'\rangle$.

On the basis of Eq. 3.19, the *Wigner-Eckart* theorem and Eq. 3.22 one can derive a general expression for the light-shift of any atomic hyperfine state $|J, F, m_F\rangle$ coupling to the manifold of final states $\{|J', F', m'_F\rangle\}_f$, which is given by

$$\Delta E(J, F, m_F) = \frac{3\pi c^2 I}{2} \sum_{J', F', m'_F} \frac{(2J'+1)(2F'+1)}{\tau_{JJ'} \Delta'_{FF'} \omega^3_{FF'}} \begin{pmatrix} J & J' & 1 \\ F' & F & I \end{pmatrix}^2_{6j} |\langle F, m_F | F', 1, m'_F, \epsilon\rangle|^2. \tag{3.23}$$

For simplicity we have introduced the effective detuning $\Delta'_{FF'}$:

$$\frac{1}{\Delta'_{FF'}} = \frac{1}{\omega_{FF'} - \omega} + \frac{1}{\omega_{FF'} + \omega}, \tag{3.24}$$

where $\omega_{FF'}$ denotes the atomic transition frequency and ω is the frequency of the classical light field.

Light-shift of the $5^2S_{1/2}$ and $5^2P_{3/2}$ state

In the case of a resolved fine-structure, but unresolved hyperfine structure, one can consider the atom in spin-orbit coupling, neglecting the coupling of the nuclear spin. The interaction with the laser field can thus be considered in the electronic angular momentum configuration of the D lines, $J = 1/2 \rightarrow J' = 1/2, 3/2$.

In this situation, illustrated in Fig. 3.3, one can first calculate the light shifts of the two electronic ground states $m_J = \pm 1/2$ with the simplified relation

$$\Delta E(J, m_j, \omega) = \frac{-|\hat{E}|^2}{4\hbar} \sum_{J'} \frac{|\langle J||e\mathbf{r}||J'\rangle|^2}{\Delta_{JJ'}} \sum_{m'_J} |\langle J, m_J | J', 1, m'_J, \epsilon\rangle|^2. \tag{3.25}$$

On the basis of this equation, one can derive a general result for the potential of

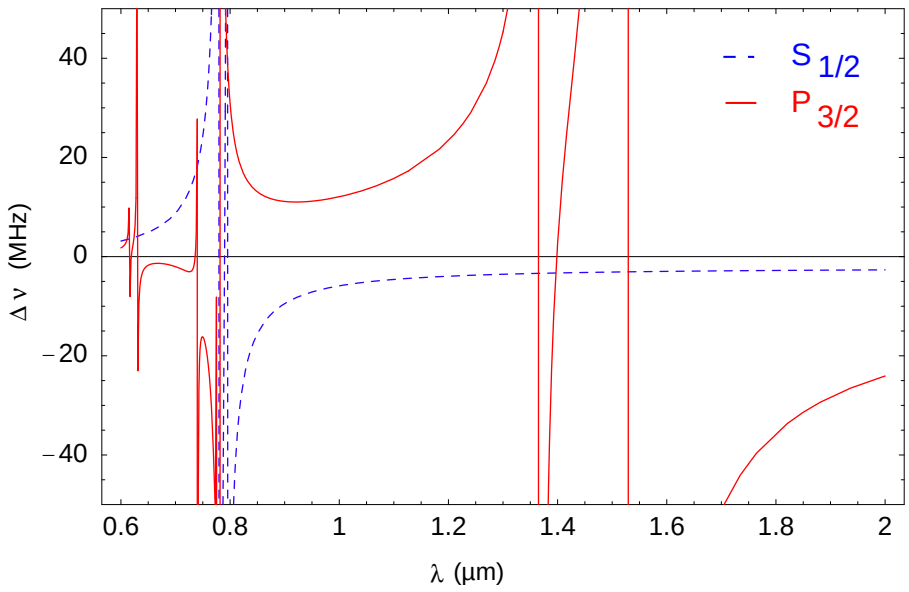

Figure 3.4: $5^2S_{1/2}$ ground- (dashed blue line) and $5^2P_{3/2}$ excited-state (solid red line) light-shift $\Delta\nu$ as a function of the dipole laser wavelength λ. At 1.4 μm both states have the same light shift. In contrast to the ground state, the excited state Zeeman sub levels m'_F experience different light shifts. Here, we assumed equal occupation of the excited state Zeeman sub-levels and calculated the mean light shift.

a ground state with total angular momentum J and magnetic quantum number m_J, which is valid for both linear and circular polarization as long as all optical detunings stay large compared to the ground- and excited-state hyperfine structure splitting:

$$U_{dip}(\mathbf{r}) = \frac{3\pi c^2}{2}\left(\frac{\Gamma_{1/2}(1-\epsilon g_J m_J)}{3\omega_{1/2}^3\Delta_{1/2}} + \frac{\Gamma_{3/2}(2+\epsilon g_J m_J)}{3\omega_{3/2}^3\Delta_{3/2}}\right) I(\mathbf{r}). \tag{3.26}$$

Here $g_J = 2$ is the well known Lande factor for alkali atoms and ϵ characterizes the laser polarization ($\epsilon = 0, \pm 1$ for linearly and $\sigma^\pm$ polarized light). The detunings $\Delta_{1/2}, \Delta_{3/2}$ of the laser frequency are referred to the atomic transitions $S_{1/2}, J \rightarrow P_{1/2}$ and $S_{1/2}, J \rightarrow P_{3/2}$ (the D_1 and D_2 line).

For *linear polarization*, both electronic ground states $m_J = \pm 1/2$ are shifted by the same amount because of simple symmetry reasons. After coupling to the nuclear spin, the resulting F, m_F states have to remain degenerate like the two original m_J states. Consequently, all magnetic sublevels show the same light shifts.

For *circular polarization*, the far-off-resonance light field lifts the degeneracy of the

two magnetic sublevels of the electronic $^2S_{1/2}$ ground state. In this sense, the circularly polarized light acts like a *fictitious magnetic field*.

With the help of Eq. 3.23 and the knowledge of the lifetimes of all coupling energy levels, it is possible to calculate the light shift of any Zeeman sub-level in the hyperfine structure of the states $5^2S_{1/2}$, $5^2P_{1/2}$ and $5^2P_{3/2}$. Due to the coupling of the excited states $5^2P_{1/2}$ and $5^2P_{3/2}$ to even higher states (see Fig. A.1), their energy shifts may have the same sign as the ground state energy shift. Thus, the dipole force can be attractive even for an atom in an excited state (see Fig. 3.4), in contrast to the simplified two-level model of Fig. 3.2. There exists a *magic* wavelength for a linear polarized dipole laser field, for which the excited state $5^2P_{3/2}$ and the ground state are equally shifted (see Fig. 3.4). This wavelength amounts to approximately $\lambda = 1.4$ μm, enabling state-insensitive optical cooling in the dipole potential.

For the photon scattering rate Γ_{Sc} of Rubidium, the same line strength factors are relevant as for the ground state dipole potential, since absorption and light shifts are determined by the same transition matrix elements. For linear polarization one explicitely obtains

$$\Gamma_{Sc}(\mathbf{r}) = \frac{\pi c^2}{2\hbar}\left(\frac{\Gamma_{1/2}^2}{\omega_{1/2}^3\Delta_{1/2}^2} + \frac{2\Gamma_{3/2}^2}{\omega_{3/2}^3\Delta_{3/2}^2}\right) I(\mathbf{r}). \tag{3.27}$$

Red-detuned focused-beam trap

A focused Gaussian laser beam tuned far below the atomic resonance frequency represents the simplest way to create a dipole trap. The spatial intensity distribution of a focused Gaussian beam with power P propagating along the z-axis is described by

$$I(r,z) = \frac{2P}{\pi w^2(z)} exp\left(\frac{-2r^2}{w^2(z)}\right) \tag{3.28}$$

where r denotes the radial coordinate. The $1/e^2$ radius $w(z)$ depends on the axial coordinate z via

$$w(z) = w_0\sqrt{1 + (\frac{z}{z_R})^2} \tag{3.29}$$

where the focal radius w_0 is called beam waist and $z_R = \pi w_0^2/\lambda$ denotes the Rayleigh length. From the intensity distribution one can derive the optical potential using Eq. 3.19, 3.23, or 3.26. The trap depth $\hat{U}$ is given by $\hat{U} = |U(r = 0, z = 0)|$. The Rayleigh length z_R is larger than the beam waist by a factor of $\pi w_0/\lambda$. Therefore the potential in the radial direction is much steeper than in the axial direction.

If the mean kinetic energy k_BT of an atomic ensemble is much smaller than the potential depth $\hat{U}$, the extension of the atomic sample is radially small compared to the beam waist and axially small compared to the Rayleigh range. In this case, the optical potential can be well approximated by a simple cylindrically symmetric harmonic

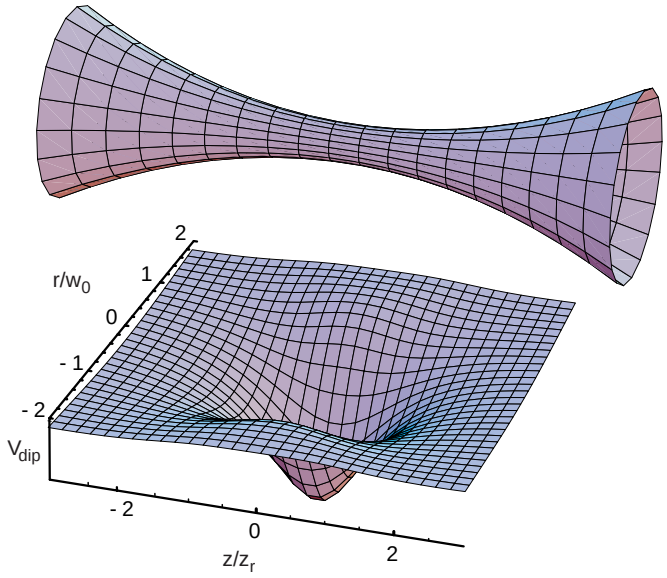

Figure 3.5: Schematical drawing of a focused Gaussian laser beam and cross section of the corresponding trapping profile for a red detuned dipole laser.

oscillator

$$U(r,z) = -\hat{U}\left[1 - 2\left(\frac{r}{w_0}\right)^2 - \left(\frac{z}{z_R}\right)^2\right]. \tag{3.30}$$

The oscillation frequencies of a trapped atom are given by $\omega_R = (4\hat{U}/mw_0^2)^{1/2}$ in the radial direction, and $\omega_z = (2\hat{U}/mz_R^2)^{1/2}$ in the axial direction. For a trap depth of $\hat{U} = 1$ mK, a beam waist of $w_0 = 3.5\mu$m, the oscillation frequencies are $\omega_R/2\pi = 26.2$ kHz and $\omega_z/2\pi = 1.3$ kHz.

3.2.2 Trap loading

The standard way to load atoms into a dipole trap is to start from a magneto-optical trap (MOT) [62] or an optical molasses, by simply overlapping the dipole trap with the atomic cloud in the MOT, before the latter is turned off. Therefore, efficient cooling techniques are an essential requirement since the attainable depths of optical dipole traps are generally below 1 mK. Once atoms are captured, further cooling can be applied to compensate possible heating mechanisms which would otherwise lead to a loss of atoms. In this section, I briefly discuss methods which are of relevance for trapping a single atom in a microscopic optical dipole trap.

Doppler cooling

Doppler cooling proposed by Hänsch & Schawlow in 1975 [63] is based on cycles of near-resonant absorption of a photon and subsequent spontaneous emission resulting in a net atomic momentum change per cycle of one photon momentum $\hbar k$ with $k = 2\pi/\lambda$ denoting the wavenumber of the absorbed photon. Cooling is counteracted by heating due to the momentum fluctuations by the recoil of spontaneously emitted photons [64]. Equilibrium between cooling and heating determines the lowest achievable temperature. For Doppler cooling of two-level atoms in standing waves ("optical molasses"), the minimum temperature T_D is given by

$$T_D = \frac{\hbar\Gamma}{2k_B}, \tag{3.31}$$

where Γ is the spontaneous decay rate of the cooling transition. For Rubidium 87 the Doppler temperature is 146 μK, which is sufficiently low to load atoms into a dipole trap. The first demonstration of dipole trapping [65] used Doppler cooling for loading the trap and keeping the atoms from beeing heated out.

Polarization gradient cooling

The Doppler temperature is a somewhat artificial limit since it is based on the simplifying assumption of a two-level atom. Atoms with a more complex level structure like Rb can be cooled far below T_D in standing waves with spatially varying polarizations [66], whereby the cooling mechanisms are based on optical pumping between ground state Zeeman sublevels [67].

With polarization-gradient molasses one can prepare atomic samples at temperatures on the order of $\sim 10T_{rec}$ with the recoil temperature

$$T_{rec} = \frac{\hbar^2 k^2}{m} \tag{3.32}$$

being defined as the temperature associated with the kinetic energy gain by emission of one photon. Polarization-gradient cooling allows efficient loading of a dipole trap, either by cooling inside a magneto-optical trap (MOT) [62, 68] or by cooling in a short molasses phase before transfer into the dipole trap.

Besides enhancing the loading efficiency, polarization-gradient cooling can be applied directly to atoms trapped in a dipole potential by subjecting them to near-resonant polarizations gradients [69]. Since the cooling mechanism relies on the modification of the ground-state Zeeman sublevels by the cooling light, a necessary condition for efficient cooling is the independency of the trapping potential from the Zeeman substate [70], which can be easily fulfilled in dipole traps.

3.2.3 Heating and losses

It is a well-known experimental fact in the field of laser cooling and trapping that collisional processes between atoms can lead to substantial trap loss. Here I will discuss the most important features of heating and cold collisions.

Heating rate

A fundamental source of heating is the spontaneous scattering of trap photons, which due to its random nature causes fluctuations of the radiation force. In a far-detuned optical dipole trap, the scattering is completly elastic (or quasi-elastic if a Raman process changes the atomic ground state).

In general both absorption and spontaneous re-emission processes show fluctuations and thus both contribute to heating [64]. At large detunings, where scattering processes follow Poisson statistics, the heating due to fluctuations in absorption corresponds to an increase of the thermal energy by exactly the recoil energy $E_{rec} = \frac{k_B T_{rec}}{2}$ per scattering event. This first contribution occurs in the propagation direction of the light field and is thus anisotropic. The second contribution is due to the random direction of the photon recoil in spontaneous emission. This heating also increases the thermal energy by one recoil energy E_{rec} per scattering event, but distributed over all three dimensions. In most cases of interest the trap mixes the motional degrees on a time scale faster than or comparable to the heating. The overall heating thus corresponds to an increase of the total thermal energy by $2E_{rec}$ in a time $\bar{\Gamma}_{sc}^{-1}$. Therefore the heating power is given by

$$P_{heat} = 2E_{rec}\bar{\Gamma}_{sc} = k_B T_{rec}\bar{\Gamma}_{sc}. \tag{3.33}$$

In thermal equilibrium, the mean kinetic energy per atom in a three-dimensional trap is $\bar{E}_{kin} = 3k_B T/2$. Introducing the parameter $\kappa \equiv \bar{E}_{pot}/\bar{E}_{kin}$ as the ratio of potential and kinetic energy, one can express the mean total energy $\bar{E}$ as

$$\bar{E} = \frac{3}{2}(1+\kappa)k_B T. \tag{3.34}$$

The relation between mean energy and temperature (Eq. 3.33) allows to reexpress the heating power resulting from photon scattering (Eq. 3.34) as a heating rate

$$\dot{T} = \frac{2/3}{1+\kappa} T_{rec}\bar{\Gamma}_{sc}, \tag{3.35}$$

describing the corresponding increase of temperature with time.

Collisions

In general, trap loss becomes important if the colliding atoms are not in their absolute ground state. In an inelastic process the internal energy can be released into the atomic

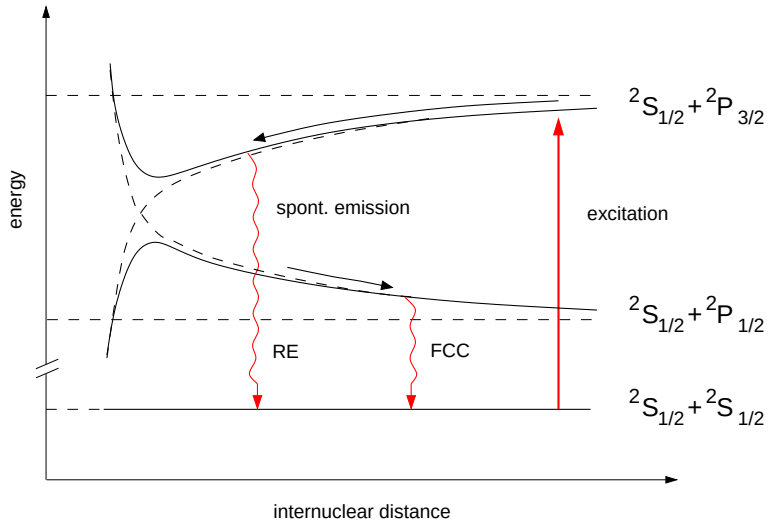

Figure 3.6: Schematic diagram of processes leading to trap loss in an optical dipole trap during the loading stage in the presence of near resonant cooling light.

motion, causing escape from the trap. Due to the shallowness of optical dipole potentials, even the collisional release of the relatively small amount of energy from transitions in the hyperfine structure of the atomic ground state $^2S_{1/2}$ will always lead to trap loss.

Trap loss can also occur as a result of light-assisted binary collisions involving atoms in the excited state (see Fig. 3.6). In *the radiative escape process* (RE) the atoms gain kinetic energy from their mutual attraction and when a spontaneous photon is emitted that has less energy than the one that was initially absorbed. The energy difference appears as kinetic energy and can be enough to eject the atoms out of the trap. In a *fine-structure changing collision* (FCC) the atoms are excited to the $^2S_{1/2}+^2P_{3/2}$ molecular potential. When they reach the short-distance region they may change the molecular state during the collision leading to the repulsive molecular potential $^2S_{1/2}+^2P_{1/2}$. The atoms gain kinetic energy from the transition, which is sufficient for ejection of one or both atoms out of the trap.

Collisional blockade in microscopic optical dipole traps

During the loading stage of an optical dipole trap, light-assisted binary collisions due to the presence of MOT light [71] dominate the trap loss. When the dipole trap volume is small enough, this binary collisions prevent loading of more than one atom [72, 73].

The number N of trapped atoms can be described by the equation

$$\frac{dN}{dt} = R - \gamma N - \beta' N(N-1), \tag{3.36}$$

where R is the loading rate, γ the *single-particle loss* coefficient taking into account

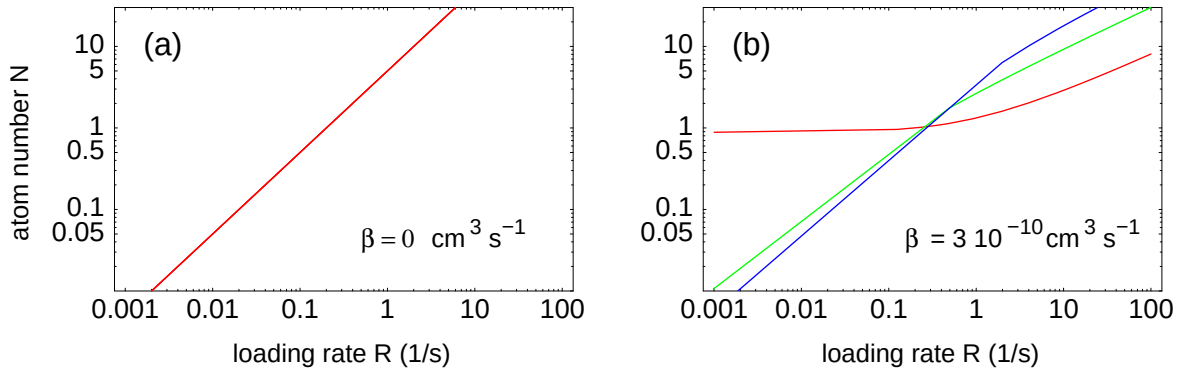

Figure 3.7: Average number N of trapped atoms as a function of the loading rate R for different values of the waist w_0 (red line: $w_0 = 4\mu$m; green line: $w_0 = 8\mu$m; blue line: $w_0 = 12\mu$m), **(a)** without and **(b)** with two-body collisions. In presence of light-induced two-body collisions a blockade regime is seen for a beam waist of $w_0 \leq 4$ μm.

collisions with the background gas in the vacuum apparatus, and β the *two-body loss* coefficient which describes cold binary collisions.

Since this equation is written for the atom number and not for the atomic density, the value of β' is inversely proportional to the volume of the trap $\beta' = \beta/V$. The volume is found by approximating the trapped sample of atoms as a cylinder with radius and length determined by the size of the trapping beam waist and the temperature of the atoms. The volume is then given by

$$V = \pi w_0^2 z_R \ln\left(\frac{1}{1-\eta}\right)\sqrt{\frac{\eta}{1-\eta}}, \tag{3.37}$$

where $\eta = k_B T/|\hat{U}|$. For ^{87}Rb the total loss rate β due to RE and FCC was measured in a far-off-resonance dipole trap experiment [71] to be $3 \times 10^{-10}...10^{-9}$cm^3 s^{-1}.

In order to get quantitative predictions for the mean atom number during the loading stage of a dipole trap, one can solve the differential equation 3.36. For the single particle loss parameter γ I will use 0.2 s^{-1}, which is consistent with our observations (see sec. 3.4.2). Figure 3.7 shows in a log-log scale the mean number of trapped atoms as a function of the loading rate. For a trapping-beam waist $w_0 \leq 4\mu$m and in presence of cooling light the mean number of trapped atoms is locked to one. This blockade effect was observed the first time by Schlosser et al. [73] in a microscopic optical dipole trap.

Atom number distribution

The solution of the differential equation 3.36 which describes the loading behaviour allows to calculate only the mean number of trapped atoms. But it does not give insight

Table 3.1: Physical processes and elementary probabilities which lead to a change in the atom number of +1, -1 and -2.

physical process	probability	change in N
loading	Rdt	+1
background collisions	$\gamma N dt$	-1
two-body collisions	$\beta' N(N-1)/2$	-2

into the atom number statistics. This information can be gathered by modelling the loading process by a *Markov process*.

In this modell the overall probability to have N single atoms at a certain time in the dipole trap is represented by a state vector $\vec{r}$. The change of this state vector per unit time is given by a transfer matrix M which describes the relevant physical processes which govern the loading and loss behaviour (see Tab.3.1). In general this matrix is of dimension $(N+1)\times(N+1)$. For simplicity I will restrict myself to the case of maximal 5 atoms in the trap and therefore the probability to have 0,1,2,3,4 or 5 atoms in the trap is given by the state vector $\vec{r} = (p_0, p_1, p_2, p_3, p_4, p_5)$ and the transfer matrix by

$$M = \begin{pmatrix} A_1 & \gamma & \beta' & 0 & 0 & 0 \\ R & A_2 & 2\gamma & 3\beta' & 0 & 0 \\ 0 & R & A_3 & 3\gamma & 6\beta' & 0 \\ 0 & 0 & R & A_4 & 4\gamma & 10\beta' \\ 0 & 0 & 0 & R & A_5 & 5\gamma \\ 0 & 0 & 0 & 0 & R & A_6 \end{pmatrix}, \tag{3.38}$$

where $A_N = 1 - (R + N\gamma + N(N-1)\beta'/2)$ for $N = 0, 1, .., 5$.

The stationary atom number distribution $\vec{r}_{stat}$ is then given by the solution of the system of linear algebraic equations which can be written as

$$(M - E)\vec{r}_{stat} = \vec{0}, \tag{3.39}$$

where E is the unity matrix.

Now one can calculate the stationary atom number distributions for different loading rates R relevant for the present experiment (see Fig. 3.8). Here we assume the situation when near-resonant colling light is present during the loading stage of the dipole trap. For a dipole laser beam waist of 10 μm we expect poissonian occupation statistics. In this regime there is a high probability to trap more than one atom at a time. When the dipole laser beam waist is 3.5μm the probability to load more than one atom is remarkably suppressed leading to subpoissonian occupation statistics. This blockade regime appears up to a maximum loading rate of 1 atom/s.

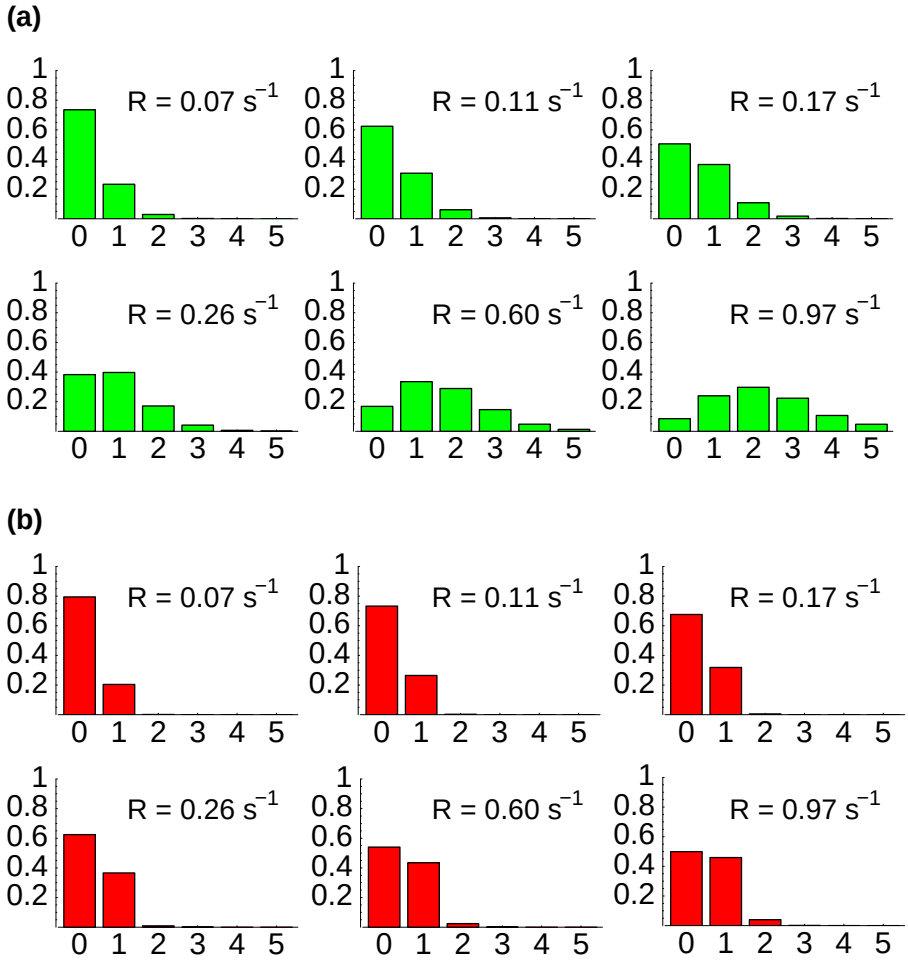

Figure 3.8: Stationary atom number distributions for different loading rates R relevant for the present experiment. Each histogram shows the probability to have 0..5 atoms in the dipole trap. **(a)** for a waist of 10μm we expect poissonian occupation statistics. **(b)**, for a beam waist of 3.5μm the number of trapped atoms is locked to one. The measured histograms in Fig. 3.18 clearly prove this "blockade effect".

3.3 Experimental setup

In order to load only single atoms into a dipole trap the waist of the focussed Gaussian dipole laser beam should be smaller than 4μm. Moreover, flexibility in optical access and no optical components inside the vaccum chamber have been the main design criteria of our experimental setup. The use of a glass cell provides the best optical access for laser beams and imaging optics. The fluorescence light scattered by a single atom in the focal spot of the dipole laser beam is collected with a confocal microscope. This simple setup [13] allows to completely suppress stray light from the dipole laser and reflexions of the cooling beams into the detection optics.

3.3.1 Vacuum system

To guarantee long storage times of atoms in a dipole trap our experiment must be performed in an ultra high vacuum (UHV) environment. Therefore we set up a compact UHV steel chamber pumped only by a ion pump (Varian, StarCell, 24 l/s). To have free access to the experimental region for laser beams and detection optics we connected a commercial spectroscopy glass cell made by Hellma with outer dimensions of $25 \times 25 \times 70$ mm^3 without antireflexion coatings directly to a milled hole in a UHV steel flange and sealed it with Indium wire. This simple and inexpensive setup yields a background gas pressure of better than 3×10^{-11} mbar. A Rubidium dispenser inside the UHV chamber operated at a current of 2.5 A serves as the source of atoms. Under this operating conditions the residual Rb gas pressure is below 10^{-10} mbar and allows to store atoms in the dipole trap up to several seconds. Details concerning the vacuum setup can be found in [13].

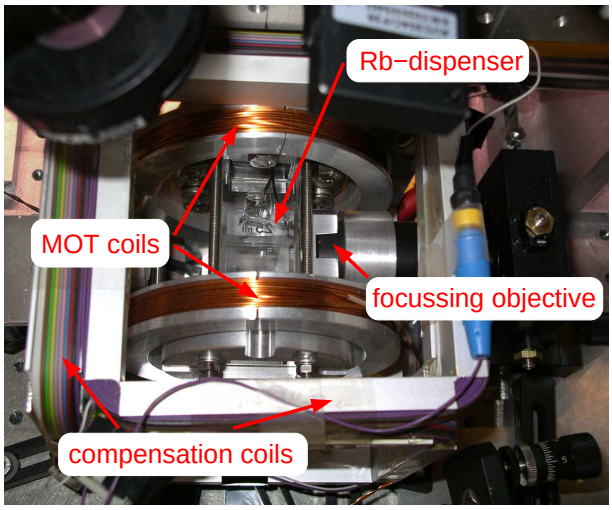

Figure 3.9: Detailed picture of the experimental setup.

3.3.2 Laser system

The application of laser cooling and the coherent manipulation of a single atom require the lasers to be stabilized onto or near atomic hyperfine transitions of the $D2$ line with a wavelength of 780 nm. For this purpose we use diode lasers locked to the Rubidium spectrum by using Doppler free saturation spectroscopy. The lock signal is generated by a heterodyne lock-in technique in the radio frequency domain [74, 75]. This technique guarantees a longterm frequency stability of less than 2 MHz. The bandwidth of the lasers is reduced to 0.6 MHz by operating them as grating stabilized external cavity lasers [76]. The mode structure of all lasers is monitored online with a confocal scanning Fabry-Perot interferometer (FPI) with a free spectral range of 375 MHz. This allows to identify mode jumps of the diode lasers and reject inappropriate experimental data.

- The **cooling laser** has to be red-detuned from the cycling transition $5^2S_{1/2}, F = 2 \rightarrow 5^2P_{3/2}, F' = 3$ up to 5 natural linewidths ($\Gamma = 6$ MHz) and will be used for the coherent manipulation (see chapter 5) of a single atom. For obvious reasons this applications require switching properties down to 10 ns which are realized in this experiment with acousto-optic modulators (AOM) in double-pass configuration [13, 77] driven by a tuneable RF signal. A laser beam passing the AOM twice shifts the laser frequency by $2 \times 150...250$ MHz. Therefore the cooling laser is locked to the crossover transition $5^2S_{1/2}, F = 2 \rightarrow 5^2P_{3/2}, F' = 1, 2$ which is red-detuned by 345.5 MHz from the cycling transition.

- **Repump laser:** Although the $5^2S_{1/2}, F = 2 \rightarrow 5^2P_{3/2}, F' = 2$ transition is detuned from the cooling transition by 45 natural linewidths, there is a finite probability of excitation to the hyperfine level $5^2P_{3/2}, F' = 2$, from where a spontaneous decay to the $5^2S_{1/2}, F = 1$ ground state can occur. To ensure efficient laser cooling a seperate repump laser transfers the atomic population back into the $5^2S_{1/2}, F = 2$ level. The repump laser is frequency stabilized via a beat signal to a master laser [13, 78, 79] which is locked to the atomic transition $5^2S_{1/2}, F = 1 \rightarrow 5^2P_{3/2}, F' = 1$. The repump laser frequency can be varied on one hand with the tunable beat signal on the other hand with the driving frequency of an AOM in double-pass configuration. This setup offers a great flexibility to tailor switchable laser pulses at different frequencies.

- **Dipole trap laser:** The far-off-resonace dipole trap is generated by a focused Gaussian laser beam of a single mode laser diode (SDL) at 856 nm with a maximum output power of 200 mW. Because the dipole laser operates at a detuning of 61 nm from atomic resonance it is sufficient to stabilize the laser wavelength on the order of a few 0.1 nm. This is achieved only by stabilizing the temperature of the laser diode within 0.05 K.

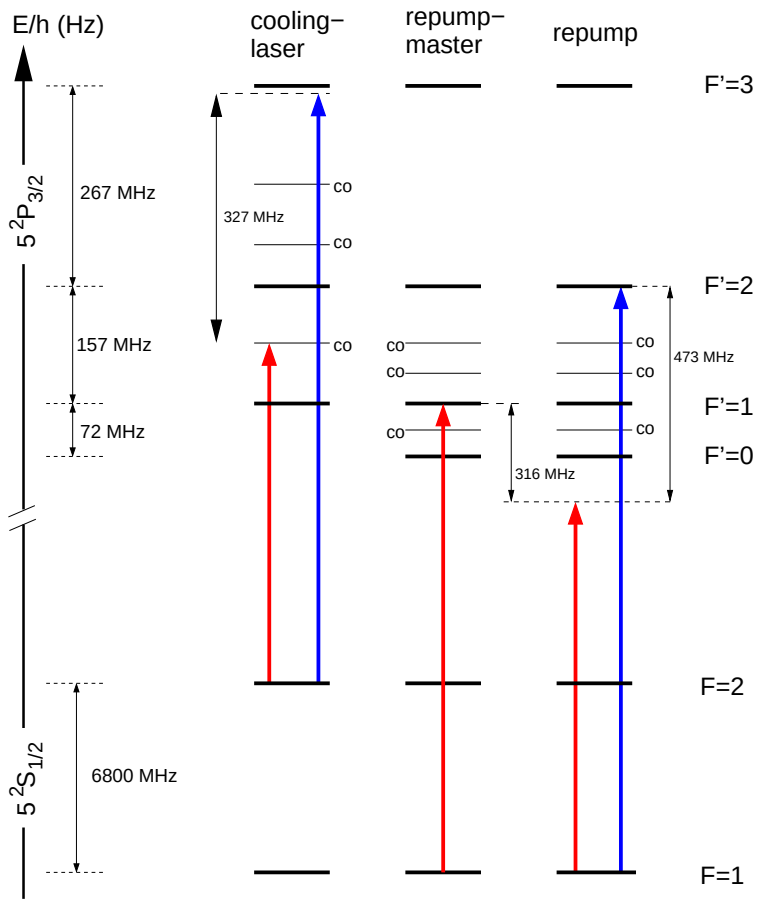

Figure 3.10: Laser frequencies used in the present experiment for laser cooling and trapping of a single ^{87}Rb atom. Red (blue) arrows: laser frequencies before (after) AOM.

3.3.3 Magneto optical trap

Because of the small potential depth of our optical dipole trap - typically 0.5 ... 1 mK - atoms have to be precooled in a magneto optical trap (MOT) to the micro-Kelvin regime [53, 80] before they can be transferred into the dipole trap. The basic idea of a MOT is to use dissipative light forces which introduce an effective friction force to slow down and cool atoms from a thermal atomic gas. At the same time an inhomogeneous magnetic field is applied which introduces a spatial dependence of the light force leading to a confinement of the atom cloud. The schematic setup for a MOT is shown in Fig. 3.11. Six red-detuned, retroreflected, and circularly polarized laser beams with a diameter of 2 mm are directed onto the center of the magnetic quadrupole field which is produced by two magnetic coils in anti-Helmholtz configuration. The coils can generate magnetic field gradients of up to $\partial B/\partial z = 11$ G/cm at a maximum current of 2 A. In contrast to a

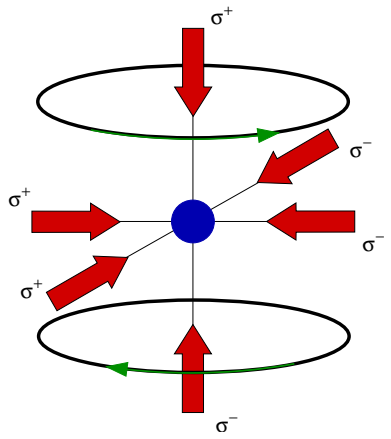

Figure 3.11: Geometry of a magneto optical trap (MOT). The magnetic quadrupole field for the MOT is generated by an anti-Helmholtz coil pair. Six circularly polarized laser beams are overlapped at the trap center.

standard MOT the two beams within the plane of the coils make an angle of 34°, instead of the usual 90° (see Fig. 3.12). Sufficiently slow atoms are captured in the MOT from the thermal ^{87}Rb background gas, whereby the pressure can be adjusted by varying the current through the Rubidium dispenser. Typically the MOT confines 3×10^4 atoms in a 1-mm-diameter cloud.

3.3.4 Dipole trap and detection optics

The detection of extremely low levels of fluorescence light scattered by a single atom requires detection optics which allow to collect atomic fluorescence from a large solid angle. On the other hand we want to suppress $|\pi\rangle$-polarized single photons from the transition $5^2P_{3/2}, F' = 0, m_{F'} = 0 \rightarrow 5^2S_{1/2}, F = 1, m_F = 0$ reducing the fidelity of the entangled atom-photon state we are interested in to generate. The smaller the solid angle of the collected atomic fluorescence light the higher the entanglement fidelity. Furthermore, we want to make use of the collisional blockade effect which can be achieved with a trapping beam waist smaller than 4 μm.

Dipole trap

To fulfill these requirements, we use a commercial achromatic laser objective (LINOS), mounted outside the vacuum chamber with a working distance of 30 mm and a numerical aperture of $NA = 0.38$, for focussing the dipole laser beam and imaging atomic fluorescence light from the dipole trap region at the same time. Before the dipole laser beam is focussed down, it is spatially filtered by a single mode optical fiber, improving the beam quality of the diode laser beam significantly. An additional plane glass plate

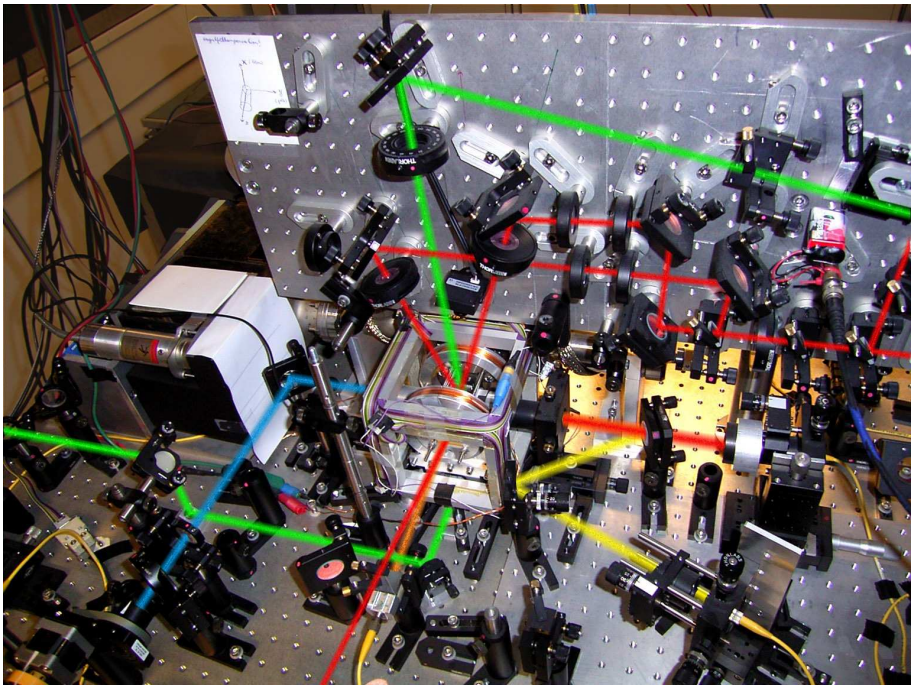

Figure 3.12: **Photograph of the experimental apparatus**. On the vertical base plate above the vacuum chamber optics for the MOT and the cycling laser can be seen. The optics on the right hand side of the MOT chamber is for focussing the dipole laser beam collecting atomic fluorescence light.

in between the glass cell of the UHV chamber and the focussing objective is inserted to improve the imaging properties of the objective [13]. This addition especially reduces the aberration of the light beam in the focal point, enabling diffraction limited imaging. For the trapping beam we achieve a minimum waist of $w_0 = 3.5 \pm 0.2$ μm with a quality factor of $M^2 = 1.1$. Here I emphasize, that this waist is used without exception in all experiments of this thesis. To adjust and to stabilize the depth of the dipole potential the power of the dipole laser beam can be controlled with an acousto-optic modulator (AOM) in single-pass configuration. For a laser power of 44 mW, a wavelength of 856 nm and a beam waist of the trapping beam we calculate a depth of the dipole potential of 1 mK and photon scattering rate of 24 s^{-1}.

Detection optics

Fluorescence light from the dipole trap region is collected with the same focusing objective in a confocal arrangement and separated from the trapping beam with a dichroic mirror. The waist of the detection beam is $w_0 = 2.2 \pm 0.2$ μm and is overlapped tranversally and longitudinally with the waist of the trapping beam. This simple setup allows

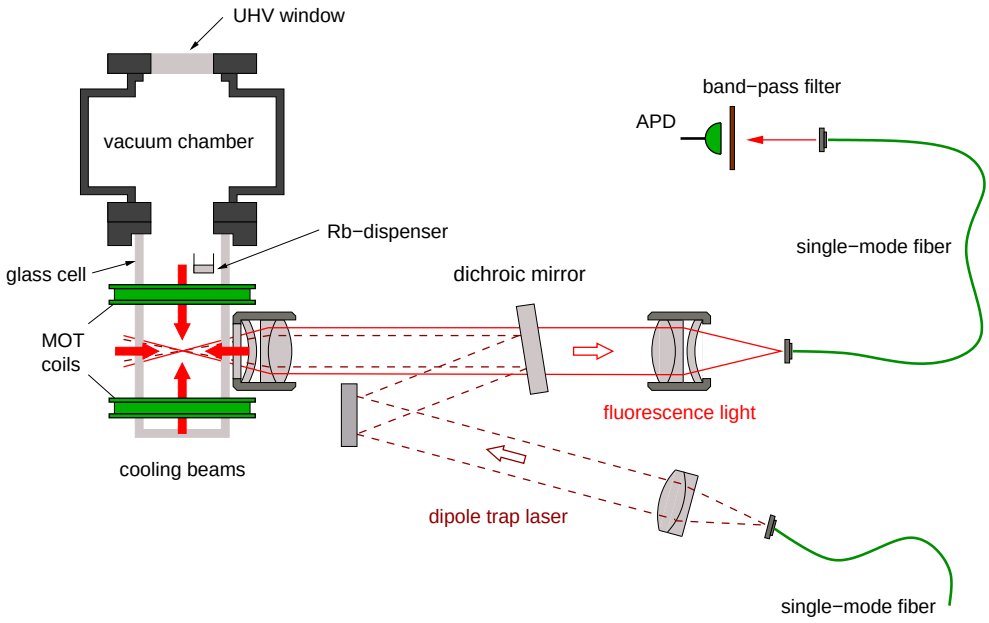

Figure 3.13: **Experimental setup of the dipole trap and fluorescence detection.** The dipole laser is focussed at the intersection of three counterpropagating laser beams for optical cooling. Fluorescence light is collected with a confocal microscope into a single-mode optical fiber and detected with a silicon APD.

to collect fluorescence light from a single atom with an effective numerical aperture of $NA = 0.29$ and guarantees a maximal entanglement fidelity F=0.99 because π-polarized photons are hardly collected [81]. To suppress stray light from the cooling beams the fluorescence light is coupled into a single mode optical fiber for spatial filtering. Finally, it is detected with single photon sensitivity with a silicon avalanche photodiode (APD) operated in the Geiger mode [82] with a typical dark count rate of 250 counts/s. If one assumes isotropic emission of unpolarized atomic fluorescence light (corresponding to the situation of a single atom in the light-field configuration of the MOT) we calculate an overall detection efficiency for single photons of 2×10^{-3} including transmission losses of optical components and the quantum efficiency $\eta_q = 0.5$ of our APDs [13].

The APD signal resulting from the detection of a photon is converted into a TTL pulse and sent to a timer card which integrates the number of detected photons in time intervals down to 10 ms. This signal serves as a real time monitor of the dipole trap and its dynamics (see Fig. 3.14) and is continously displayed on a computer screen and recorded into a data file.

3.4 Observation of single atoms in a dipole trap

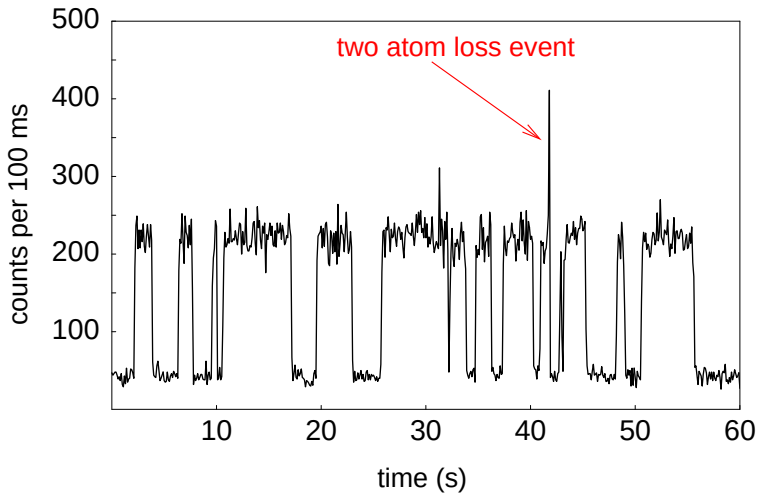

Figure 3.14: **Single atom detection**. Number of photons counted by an avalanche photodiode per 100 ms. Due to the small trap volume and light induced two-body collisions we observe either one or no atom at a time.

The dipole trap is loaded by simply overlapping it with the atomic cloud in the MOT, where the atoms are precooled into the μK regime. Typically the cooling laser is red detuned to the hyperfine transition $5^2S_{1/2}, F = 2 \rightarrow 5^2P_{3/2}, F = 3$ by 3..5Γ and the repump laser on resonance with the hyperfine transition $5^2S_{1/2}, F = 1 \rightarrow 5^2P_{3/2}, F = 2$ of the D2 line. When both the dipole trap and the pre-cooling MOT are turned on together, we observe characteristic steps in the detected fluorescence signal (Fig. 3.14), corresponding to individual atoms entering and leaving the dipole trap. By changing the magnetic field gradient of the MOT we can adjust the density of the atomic cloud and therefore the loading rate of atoms into the dipole trap from $R = 1$ atom/15 s to $R = 1$ atom/s (see Fig. 3.17, inset (a)). If a second atom enters the trap both are immediately lost. This effect that atoms leave the trap in pairs is a result of light-induced binary collisions and will be investigated in detail in 3.4.2.

The fluctuations of the photon count rate originate in the poissonian counting statistics. A typical histogram of photon counts is shown in Fig. 3.15. The dark count rate of the APD and background gas fluorescence cause a first peak in the histogram at $N_0 = 45$ counts/100 ms and a rms width of $\sigma_0 = 7$ counts/100 ms, whereby the dark count rate of the APD (400 counts/s) dominates the background. Atomic fluorescence light radiated by cold atoms in the surrounding MOT determine the residual contribution. Cooling laser light reflected by optical components is completely suppressed in the present setup. The second peak in Fig. 3.15 at $N_1 = 225$ counts/100 ms and a rms width of $\sigma_1 = 19$ counts/100 ms is caused by resonance fluorescence of a single atom in the dipole trap.

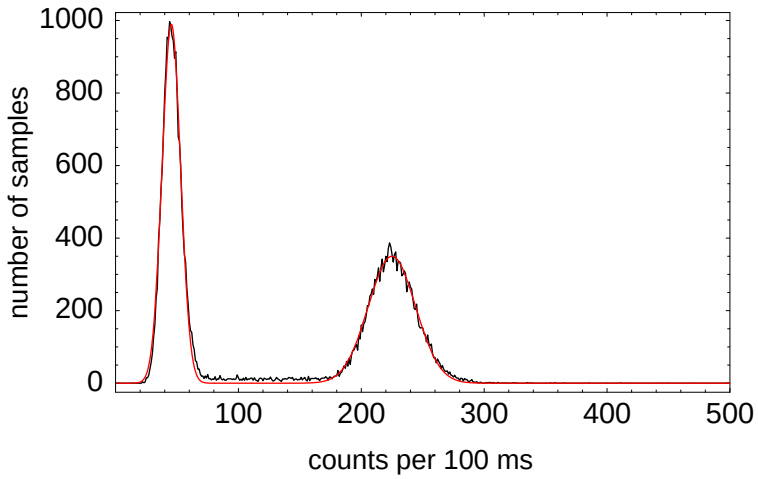

Figure 3.15: Single atom detection. Histogram of photon counts per 100 ms of Fig. 3.14.

Typical photon counting rates are 500 - 1800 s^{-1} per atom depending on the detuning and intensity of the cooling laser. For a maximum counting rate of 1800 s^{-1} per atom we determine a minimum time interval of 10 ms to be able to distinguish 1 atom from the background counts. As a criterion we require that the difference of count rates of "1" atom and "0" atom, $\Delta N = N_1 - N_0$, is 4 times larger than the statistical fluctuations of N_1. Provided the fluctuations of the photon count rate are caused only by the poissonian counting statistics the expected error of this method is 4 percent.

3.4.1 Trap lifetime

The lifetime of single atoms in the dipole trap depends on one hand on collisions with atoms from the background gas, whereby the collision rate is determined by the residual background gas pressure in the vacuum chamber. For a gas pressure below 10^{-10} mbar we expect a lifetime up to several seconds. On the other hand, this value can drop by many orders of magnitude during the loading stage because light-induced binary collisions dominate the trap loss.

Depending on the trap depth and the loading rate we observe a mean $1/e$ lifetime between 0.5 and 2.2 s (see Fig. 3.17, inset (b)). Here the lifetime is extracted directly by histogramming the length of fluorescence steps. Because the cooling and the repump laser of the MOT are present during the loading stage of the dipole trap, light-induced two-body collisions dominate the trap loss and therefore the measured lifetime.

In a different experiment the characteristic lifetime of single atoms limited only by background gas collisions is measured. Therefore, we switch on the cooling and repump laser of our MOT and wait for a single atom. If the observed fluorescence exceeds a threshold of 1200 counts/s the MOT lasers are switched off. After a variable delay time

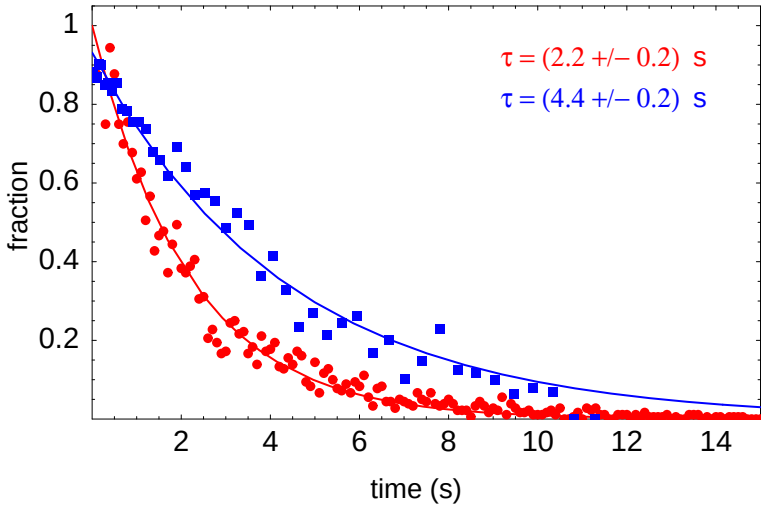

Figure 3.16: Fraction of single atoms in the dipole trap as a function of time with (red data points) and without (blue data points) cooling light. A fit of the experimental data with a simple exponential decay yields a 1/e lifetime of 2.2 ± 0.2 s and 4.4 ± 0.2 s, respectively.

t, the MOT lasers are switched on again and atomic fluorescence light is collected for 50 ms. If the measured fluorescence still exceeds the threshold, the atom has stayed in the trap. If we do not observe atomic fluorescence light, the atom is lost due to collisions with the background gas. This experimental sequence is repeated for a range of delay times t and for each delay value many times. Finally, we derive a histogram, where the probability to redetect a single atom in the dipole trap is given as a function of the delay time and fit this data set with an exponential decay yielding a $1/e$ lifetime of 4.4 ± 0.2 s.

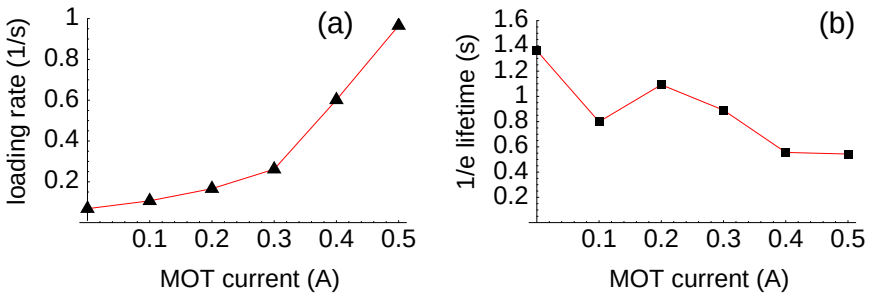

Figure 3.17: **(a)** Loading rate R and **(b)** $1/e$ lifetime in presence of cooling light as a function of the MOT current. Increasing the MOT current reduces the trap lifetime due to an increase of the loading rate.

3.4.2 Atom number statistics

One important fact concerning the fluorescence detection in our experiment is, that photon count rates corresponding to more than one atom never occur up to a maximum MOT current of 0.5 A corresponding to a maximum loading rate of $R = 1\ \mathrm{s}^{-1}$. This can be seen directly from the histogramms of photon counts in Fig. 3.18.

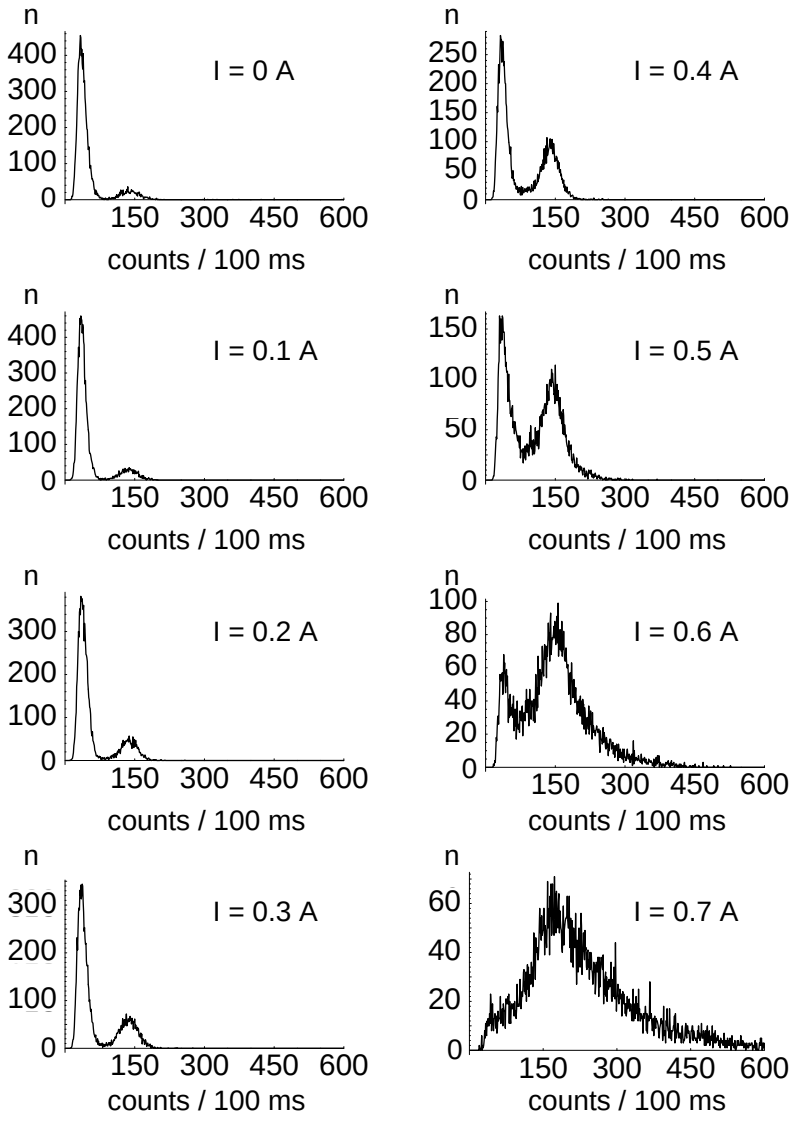

Figure 3.18: Histograms of detected photon counts in 100 ms for different MOT currents (I). Up to 0.5 A only single atoms are observed in the dipole trap.

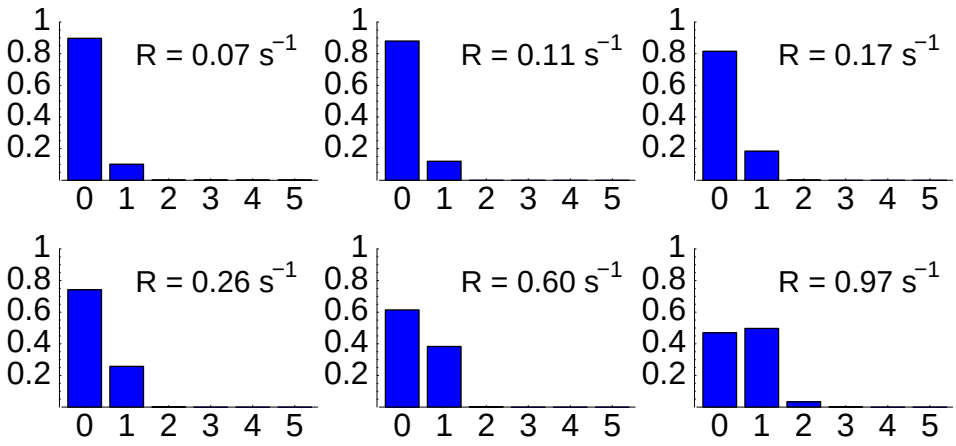

Figure 3.19: Measured atom number distributions for different loading rates. Due to the small dipole trap volume and the presence of light-induced two-body collisions during the loading stage the number of trapped atoms is locked to one up to a loading rate of 1 atom/s.

To compare the measured atom number distributions directly with the calculated distributions for a trapping beam waist of 3.5μm (see Fig. 3.8), the continuous photon counting histograms are converted by numerical integration into bar-histograms where the probability to load atoms into the dipole trap is plotted as a function of the atom number N (see Fig. 3.19). As expected, our measurement results confirm the "blockade effect" [73], locking the maximum number of trapped atoms to one.

3.4.3 Temperature measurement of a single atom

In the present experiment a single optically trapped atom is cooled during fluorescence detection by three-dimensional polarization gradients in an optical molasses. This leads to a final kinetic energy on the order of 100 μK [70]. Information about the kinetic energy can be gathered by the spectral analysis of the emitted resonance fluorescence, because Doppler effects due to the motion in the confining potential lead to a line broadening in the emitted fluorescence spectrum.

For low excitation intensities the fluorescence spectrum of a two-level atom exhibits an elastic peak centered at the incident laser frequency ω_L, while for higher intensities an inelastic component becomes dominant, with contributions at the frequencies ω_L and $\omega_L \pm \Omega_0$ [83], where Ω_0 denotes the Rabi frequency. This so so-called "Mollow triplet" arises from the dynamical Stark splitting of the two-level transition and has been observed in a number of experiments [84, 85, 86], using low-density atomic beams or a single trapped and laser-cooled Ba^+ ion [87]. Surprisingly, there are only a few experimental investigations of the *coherent* scattering process, with a frequency distribution determined by the exciting laser. Subnatural linewidths were demonstrated with atomic

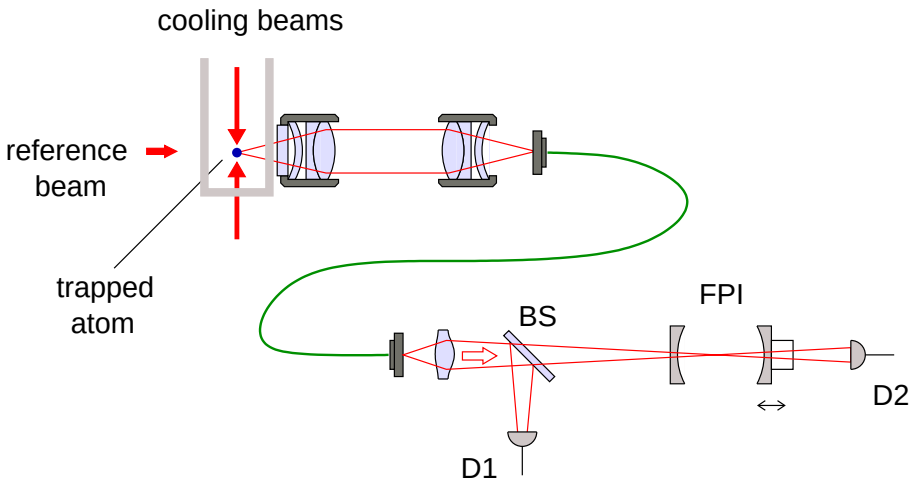

Figure 3.20: Setup for the measurement of the resonance fluorescence spectrum of light scattered by a single atom in an optical dipole trap. The fluorescence and excitation laser light is collected confocally to the trapping beam (see Fig. 3.13) and analyzed with a scanning Fabry-Perot Interferometer (FPI). The reference laser is used to monitor length drifts of the resonator and to determine the instrumental function of the FPI.

beam experiments [86, 88], atomic clouds in optical molasses [89, 90] and a single trapped and laser-cooled Mg^+ ion [91, 92].

For our laser cooling parameters the fluorescence spectrum is dominated by elastic Rayleigh scattering [47]. Hence, the emitted fluorescence light exhibits the frequency distribution of the exciting laser (0.6 MHz FWHM) field broadened by the Dopper effect. Position-dependent atomic transition frequencies in the dipole trap due to the inhomogeneous AC-Stark shift give no additional broadening because the spectrum of the elastically scattered fluorescence light is determined only by the frequency distribution of the exciting light field and not by the atomic transition frequencies.

The resolution achieved with narrow-band Fabry-Perot filter resonators for spectral analysis is limited to approximately 1 MHz and allows to measure an effective line broadening on the order of several 10 kHz. This resolution is sufficient to determine the kinetic energy with sufficient accuracy.

Experimental setup

The scattered fluorescence spectrum is analyzed via a scanning Fabry-Perot interferometer (FPI) with a frequency resolution of 0.45 MHz (full width half maximum), a transmission of 40% and a finesse of 370. To measure the spectrum only at times we trap single atoms, a part of the fluorescence light is monitored separately with a reference APD (D1) (see Fig. 3.20). Since the broadening of the atomic emission spectrum

due to the Doppler effect is expected to be a small effect, the instrumental function of the spectrometer and the exciting laser line width have to be known accurately. In order to achieve this, we shine a fraction of the exciting light (reference beam) into the collection optics (see Fig. 3.20). This way, both reference and scattered light are subject to the identical spectrometer instrumental function whereby the reference laser spectrum is also used to monitor length drifts of the filter cavity. In the experiment the spectrum of the reference beam and the fluorescence light scattered by a single atom in the dipole trap were recorded alternately. After each measurement a compensation of the cavity drift was performed by referencing the cavity frequency to the maximum transmission of the reference laser.

Experimental results

With this procedure we obtained the two (normalized) data sets in Fig. 3.21. As expected, the fluorescence spectrum scattered by a single atom exhibits a "subnatural" linewidth of 1.04 ± 0.01 MHz (FWHM) because the elastic Rayleigh contribution dominates the scattering process. The exciting laser light field exhibits a linewidth of 0.94 ± 0.01 MHz (FWHM) which is the convolution of the transmission function of the Fabry-Perot filter with the spectral width of the excitation laser. The depicted error bars reflect the statistical error from the individual count rates of each data point. For the reference laser this error is too small to be visible in this graph.

For an atom at rest the resonance fluorescence spectrum should show the same linewidth as the exciting light field. Any finite kinetic energy of the atom will lead to a broadening of the atomic emission spectrum and therefore can be used for a determination of the "temperature". To extract a mean kinetic energy from the measured spectra in Fig. 3.21, we assume the same stationary Gaussian velocity distribution in all directions. According to this assumption we convolve a Gaussian distribution with the measured reference laser line profile. The resulting function is fitted to the data points of the fluorescence spectrum with the variance of the Gaussian profile being the only free fit parameter [93]. From this fitted variance we directly obtain the mean kinetic energy E_{kin} of a single atom in the dipole trap of

$$E_{kin} = \frac{1}{2} m \langle \Delta v^2 \rangle = (110 \pm 15)^{+14}_{-25}\ \mu\mathrm{K} \cdot k_B, \tag{3.40}$$

with a statistical error of $\pm 15 \mu$K. k_B denotes the Boltzmann constant, m the atomic mass and $\langle \Delta v^2 \rangle$ the mean quadratic velocity.

The calculation of the mean kinetic energy contains a systematic error because the cooling beams have different angles relative to the axes defined by the dipole trap and the detection optics. The overall Doppler broadening of the elastic scattered fluorescence light depends on these angles. Therefore, an upper bound for this error is estimated by assuming that the atoms scatter light only from the beams which would give the highest or lowest velocities, respectively. Within the experimental errors, the measured temperature is equal to or smaller than the Doppler temperature of ^{87}Rb (146 μK).

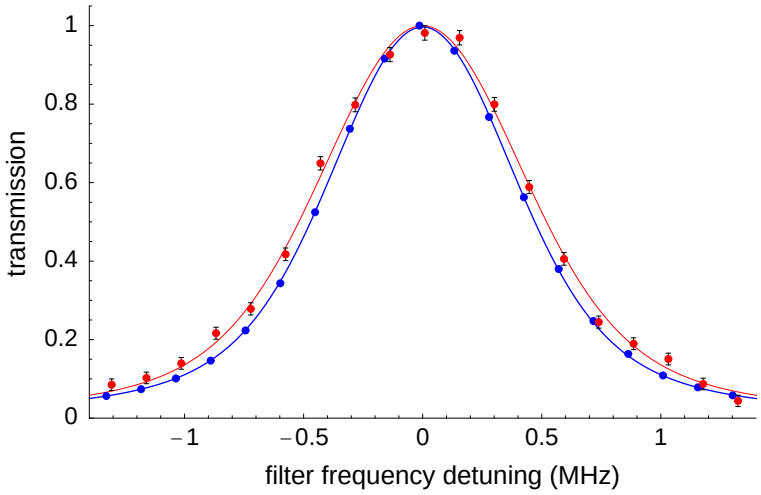

Figure 3.21: Measured spectra of the single atom resonance fluorescence (red data points) and the excitation light (blue data points). The spectra exhibit a width of 0.94 ± 0.01 MHz and 1.04 ± 0.1 MHz (FWHM) for the excitation and the fluorescence light, respectively. Experimental parameters: $I_{CL} = 80$ mW/cm^2, $I_{RL} = 12$ mW/cm^2, $\Delta_{CL} = -2\pi \times 19$ MHz, $\hat{U} = (0.62 \pm 0.06)$ mK.

3.5 Conclusion and discussion

A single ^{87}Rb atom is loaded from a magneto-optical-trap (MOT) into an optical dipole trap that operates at a detuning of 61 nm from atomic resonance. Atoms stored in this far-off-resonance optical dipole trap have a very small scattering rate and therefore negligible photon recoil heating. Confinement times up to 5 s are achieved with no additional cooling. For loading the dipole trap, the MOT cooling lasers are switched on, and atomic fluorescence light is collected with a microscope objective and detected with a single photon avalanche diode (APD). Well seperated equidistant steps in the detected fluorescence signal allow to monitor the number of trapped atoms in a "noninvasive" way and in real time. Because of the small dipole trap volume (beam waist $w_0 = 3.5\mu$m), cold binary collisions assisted by cooling light lock the maximum number of trapped atoms to one. Measurements for different loading rates clearly prove this "blockade effect". The overall detection efficiency of single photons is 0.2 percent including transmission losses and the quantum efficiency of the APD.

Using a scanning filter-cavity we determined the spectrum of the emitted single atom resonance fluorescence. Due to Rayleigh-scattering the measured atomic fluorescence spectrum is dominated mainly by the spectral profile of the exciting light field. In addition we observe a Doppler broadening of the scattered atomic fluorescence spectrum, which allowed us to determine an upper bound of the mean kinetic energy of the trapped

atom corresponding a temperature of 110 μK.

4 Single photons from single atoms

4.1 Introduction

The experimental results from the previous chapter (see Fig. 3.14) suggest that we observe only single atoms in our dipole trap. This assumption can be verified by a detailed statistical analysis of the measured stream of photon counts. In particular, nonclassical features of the resonance fluorescence are observed in the second-order correlation function $g^{(2)}(\tau)$, whereby, most prominently, the so-called *antibunching* behaviour indicates the single particle character of the radiating source.

To prove that only a single atom is stored in our trap we have set up a Hanbury-Brown-Twiss (HBT) experiment [94, 95] and studied the statistical properties of the detected fluorescence light. The measured second-order correlation function exhibits strong photon antibunching verifying the presence of a single atom. In addition the two-photon correlations show the internal quantum dynamics of the population occupation of the atomic hyperfine levels involved in the excitation process, whereby the observed oscillations can be explained with a four-level model. To compare the theoretical model with the experimental data we numerically solve optical Bloch equations and calculate the second order correlation function of the emitted fluorescence light. We find good agreement with the measured data.

Due to the complex structure of photon-pair correlations which depend on the internal and external dynamics of the atom-light interaction, I will first introduce theoretical aspects relevant for the understanding of the present experiment before I will discuss measured experimental data.

4.2 Theoretical framework

4.2.1 Second-order correlation function

For the scattered light field of atomic resonance fluorescence described by the electric field operators $\mathbf{E}^+$ and $\mathbf{E}^-$, the two-photon correlation function $g^2(\tau)$ is given, according to Glauber [96] (see also [97]), by

$$g^{(2)}(\tau) = \frac{\langle \mathbf{E}^-(t)\mathbf{E}^-(t+\tau)\mathbf{E}^+(t+\tau)\mathbf{E}^+(t)\rangle}{\langle \mathbf{E}^-(t)\mathbf{E}^+(t)\rangle^2}, \tag{4.1}$$

where $\tau \geq 0$. For almost monochromatic light fields and a small detection probability, this function is the conditional probability of detecting a photon at time $t+\tau$, given the previous detection of another photon at time t, normalized by the factorized value for statistically independent photons. Whereas classical fields show correlation functions $g^{(2)}(0) \geq 1$ and $g^{(2)}(\tau) \leq g^{(2)}(0)$, the nonclassical resonance fluorescence of a single atom exhibits the so-called *antibunching* behaviour, i.e., $g^{(2)}(0) = 0$ and $g^{(2)}(\tau) > g^{(2)}(0)$. This condition signals sub-Poissonian emission probability.

4.2.2 Two-level atom

The resonance scattering from an atom can be described by the electromagnetic field operators in the Heisenberg picture. For a two-level atom at position $\mathbf{R}$ with a dipole transition, the electric field operator $\mathbf{E}^+(\mathbf{r},t)$ at a point $\mathbf{r}$ is given in the far-field region by

$$\mathbf{E}^+(\mathbf{r},t) = \mathbf{E}^+_{free}(\mathbf{r},t) + \mathbf{E}^+_S(\mathbf{r},t), \tag{4.2}$$

where $\mathbf{E}^+_{free}(\mathbf{r},t)$ is the field unperturbed by the atom. This part contains the vacuum fluctuations and the externally applied (laser) light. The point of detection $\mathbf{r}$ is chosen such that the excitation light field is negligible and therefore the freely-propagating part can be dropped. The second contribution in Eq. (4.2) is the source field part $\mathbf{E}^+_S(\mathbf{r},t)$ which represents the field scattered by the atom. It is given by [97]

$$\mathbf{E}^+_S(\mathbf{r},t) = -\frac{\omega_0^2 |\langle g|\mathbf{d}|e\rangle| \sin\theta}{4\pi\epsilon_0 c^2 |\mathbf{r}-\mathbf{R}|} \vec{\epsilon}_S \hat{\pi}(t - \frac{|\mathbf{r}-\mathbf{R}|}{c}). \tag{4.3}$$

Here, ω_0 is the angular frequency of the atomic transition $|g\rangle \rightarrow |e\rangle$, $\langle g|\mathbf{d}|e\rangle$ is the corresponding dipole matrix element, and $\mathbf{R}$ is the center-of-mass coordinate of the atom. The operator $\hat{\pi}(\mathbf{r},t)$ contains the spatio-temporal dependence of the light field and is defined by $\hat{\pi} = |g\rangle\langle e|$. For the negative part of the electric field the corresponding operator is defined by $\hat{\pi}^\dagger = |e\rangle\langle g|$ respectively. The angle θ is subtended between the dipole matrix element and the direction of observation, $\mathbf{r}-\mathbf{R}$. The linear polarization of the emitted field, $\vec{\epsilon}_S$, is in the plane perpendicular to the direction of observation, and parallel to the projection of the dipole matrix element into this plane.

The coherence properties of the light emitted by a single two-level atom in free space can now be calculated with the use of the source-field expression (4.3), and we get for the second-order correlation function of the emitted fluorescence light

$$g^{(2)}(\tau) = \frac{\langle \hat{\pi}^\dagger(t)\hat{\pi}^\dagger(t+\tau)\hat{\pi}(t+\tau)\hat{\pi}(t)\rangle}{\langle \hat{\pi}^\dagger(t)\hat{\pi}(t)\rangle^2}, \tag{4.4}$$

where the time delay τ is always positive. This relation contains the expectation value of two observables at different times. With the help of the *quantum regression theorem* [98] the two-time expectation values can be reduced to particular one-time expectation

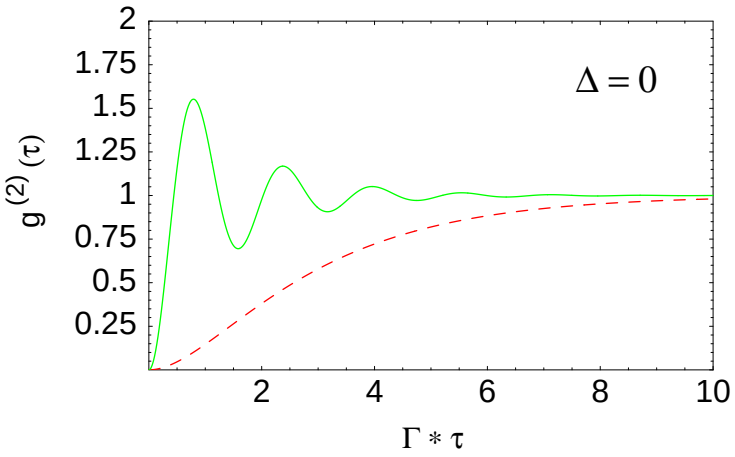

Figure 4.1: Second-order correlation function $g^{(2)}(\tau)$ of a two-level atom versus the dimensionless delay time $\Gamma\tau$ for $\Omega_R/\Gamma = 4$ (green solid line) and $\Omega_R/\Gamma = 0.4$ (red dashed line, respectively).

values. Performing some calculations [49], the second-order correlation function is found to be:

$$g^{(2)}(\tau) = \frac{\rho_{ee}(\tau)}{\rho_{ee}(\infty)}. \tag{4.5}$$

Here $\rho_{ee}(\tau)$ is the element of the atom's density matrix that represents the population of the excited atomic state at the time τ. This element can be calculated from optical Bloch equations (OBE) [80] with the initial conditions $\rho_{ee}(0) = \rho_{eg}(0) = \rho_{ge}(0) = 0$, and $\rho_{gg}(0) = 1$, which describe the state of the atom immediately after the emission of a photon. The theoretically predicted correlation function is given by [99]

$$g^{(2)}(\tau) = 1 - e^{-3\Gamma\tau/4}[\cos(\Omega_R\tau) + \frac{3\Gamma}{4\Omega_R}\sin(\Omega_R\tau)], \tag{4.6}$$

where $\Omega_R^2 = \Omega_0^2 + \Delta^2 - (\Gamma/4)^2$, with the Rabi frequency Ω_0 at resonance, the natural linewidth Γ, and the detuning Δ.

In Fig. 4.1, the second-order correlation function is plotted as a function of the time delay τ for different values of the generalized Rabi frequency Ω_R of the driving field. For $\tau = 0$ the two-photon correlation function $g^{(2)}(\tau) = 0$, which corresponds to the phenomenon of *photon antibunching*. Once a photon is emitted, the atom is found in the ground state and it takes the driving field some time to reexcite the atom to the upper level, from which the next photon can be emitted. On average, this delay is of the order of the Rabi period Ω_R^{-1}. For a weak driving field, $\Omega_R/\Gamma < 1$, $g^{(2)}(\tau)$ increases monotonically from 0 to 1 as τ is increased. For a strong driving field, $\Omega_R/\Gamma >$

1, i.e. the generalized Rabi frequency Ω_R and thus the frequency of populating and depopulating the excited state is greater than the decay rate Γ. Therefore $g^{(2)}(\tau)$ shows an oscillatory dependence on τ. The magnitude of these oscillations decreases as τ is increased and $g^{(2)}(\tau)$ approaches unity as $\tau \to \infty$. The upper limit of $g^{(2)}(\tau)$ for the resonance fluorescence of a two-level atom is 2.

Both antibunching and sub-Poissonian statistics in resonance fluorescence have been observed in quantum optical experiments with atoms [100, 101]; however corrections for the fluctuating atom numbers in the atomic beam had to be taken into account. With a single trapped Mg^+ ion Diedrich *et al.* [102] observed antibunching of an individual two-level atom. In that experiment antibunching in the resonance fluorescence of one, two, and three trapped ions was observed and the antibunching property decreased as predicted for increasing ion numbers, since for an increasing number of independent atoms the photon counts become more and more uncorrelated.

Aside from antibunching and sub-Poissonian statistics, Schubert *et al.* [103] observed two-photon correlations in the resonance fluorescence of a single Ba^+ ion with a maximum much larger than what is possible with two-level atoms, as well as photon antibunching with much larger time constants of the initial photon anticorrelation. A detailed study of the internal eight-level dynamics on the basis of optical Bloch equations allowed a quantitative description of the observed $g^{(2)}(\tau)$ functions [104].

4.2.3 Four-level model

For the fluorescence detection of a single atom in the dipole trap we use the MOT cooling laser (CL) red detuned to the unperturbed hyperfine transition $5^2S_{1/2}, F = 2 \to 5^2P_{3/2}, F' = 3$ (Fig. 4.2) by $\Delta = 4..5\Gamma$. To avoid optical pumping to the hyperfine ground level $F = 1$ during the loading process we additionally shine in a repump laser (RL) on resonance with the hyperfine transition $5^2S_{1/2}, F = 1 \to 5^2P_{3/2}, F' = 2$. Because the atom is stored in a dipole trap, the AC Stark-effect additionally shifts the cooling and repump laser to the red of resonance and leads to significant optical pumping to $F = 1$. Hence, we expect a more detailed multi-level model - which includes also this pumping effect - to correctly describe the internal dynamics of the atom-light interaction.

In general it is quite complicated to describe the situation of a laser-cooled single atom in a dipole trap, because the six counter-propagating circularly polarized cooling laser beams of the MOT form an intensity lattice in space and a discrete set of points with zero intensity. The form of this interference pattern is specific to the set of phases chosen. Due to the finite kinetic energy corresponding to a temperature of approximately 110 μK (see preceding chapter) the atom oscillates in a classical picture with an amplitude corresponding to several optical wavelengths. During this oscillatory movement the atom experiences both a changing intensity and polarization. This situation suggests to simplify the internal atomic dynamics neglecting the Zeeman substructure of the involved hyperfine levels and to treat the exciting cooling and repump light as two unpolarized laser fields with an average intensity of six times the single beam intensity.

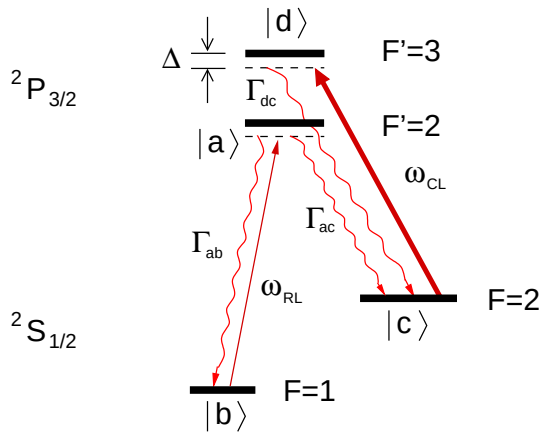

Figure 4.2: Effective level structure in ^{87}Rb used for fluorescence detection. The cooling laser field (CL) couples $F = 2 \rightarrow F' = 3$ and $F = 2 \rightarrow F' = 2$, whereas the repump laser field (RL) couples only $F = 1 \rightarrow F' = 2$.

Optical Bloch equations

In the following I will focus on an atomic four-level system as indicated in Fig. 4.2 and the interaction with two classical light fields. The Hamiltonian H of the system reads

$$H = H_0 + H_{int}, \tag{4.7}$$

where H_0 denotes the Hamiltonian of the free atom and H_{int} the interaction with the repump laser field $\mathbf{E}_{RL}$ of angular frequency ω_{RL} and the cooling laser field $\mathbf{E}_{CL}$ of angular frequency ω_{CL} respectively.

The equation of motion for the atomic density matrix ρ of the system is given by

$$\dot{\rho} = \frac{-i}{\hbar}[H, \rho] + R, \tag{4.8}$$

where the brackets [,] are defined by $[H, \rho] = H\rho - \rho H$ and the relaxation term R represents the spontaneous decay process. In the rotating-wave approximation (RWA) we obtain for the Hamiltonian H the matrix representation in the basis of the bare atomic states $|a\rangle$, $|b\rangle$, $|c\rangle$ and $|d\rangle$ corresponding to the hyperfine states $|F' = 2\rangle$, $|F = 1\rangle$, $|F = 2\rangle$ and $|F' = 3\rangle$:

$$H = \hbar \begin{pmatrix} \omega_a & -\frac{\Omega_1}{2}e^{-i\omega_{RL}t} & -\frac{\Omega_2}{2}e^{-i\omega_{CL}t} & 0 \\ -\frac{\Omega_1}{2}e^{i\omega_{RL}t} & \omega_b & 0 & 0 \\ -\frac{\Omega_2}{2}e^{i\omega_{CL}t} & 0 & \omega_c & -\frac{\Omega_3}{2}e^{i\omega_{CL}t} \\ 0 & 0 & -\frac{\Omega_3}{2}e^{-i\omega_{CL}t} & \omega_d \end{pmatrix}. \tag{4.9}$$

We assume the repump laser to excite the $F' = 2$ level, whereas the cooling laser excites both hyperfine levels $F' = 2$ and $F' = 3$. The strength of these couplings are described

by the on-resonance Rabi frequencies Ω_1, Ω_2 and Ω_3 respectively. They are defined by

$$\Omega_1 = \Gamma\sqrt{\frac{I_{RL}}{2I_s^{12}}}, \quad \Omega_2 = \Gamma\sqrt{\frac{I_{CL}}{2I_s^{22}}} \quad \text{and} \quad \Omega_3 = \Gamma\sqrt{\frac{I_{CL}}{2I_s^{23}}}, \tag{4.10}$$

where $\Gamma = 2\pi \times 6 \times 10^6$ Hz is the decay rate of the transition $5^2P_{3/2} \rightarrow 5^2S_{1/2}$. For an *isotropic* excitation light field (i.e. a pumping field with equal components in all *three* possible polarizations) the saturation intensities of the hyperfine transitions $F = 1 \rightarrow F' = 2$, $F = 2 \rightarrow F' = 2$ and $F = 2 \rightarrow F' = 3$ can be calculated [61] to $I_s^{12} = 6.01$ mW/cm^2, $I_s^{22} = 10.01$ mW/cm^2 and $I_s^{23} = 3.58$ mW/cm^2. I_{CL} and I_{RL} denote the intensities of the cooling and repump laser, respectively.

The relaxation term R in the master equation represents spontaneous decay [105, 59] from the excited hyperfine levels a and d. In matrix representation we obtain

$$R = \begin{pmatrix} -(\Gamma_{ab} + \Gamma_{ac})\rho_{aa} & -\gamma_{ab}\rho_{ab} & -\gamma_{ac}\rho_{ac} & -\gamma_{ad}\rho_{ad} \\ -\gamma_{ab}\rho_{ba} & \Gamma_{ab}\rho_{aa} & 0 & -\gamma_{bd}\rho_{bd} \\ -\gamma_{ac}\rho_{ca} & 0 & \Gamma_{ac}\rho_{aa} + \Gamma_{dc}\rho_{dd} & -\gamma_{dc}\rho_{cd} \\ -\gamma_{ad}\rho_{da} & -\gamma_{bd}\rho_{db} & -\gamma_{dc}\rho_{dc} & -\Gamma_{dc}\rho_{dd} \end{pmatrix}, \tag{4.11}$$

where Γ_{ab}, Γ_{ac}, and Γ_{dc} are the energy and γ_{ab}, γ_{ac}, γ_{ad}, γ_{bd}, and γ_{dc} are the respective phase relaxation rates. Energy relaxation from $c \rightarrow b$ is neglected.

The energy relaxation rates appear in the diagonal elements of R and describe population loss of all involved levels due to spontaneous emission. In detail, Γ_{dc} is given by the spontaneous emission rate Γ of the $^2P_{3/2}$ excited state in ^{87}Rb, whereas Γ_{ac} and Γ_{ab} refer to spontaneous decay from $a \rightarrow c$ and $a \rightarrow b$. The ratio of Γ_{ab}/Γ_{ac} is given by the branching ratio of the respective hyperfine transitions and obeys the relation

$$\Gamma = \Gamma_{ac} + \Gamma_{ab}. \tag{4.12}$$

In the case of an isotropically polarized excitation light field the respective branching ratio is 1/2. Population loss acts also on the nondiagonal matrix elements of R. In general, the phase relaxation rate of a transition $n \rightarrow m$ is given by [59]

$$\gamma_{nm} = \frac{1}{2}(\Gamma_n + \Gamma_m), \tag{4.13}$$

where Γ_n denotes the sum of any population loss of level n, and Γ_m of m respectively. In our case the phase relaxation rates are given by

$$\gamma_{ab} = \frac{1}{2}(\Gamma_{ab} + \Gamma_{ac}), \qquad \gamma_{ac} = \tfrac{1}{2}(\Gamma_{ab} + \Gamma_{ac}), \qquad \gamma_{ad} = \frac{1}{2}(\Gamma_{ab} + \Gamma_{ac} + \Gamma_{dc}) \tag{4.14}$$

$$\gamma_{bd} = \frac{1}{2}\Gamma_{dc}, \qquad \gamma_{dc} = \tfrac{1}{2}\Gamma_{dc}. \tag{4.15}$$

From Eq. (4.8) we derive optical Bloch equations (OBE) for the four-level system as shown in Fig. 4.2. As this set of 16 coupled ordinary differential equations entails no new physics, they are not shown explicitly.

To solve the OBE by numerical integration [106] it is convenient to suppress any explicit time dependence in the coefficients of the OBE. Hence we introduce new variables $\hat{\rho}_{ik}$ $(i,k = a,b,c,d)$ which are given in matrix representation by

$$\hat{\rho} = \begin{pmatrix} \rho_{aa} & \rho_{ab}e^{i\omega_{RL}t} & \rho_{ac}e^{i\omega_{CL}t} & \rho_{ad} \\ \rho_{ba}e^{-i\omega_{RL}t} & \rho_{bb} & \rho_{bc}e^{-i(\omega_{RL}-\omega_{CL})t} & \rho_{bd}e^{-i\omega_{RL}t} \\ \rho_{ca}e^{-i\omega_{CL}t} & \rho_{cb}e^{i(\omega_{RP}-\omega_{CL})t} & \rho_{cc} & \rho_{cd}e^{-i\omega_{CL}t} \\ \rho_{da} & \rho_{db}e^{i\omega_{RL}t} & \rho_{dc}e^{i\omega_{CL}t} & \rho_{dd} \end{pmatrix}. \tag{4.16}$$

Photon correlation function

The photon correlation function as defined in Eq. (4.1) is a two-time expectation value of the electric field operators $\mathbf{E}^-$ and $\mathbf{E}^+$ of the scattered light field. Hence, features of the photon correlation function originate from the structure of $\mathbf{E}$. For the present case of a four-level atom Eq. (4.2) can be generalized by assuming that each dipole transition of the atom contributes to the field a term like $\mathbf{E}_S^+$ in Eq. (4.3). With the help of the quantum regression theorem [98] the resulting correlation function is given by

$$g^{(2)}(\tau) = \frac{\rho_{aa}(\tau) + \rho_{dd}(\tau)}{\rho_{aa}(\infty) + \rho_{dd}(\infty)}, \tag{4.17}$$

the ratio of the excited state populations at time τ and in the steady state ($\tau = \infty$). To evaluate this expression, the optical Bloch equations have to be solved for both steady-state and time-dependent cases.

The time-dependent solution depends on the initial conditions for the density matrix, and it is this point where different correlation functions can be distinguished [104]. Physically, the initial conditions describe the state of the atom after the emission of the first photon and consequently depend on the properties of that photon. Thus the correlation function depends on the wavelength of the first photon, but does not depend on the properties of the second photon.

In the HBT experiment performed (see next section) we do not distinguish from which transition the first photon came from. In this case the initial conditions for the numerical calculation of the density matrix elements $\rho_{aa}(\tau)$ and $\rho_{dd}(\tau)$ can be determined from the steady-state solution. All matrix elements vanish, $\rho_{ij}(0) = 0$, except

$$\rho_{bb}(0) = \frac{\Gamma_{ab}\rho_{aa}(\infty)}{(\Gamma_{ab}+\Gamma_{ac})\rho_{aa}(\infty) + \Gamma_{dc}\rho_{dd}(\infty)} \quad \text{and} \tag{4.18}$$

$$\rho_{cc}(0) = \frac{\Gamma_{ac}\rho_{aa}(\infty) + \Gamma_{dc}\rho_{dd}(\infty)}{(\Gamma_{ab}+\Gamma_{ac})\rho_{aa}(\infty) + \Gamma_{dc}\rho_{dd}(\infty)}. \tag{4.19}$$

These initial conditions characterize the state of the atom immediately after the emission of any photon: the atom is in the $^2S_{1/2}$ levels $|b\rangle$ and $|c\rangle$, whose relative population is given by the probabilities for spontaneous emission on the transitions $|a\rangle \to |b\rangle$, $|a\rangle \to |c\rangle$ and $|d\rangle \to |c\rangle$.

Following the described procedure we calculated the second-order correlation function $g^{(2)}(\tau)$ for different detunings Δ of the cooling laser (see Fig. 4.3). The repump laser is supposed to be on resonance. Increasing Δ leads to significant optical pumping to the $F = 1$ hyperfine ground level and to a breakdown of the two-level model. To demonstrate this effect, we calculated the photon correlation function for a two-level and four-level model for equal experimental parameters. For small detunings of the cooling laser, the second-order correlation functions based on a two-level and four-level model are indistinguishable.

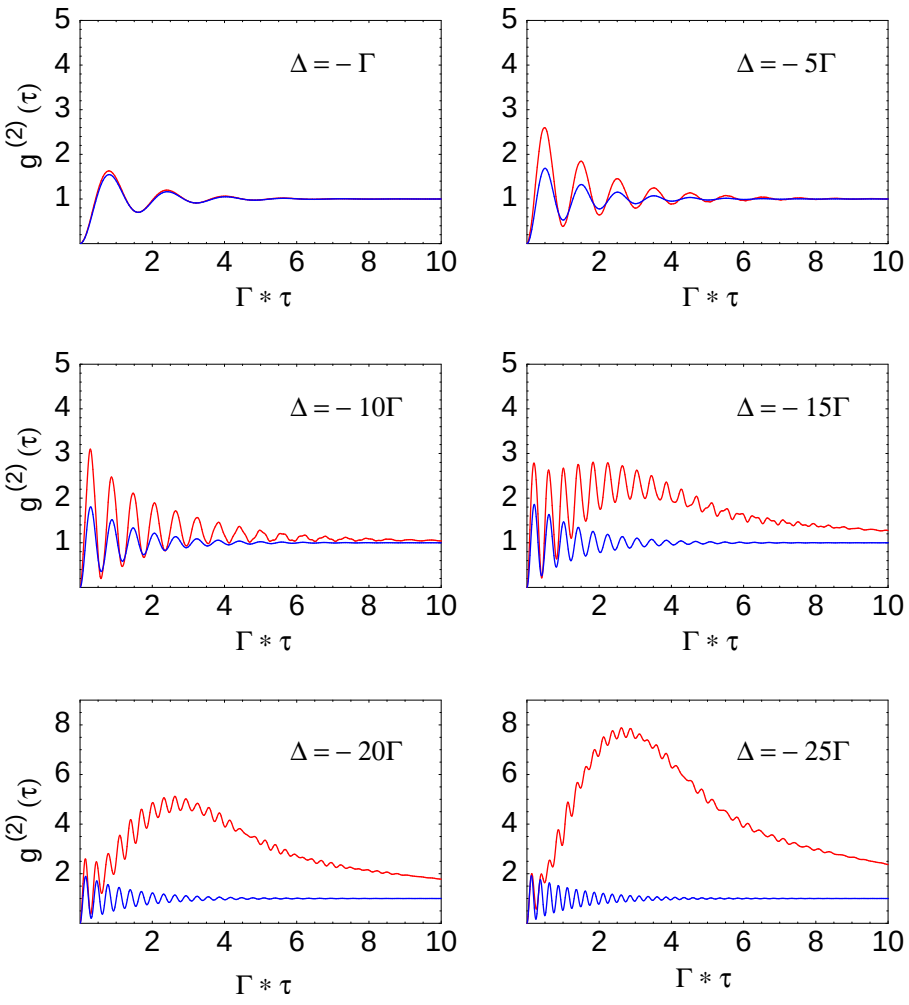

Figure 4.3: Calculated intensity correlation function $g^{(2)}(\tau)$ for different detunings Δ of the cooling laser. Blue line: two-level model; red line: four-level model. Experimental parameters: $I_{CL} = 100$ mW/cm^2, $I_{RL} = 12$ mW/cm^2

For larger detunings, corresponding to the situation of a single ^{87}Rb atom in a MOT or an optical dipole trap ($\Delta = -5.. - 10\Gamma$), the photon-pair correlation function of the four-level model shows deviations from the predictions of a simple two-level model. Most prominently the amplitudes of the Rabi oscillations exceed the upper limit of 2, which is predicted by a two-level model. Increasing the detuning of CL further increases the coupling to the level $|a\rangle$. Hence, the multi-level structure becomes more and more dominant. On the one hand this gives rise to several generalized Rabi frequencies, on the other hand to significant optical pumping to $F = 1$. For large detunings of the cooling laser ($\Delta > -20\Gamma$) the envelope of the correlation function shows the predicted feature of a three-level Λ-type atom [107]. The calculated correlation functions in Fig. 4.3 demonstrate this behavior very well.

4.2.4 Motional effects

Since the correlation function of the emitted light depends on the incident field, the motion of the atom will modify the photon correlations. Moving through the dipole trap the atom crosses various spots of a light interference pattern with different intensity and polarization. In our experiment this interference pattern is formed by the intersection of three pairs of counterpropagating σ^+-σ^- polarized laser beams used for laser cooling and fluorescence detection. The polarization of resonance fluorescence is determined by the magnetic orientation of the atom, which in turn depends on the local light field and changes on the time scale of atomic motion over an optical wavelength λ. Thus, in addition to correlations of the total intensity (4.1) one expects polarization effects to be visible in two-photon correlations [108].

Our measurements of the photon statistics are only sensitive to total intensity correlations caused by a standing light field pattern. Hence, I will restrict the following theoretical considerations only to total intensity correlations. Because of the entanglement of internal and external degrees of freedom, a proper description of the atomic dynamics is a non-trivial problem [109, 110]. I do not intend here to present a sophisticated theory but rather to describe the atomic motion in a simple phenomenological way.

Fokker-Planck equation

The trapping force in a dipole trap with a superimposed 1D σ^+-σ^- polarization gradient cooling includes two partial forces, i.e., the gradient force of the dipole potential (see Eq. 3.4) and the radiation pressure force [70] and can be expressed as a damped harmonic oscillation with spring constant κ and friction parameter α. In a simple model random fluctuations of the friction force may be characterized by a diffusion constant $D = k_B T/\alpha$, where T is the temperature (which has the meaning of an average kinetic energy of the trapped atom) and k_B denotes the Boltzmann constant. Treating the dipole potential as an effective harmonic potential, the theory of Brownian motion [80] can be

used to derive a Fokker-Planck equation for the atomic motion:

$$\frac{\partial}{\partial t}f = \frac{\kappa}{\alpha}\frac{\partial}{\partial z}(zf) + \frac{kT}{\alpha}\frac{\partial^2}{\partial z^2}f. \tag{4.20}$$

Here the function $f = f(z, z_0, t)$ describes the probability density for the atom to be at time t at position z for the initial atomic position $z(t = 0) = z_0$.

For atomic motion in potential-free space (situation in an optical molasses), the Fokker-Planck equation reduces to a diffusion equation

$$\frac{\partial}{\partial t}f = D\frac{\partial^2}{\partial z^2}f. \tag{4.21}$$

The probability function f which solves this differential equation has the form

$$f(z, z_0, t) = \frac{1}{\sqrt{2\pi}\sigma(t)}e^{-\frac{(z-z_0)^2}{2\sigma^2(t)}}, \tag{4.22}$$

where $\sigma(t) = \sqrt{2Dt}$ describes the temporal spread of the atomic positional probability, which is an expanding Gauss if there is no potential.

Total intensity correlation function

In order to gain physical insight how the diffusive motion of a single atom in an intensity modulated standing light field will influence the total intensity correlation function, I will start with an atom modeled by a classical emitter with an induced dipole moment proportional to the local light field. Then the corresponding total correlation function is given by

$$g^{(2)}_{tot}(\tau) = \frac{\int\int_{-\infty}^{\infty} I(z_0)I(z)f(z_0, z_0, \infty)f(z, z_0, \tau)dzdz_0}{\langle I(t)\rangle^2}, \tag{4.23}$$

where the position dependent fluorescence intensity is given by $I(z)$ and the probability density for the atom to be at time t at z, if its initial position was $z(t = 0) = z_0$, is $f(z, z_0, t)$.

Let's assume that the atom moves "diffusively" in potential-free space in a one-dimensional light field configuration, produced by two plane waves counterpropagating along z with the same frequency, equal amplitudes and equal linear polarizations ($I(z) \propto \cos^2(kz)$). Then the total second-order correlation function $g^{(2)}_{tot}(\tau)$ of the emitted fluorescence light is given by [108]

$$g^{(2)}_{tot}(\tau) = 1 + \frac{1}{2}e^{-2k^2\sigma^2(\tau)}. \tag{4.24}$$

This correlation function contains information on the character of the atomic motion. For instance, diffusion ($\sigma \propto \sqrt{t}$) is indicated by an exponential decay whereas ballistic

motion ($\sigma \propto t$) yields a Gaussian decay. All correlations vanish after the atom has moved more than a distance of $\lambda/2$. The corresponding decay time constant τ_0 is then given by

$$\tau_0 = \frac{1}{4k^2 D}, \tag{4.25}$$

where $k = 2\pi/\lambda$. As the diffusion constant D depends on the atomic temperature T and the friction parameter α, the preceding relation allows to determine the atomic temperature provided the friction parameter was calculated [70] or measured.

4.3 Experimental determination of the photon statistics

4.3.1 Setup

The correlation function $g^{(2)}(\tau)$ of the collected fluorescence light is measured in a standard Hanbury-Brown-Twiss configuration with two single photon detectors ($D1$ and $D2$) behind a beam splitter (BS, Fig. 4.4). To suppress cross talk in the optical setup, infront of each detector we insert a bandpass filter (IF) blocking unwanted fluorescence light caused by the breackdown flash of the other silicon avalanche photo diode which follows the detection of a photon [111]. The differences of detection times $\tau = t_1 - t_2$ of photon pair events are then recorded in a storage oscilloscope with a time resolution of 100 ps. However, the minimum bandwidth of the measurements is limited by the 1.4 ns timing jitter of the detectors.

The normalized distribution of time differences τ is equivalent to the second order correlation function $g^{(2)}(\tau)$ as long as τ is much smaller than the mean time difference between two detection events [112]. For correct normalization of the measured $g^{(2)}(\tau)$ we divide the coincidences in each time bin $\Delta\tau$ by $r_1 \times r_2 \times \Delta\tau \times T_{int}$, where r_1 and r_2 are the mean count rates of the two detectors, and T_{int} is the total integration time with an atom in the trap.

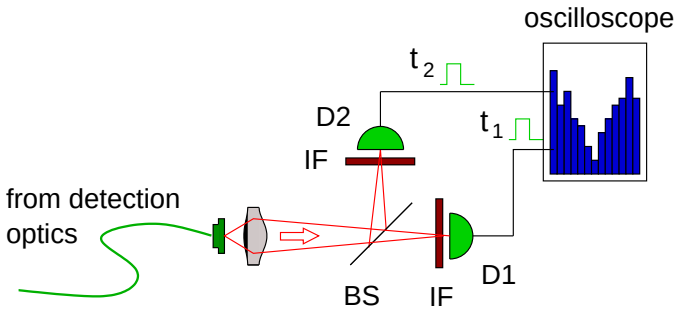

Figure 4.4: Hanbury-Brown-Twiss setup to measure the photon pair correlation function $g^{(2)}(\tau)$. The fluorescence light is sent through a beam splitter BS onto two single photon detectors D1, D2 to record detection time differences $\tau = t_1 - t_2$.

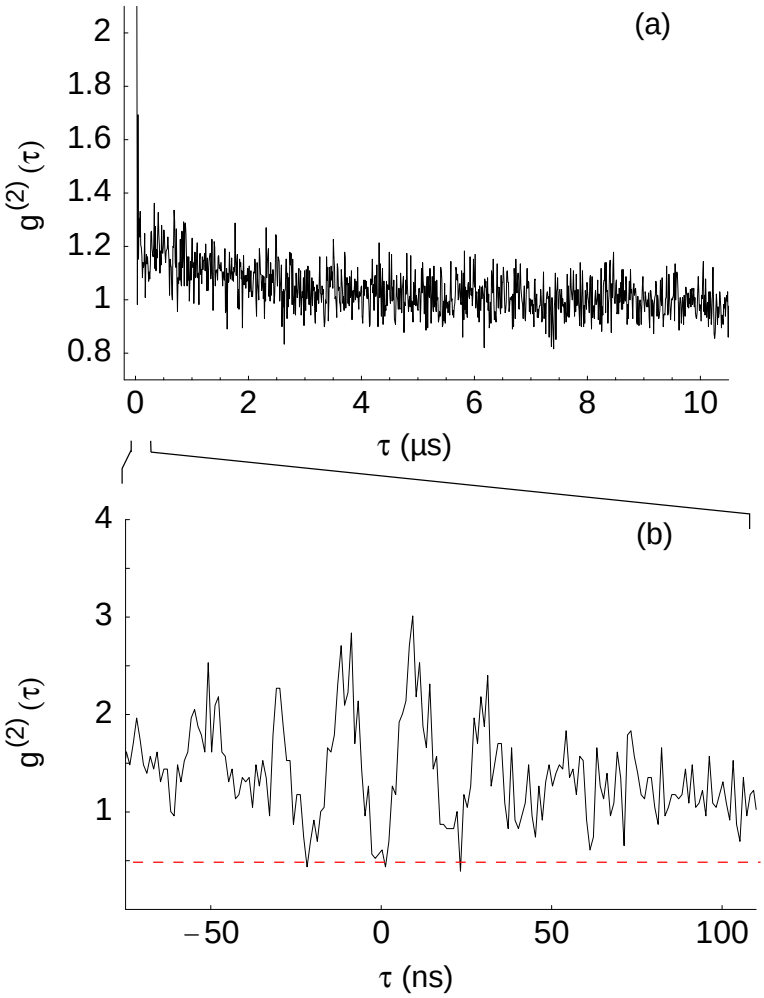

Figure 4.5: Second-order correlation function $g^{(2)}(\tau)$ of the resonance fluorescence of a single ^{87}Rb atom. **(a)** On long timescales, $g^{(2)}(\tau)$ shows a monotonous decay for $\mid \tau \mid \leq 2..3\mu$s. **(b)** On short timescales, clear photon anti-bunching at $\tau = 0$ and oscillations due to Rabi flopping are observed. The red dashed line indicates accidental coincidences due to the dark count rate of the detectors. Experimental parameters: $I_{CL} = 103\,\mathrm{mW/cm^2}$, $I_{RL} = 12\,\mathrm{mW/cm^2}$, $\Delta/2\pi = -31$ MHz, $\hat{U} = 0.38$ mK.

4.3.2 Experimental results

In a first experiment we measured the second-order correlation function of the light collected from the center of our dipole trap potential in the continous loading mode of the trap (cooling and repump lasers are present during the whole measurement time). In this operating regime we observe characteristic steps in the detected fluorescence signal (see Fig. 3.14). To minimize background contributions, photon correlations are acquired only at times we observe fluorescence exceeding a threshold of 1200 counts per second (cps), i.e. when an atom was inside the trap.

Fig. 4.5 shows the resulting correlation function $g^{(2)}(\tau)$ for a dipole potential of $\hat{U} = 0.38 \pm 0.04$ mK, a total cooling laser intensity $I_{CL} \approx 103\text{mW/cm}^2$ and detuning $\Delta/2\pi$ of -31 MHz respectively. On a μs timescale the correlation function shows an exponential decay from the asymptotic value 1.24 at $\tau = 0$ to 1.0 for large τ with a time constant of 1.8 μs. This decay is caused by the fluorescence of an atom undergoing diffusive motion in the intensity-modulated light field of the cooling beam configuration (see 4.2.4).

On short timescales, most prominently the uncorrected minimum value $g^{(2)}(0) = 0.52 \pm 0.14$ at zero delay $\tau = 0$ clearly proves photon anti-bunching of the emitted fluorescence. Including accidental coincidences due to a dark count rate of 300 s^{-1} of each detector (dashed red line in Fig. 4.5), we derive a corrected minimum value $g^{(2)}_{corr}(\tau = 0) = 0.02 \pm 0.14$. Within our experimental errors this is compatible with perfect photon anti-bunching verifying the presence of only one single atom in the dipole trap. Furthermore, the signature of Rabi-oscillations is observed due to the coherent interaction of the cooling and repump laser fields with atomic hyperfine levels involved in the excitation process. The oscillation frequency is in good agreement with the simple two-level model [99] and the oscillation amplitude is damped out on the expected timescale of the $5^2P_{3/2}$ excited state lifetime. Increasing the dipole laser power from 16.7 mW to 35.5 mW without changing the laser cooling parameters increases the detuning of the cooling laser to the hyperfine transition $5^2S_{1/2}(F = 2) \rightarrow 5^2P_{3/2}(F' = 3)$ due to an increase of the AC Stark-shift of the atomic levels in the dipole trap laser field. This effect was observed as the expected increase of the oscillation frequency from 47.5 MHz to 62.5 MHz (see Fig. 4.7).

In contrast to a two-level atom, the measured and background corrected correlations in Fig. 4.7(b) show a maximum value of 6 close to $\tau = 0$. This increase of the oscillation amplitude is a consequence of the atomic multi-level structure and can be explained very well by the four-level model presented in the theory section of this chapter.

For a detailed interpretation of the measured $g^{(2)}(\tau)$ functions on a short timescale we calculated $g^{(2)}(\tau)$ on the base of the four-level model for given experimental parameters and multiplied it with the function $1 + Ae^{-\tau/\tau_0}$, describing the additional decay contribution due to motion in the intensity modulated light field of the cooling beam configuration. The parameters A and τ_0 we determined from an extra fit to the background corrected correlation function on the μs time scale (see Fig. 4.6). The light-shift

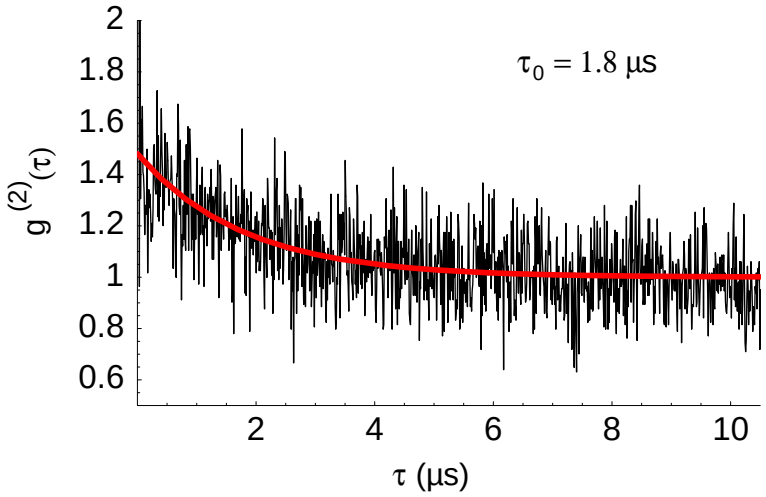

Figure 4.6: Background corrected second-order correlation function $g^{(2)}(\tau)$ in the resonance fluorescence of a single atom in the dipole trap and fit with model-function (4.24). Experimental parameters: $I_{CL} = 103$ mW/cm^2, $I_{RL} = 12$ mW/cm^2, $\Delta/2\pi = -31$ MHz, $\hat{U} = 0.38$ mK.

of the atomic hyperfine levels is calculated on the basis of Eq. 3.23 for both the ground levels $F = 1$ and $F = 2$ as well as the relevant hyperfine levels $F' = 2$ and $F' = 3$ of the $5^2P_{3/2}$ state and included into the four-level model. Furthermore a reduction of the light-shift potential is incorporated in the calculations due to a finite kinetic energy of the atom of approximately 100 μK. For two different depths of the optical trapping potential we find good agreement of the measured second order correlation function $g_\tau^{(2)}$ with the calculated one (see Fig. 4.6).

4.4 Conclusion and discussion

To prove that only single atoms are stored in our dipole trap, the statistical properties of the detected fluorescence light were studied with a Hanbury-Brown-Twiss setup. The measured second-order correlation function $g^{(2)}(\tau)$ of the detected fluorescence light exhibits strong photon antibunching verifying the presence of a single atom. In addition the measured two-photon correlations show the internal and external dynamics of the atomic hyperfine levels involved in the excitation process. Due to the AC Stark-shift of the atomic levels in the dipole potential and the resulting increase of the detuning of the cooling light, significant population is continuously transferred to the second hyperfine ground state $5^2S_{1/2}, F = 1$. Thus the atom-light interaction can not be modeled with a simple two-level model. An atomic four-level model is developed and its predictions are

compared with measured experimental data. Within our experimental errors we find good agreement of the calculated second order correlation function with the measured correlation function.

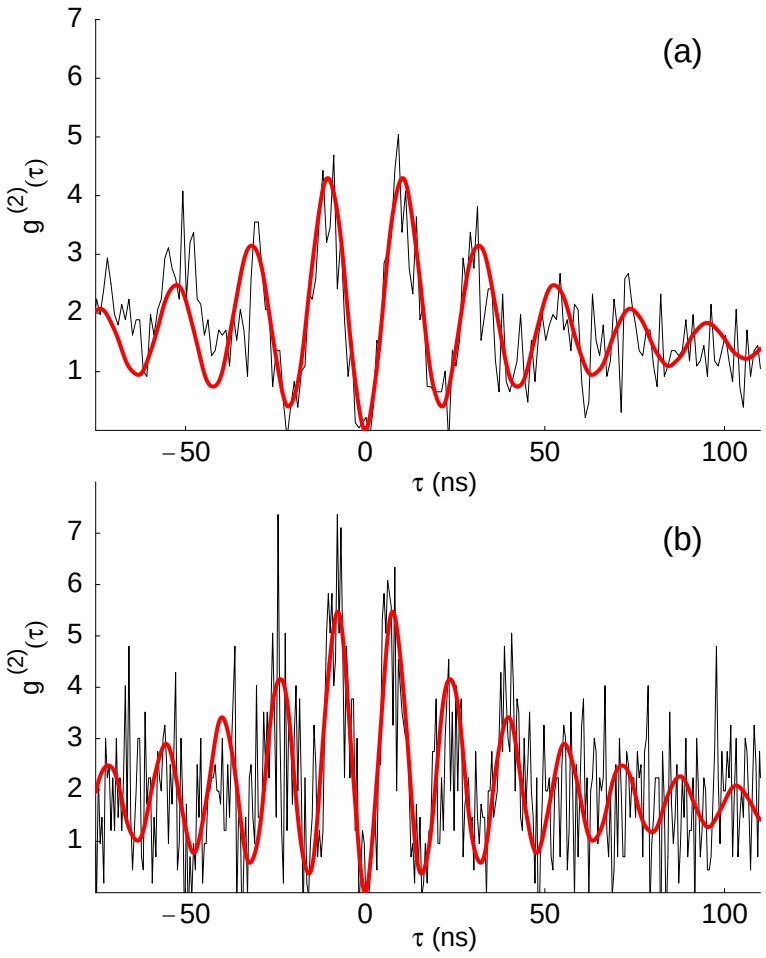

Figure 4.7: Intensity correlation function $g^{(2)}(\tau)$ (background corrected) of the resonance fluorescence from a single ^{87}Rb atom in the dipole trap for two different trap depths. Red solid line: calculation. Experimental parameters: $I_{CL} = 103$ mW/cm^2, $I_{RL} = 12$ mW/cm^2, $\Delta/2\pi = -31$ MHz, **(a)** $\hat{U} = 0.38$ mK, **(b)** $\hat{U} = 0.81$ mK.

5 Detection of atomic superposition states

5.1 Introduction

To verify entanglement between the spin state of a single atom and the polarization of a spontaneously emitted photon, one has to perform correlated local measurements of the internal quantum states of the atom and the photon. The polarization state of a single photon can be measured relatively simply by a combination of a polarization filter and a single photon detector. However, the measurement of the spin state of a single atom is not trivial and therefore the primary experimental challenge of the present work.

In experiments with trapped ions, the state of an atomic qubit encoded in the internal atomic level structure can be measured with almost perfect detection efficiency on the basis of the "electron shelving" method [113]. This technique has the relevant property that depending on the internal quantum state, the atom scatters fluorescence light from an incident laser light field. Hence, the presence or absence of atomic fluorescence light indicates directly the quantum state of the atom.

In this chapter I will show how the experimental techniques of coherent population trapping (CPT) and stimulated Raman adiabatic passage (STIRAP) can be used for phase-sensitive probing of coherent superposition states of a single atom. Therefore I will first give a short theoretical review on coherent population trapping and adiabatic population transfer in three- and four-level systems, before I present experiments that allow to detect a single Rubidium 87 atom in a coherent superposition $|m_F = -1\rangle + e^{i\phi}|m_F = +1\rangle$ of the Zeeman sublevels $m_F = \pm 1$ of the hyperfine ground state $^2\mathrm{S}_{1/2}$, $F = 1$.

5.2 Theoretical framework

Atomic states that do not couple to an incident light field are called dark states and are used in the present work in various ways to prepare and analyze atomic states. In general one can distinguish three kinds of dark states. (1) The atom is in a state that can couple to a light field due to selection rules of electromagnetic dipole transitions. But the incident light field is detuned far-off-resonance and therefore couples negligibly to the incident light. (2) The atom is in a state that can not couple to a light field due to atomic selection rules. (3) The atom is in a coherent superposition of two ground states

and exposed to respective resonant light fields. But due to destructive interference of the excitation amplitudes the absorption is canceled and the atom remains dark.

Dark states of the first two kinds can be populated relatively simply by optical pumping and are insensitive to experimental parameters, provided the atomic states do not mix due to a strong perturbation effect, e.g. the interaction with a strong electric or magnetic field. Coherent dark states of the third case are much more sensitive to experimental parameters because they depend on the phase coherence of the incident light fields and on the temporal evolution of the respective atomic energy levels. The understanding for the preparation and the analysis of coherent dark states is essential for the state selective detection of the atomic qubit. Hence, I will give a short review on coherent population trapping and its applications.

5.2.1 Coherent population trapping - dark states

We consider now coherent population trapping in a three-level atom interacting with two classical light fields of angular frequencies ω_1 and ω_2 as shown in Fig. 5.1. We assume the atom has only three energy levels in a so-called Λ configuration in which two lower levels $|b\rangle$ and $|c\rangle$ are coupled to a single upper level $|a\rangle$.

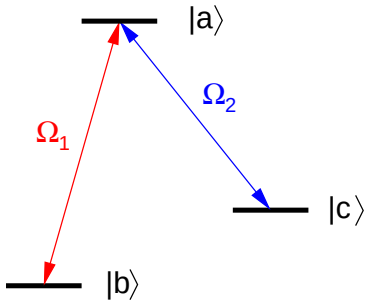

Figure 5.1: Three-level system coupled by two lasers of angular frequencies ω_1 and ω_2, respectively. Due to destructive interference of the respective transition amplitudes the linear superposition $|b\rangle - e^{i\phi}|c\rangle$ of the ground states does not couple to the resonant light fields (see Eq. 5.6).

The Hamiltonian H for the system, in the rotating-wave approximation, is given by

$$H = H_0 + H_1, \tag{5.1}$$

where

$$H_0 = \hbar(\omega_a|a\rangle\langle a| + \omega_b|b\rangle\langle b| + \omega_c|c\rangle\langle c|), \tag{5.2}$$

$$H_1 = -\frac{\hbar}{2}(\Omega_1 e^{-i(\omega_1+\phi_1)t}|a\rangle\langle b| + \Omega_2 e^{-i(\omega_2+\phi_2)t}|a\rangle\langle c|) + H.c. \tag{5.3}$$

Here $\Omega_1 \exp(-i\phi_1)$ and $\Omega_2 \exp(-i\phi_2)$ are the Rabi frequencies associated with the coupling of the field modes to the atomic transitions $|a\rangle \rightarrow |b\rangle$ and $|a\rangle \rightarrow |c\rangle$, respectively. The atomic wave function of the system can be written in the form

$$|\psi(t)\rangle = c_a(t)e^{-i\omega_a t}|a\rangle + c_b(t)e^{-i\omega_b t}|b\rangle + c_c(t)e^{-i\omega_c t}|c\rangle, \tag{5.4}$$

where the $c_i(t)$ are the complex amplitudes of the respective atomic basis states $|i\rangle$. Its dynamics is governed by the time-dependent Schrödinger equation $i\hbar|\dot{\psi}(t)\rangle = H|\psi(t)\rangle$.

We now assume the initial atomic state to be a superposition of the two lower levels $|b\rangle$ and $|c\rangle$

$$|\psi(0)\rangle = \cos\theta|b\rangle + \sin\theta e^{-i\psi}|c\rangle. \tag{5.5}$$

For $\Omega_1 = \Omega_2$, $\theta = \pi/4$, and $\phi_1 - \phi_2 - \psi = \pm\pi$ it can be verified [49] that

$$|\psi_d(0)\rangle = \frac{1}{\sqrt{2}}(|b\rangle - e^{i\phi}|c\rangle) \tag{5.6}$$

is one of three eigenstates of the Hamiltonian H, whereby the phase $\phi = \phi_1 - \phi_2$ is given by the phase difference between Ω_1 and Ω_2. The mentioned eigenstate has a zero eigenvalue and it is the only eigenstate which does not include a contribution of the excited level $|a\rangle$. Due to destructive interference of the transition amplitudes the atomic population is *trapped* in a coherent superposition of the lower states and there is no absorption or scattering even in the presence of resonant light fields. So this state is called "dark". However, the orthogonal state $|b\rangle + e^{i\phi}|c\rangle$ couples to the incident light fields Ω_1 and Ω_2 because of constructive interference of Ω_1 and Ω_2. Hence, this state is called "bright".

5.2.2 Stimulated Raman adiabatic passage

An interesting and powerful application of coherent population trapping in three-state atoms is the transfer of population with a counter-intuitive sequence of pulses [115]. This technique called stimulated Raman adiabatic passage (STIRAP) allows, in principle, a complete coherent population transfer from a single initial to a single final quantum state [115, 114, 116, 117, 118, 119]. The underlying physical mechanism is the existence of an adiabatically decoupled (or dark) state, which at early and late times coincides with the initial and target quantum state respectively. This process is robust against moderate variations of the pulse form, area and delay between the pulses and therefore is well suited for experimental applications.

Consider again the three-level system in Fig. 5.1. Provided we start at $t = 0$ with the atom in state $|b\rangle$ and $\Omega_1 = 0$ with Ω_2 finite and then proceed to turn Ω_2 off while adiabatically turning Ω_1 on (see Fig.5.2), we will end up with the atom in the state $|c\rangle$. This is made clear by realizing that the atom is in the time-dependent dark state [114]

$$|\psi_d(t)\rangle = \cos\theta(t)|b\rangle - \sin\theta(t)e^{i\phi}|c\rangle, \tag{5.7}$$

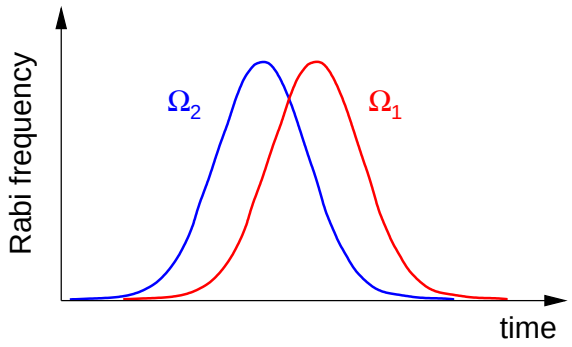

Figure 5.2: Time dependence of the Rabi frequencies required for efficient population transfer from the initial state $|b\rangle$ to the final state $|c\rangle$ under adiabatic following conditions [114].

where

$$\tan\theta(t) = \frac{\Omega_1(t)}{\Omega_2(t)}, \tag{5.8}$$

and ϕ is the relative phase between Ω_1 and Ω_2. When the pulse Ω_2 precedes the pulse Ω_1, the mixing angle θ is initially zero. Therefore the trapped state $|\psi_d(t)\rangle$ coincides initially with state $|b\rangle$ while $\langle c|\psi_d(t=0)\rangle = 0$. When the pulse areas are sufficiently large, $\Omega_{eff}T \gg 1$, where $\Omega_{eff} = \sqrt{\Omega_1^2 + \Omega_2^2}$ is the effective two-photon Rabi frequency and T is the interaction time, non-adiabatic coupling to intermediate state $|a\rangle$ is small. According to (5.7) the population then remains in the dark state $|\psi_d(t)\rangle$ and evolves into $|c\rangle$, depending on the evolution of the mixing angle θ.

5.2.3 Tripod STIRAP

An interesting and powerful extension of STIRAP is tripod-STIRAP which allows to create or probe, in a robust way, a superposition of atomic states [120, 121, 122, 123].

In this case the coupling scheme consists of four atomic levels coupled by three lasers (see Fig. 5.3). The Hamiltonian of a resonant tripod system has four adiabatic states [120] that are parametrized by two mixing angles $\theta(t)$ and $\Phi(t)$, defined by

$$\tan\theta(t) = \frac{\Omega_1(t)}{\Omega_2(t)}, \quad \text{and} \quad \tan\Phi(t) = \frac{\Omega_{1^-}(t)}{\Omega_{1^+}(t)}, \tag{5.9}$$

where Ω_{1^-}, Ω_{1^+} and Ω_2 are the Rabi frequencies of the coupling lasers and $\Omega_1(t) = \sqrt{\Omega_{1^+}^2(t) + \Omega_{1^-}^2(t)}$. Two of the adiabatic states are orthogonal degenerate dark states, i.e., states without components of the intermediate state $|a\rangle$,

$$|\psi_d^1(t)\rangle = \cos\theta(t)\left(\sin\Phi(t)|b^-\rangle + \cos\Phi(t)e^{i\phi_1}|b^+\rangle\right) - \sin\theta(t)e^{i\phi_2}|c\rangle, \tag{5.10}$$

$$|\psi_d^2(t)\rangle = \cos\Phi(t)|b^-\rangle - \sin\Phi(t)e^{i\phi_1}|b^+\rangle, \tag{5.11}$$

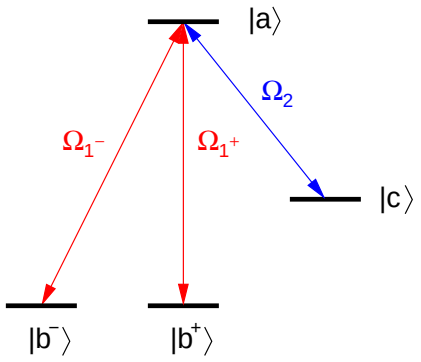

Figure 5.3: Four-level system of tripod-STIRAP coupled by three lasers. The Rabi frequencies of the pump and Stokes laser are Ω_1 and Ω_2, respectively.

where ϕ_1 and ϕ_2 are the relative phase between Ω_{1^-} and Ω_{1^+}, and Ω_{1^-} and Ω_2 respectively.

In the present experiment, there is only one linearly polarized pump laser, which produces two coincident and copropagating σ^+ and σ^- polarized fields with the same intensity; hence $\Omega_{1^-} = \Omega_{1^+}$ and $\Phi = \pi/4$. Moreover, because the pump field Ω_1 is delayed with respect to the Stokes field Ω_2, we have $\theta(0) = 0$ and $\theta(+\infty) = \pi/2$. Hence, in the adiabatic limit, the atom evolves along the adiabatic path $|\psi_d^1(t)\rangle$ [120] from the initial state

$$|\psi_i\rangle = \frac{1}{\sqrt{2}}\left(|b^-\rangle + e^{i\phi_1}|b^+\rangle\right) \tag{5.12}$$

to the final state $|c\rangle$. If the atom was initially prepared in the orthogonal state $1/\sqrt{2}(|b^-\rangle - e^{i\phi_1}|b^+\rangle)$, the population will remain in this dark state during the STIRAP pulse sequence and will not be transferred to $|c\rangle$.

Choice of the atomic measurement basis

For $\phi_1 = 0$, the associated bright and dark states

$$\frac{1}{\sqrt{2}}(|b^-\rangle + |b^+\rangle) \quad \text{and} \quad \frac{1}{\sqrt{2}}(|b^-\rangle - |b^+\rangle), \tag{5.13}$$

form an orthonormal basis for the two ground states $|b^-\rangle$ and $|b^+\rangle$. This basis is denoted in the following chapter the σ_x basis, provided that the ground states $|b^-\rangle$ and $|b^+\rangle$ are identified with the respective eigenstates $|\uparrow\rangle$ and $|\downarrow\rangle$ of σ_z. To measure the atomic qubit in the complementary σ_y basis one has to set the relative phase ϕ_1 of Ω_{1^-} and Ω_{1^+} to $\pi/2$. We find, that the corresponding set of orthogonal bright and dark states

$$\frac{1}{\sqrt{2}}(|b^-\rangle + i|b^+\rangle) \quad \text{and} \quad \frac{1}{\sqrt{2}}(|b^-\rangle - i|b^+\rangle). \tag{5.14}$$

are the eigenstates of σ_y.

5.3 Phase-sensitive probing of Zeeman superposition states

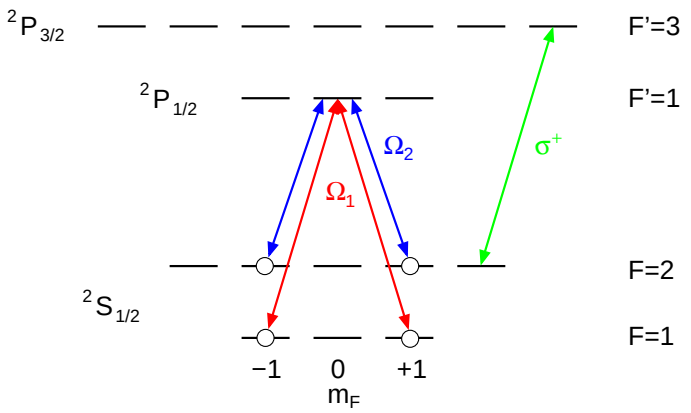

Figure 5.4: Coupling scheme for the analysis of coherent superposition states. The STIRAP process transfers the superposition $\frac{1}{\sqrt{2}}(|1,-1\rangle+e^{i\phi}|1,+1\rangle)$ to the $F=2$ ground state whereas the orthogonal state $\frac{1}{\sqrt{2}}(|1,-1\rangle-e^{i\phi}|1,+1\rangle)$ remains in $F=1$. To distinguish the hyperfine ground states, a σ^+ polarized detection laser pulse resonant to the cycling transition $^2S_{1/2}, F=2 \rightarrow {}^2P_{3/2}, F'=3$ is used.

5.3.1 Introduction

For the detection of atomic superposition states we set up a STIRAP-laser system which couples a superposition of the Zeeman sub-levels $m_F=-1$ and $m_F=+1$ of the hyperfine ground level $F=1$ to a superposition of Zeeman sublevels of $F=2$. Because the adiabatic population transfer has to evolve via a dark state that contains only the initial levels (here $|1,-1\rangle$ and $|1,+1\rangle$) and the target state $F=2$ (a certain superposition of Zeeman sublevels), a proper readout of the atomic phase information can only be realized if the intermediate level of the STIRAP process has the same or less Zeeman manifold as the hyperfine ground level $F=1$.

In the present experiment the atomic state detection is performed in two steps.

- A linearly polarized STIRAP-laser pulse, propagating along the quantization axis z (parallel to the observation direction of atomic fluorescence light), couples to a superposition $\frac{1}{\sqrt{2}}(|F=1,m_F=-1\rangle+e^{i\phi}|F=1,m_F=+1\rangle)$ and transfers the atomic population adiabatically via the intermediate level $^2P_{1/2}, F=1, m_F=0$ to the final level $F=2$ while the orthogonal state $\frac{1}{\sqrt{2}}(|F=1,m_F=-1\rangle-$

$e^{i\phi}|F=1, m_F=+1\rangle$) remains in $F=1$. The relative phase $\phi = 2\alpha$ between $|F=1, m_F=-1\rangle$ and $|F=1, m_F=+1\rangle$ is determined by the linear polarization angle α of the pump field Ω_1 with respect to the x axis.

- After the state-selective population transfer the atom is in a superposition of the two hyperfine ground states $F=1$ and $F=2$. To discriminate these states we apply a detection laser pulse resonant to the cycling transition ${}^2S_{1/2}, F=2 \rightarrow {}^2P_{3/2}, F'=3$. Provided the atom is in $F=2$ it scatters photons from this laser beam, and with each scattering event the atom acquires an additional photon momentum $\hbar\vec{k}$. After approximately 40 to 50 scattering events the atom is pushed out of the trap. Finally, to read out the atomic state the cooling and repump lasers of the MOT are switched on and the atomic fluorescence light is integrated for 30..60 ms to decide if the atom is still in the trap or not.

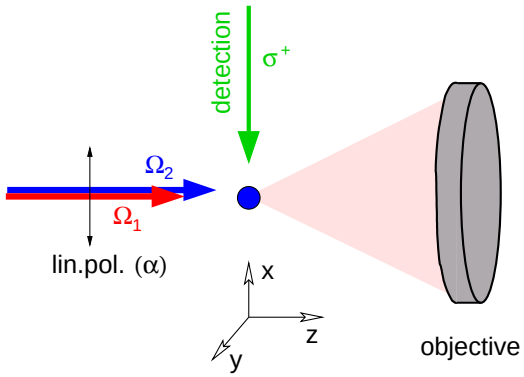

Figure 5.5: Geometry of the experiment. The two circularly polarized pump laser components (here denoted by Ω_1) are generated by a linearly polarized laser propagating in the z direction, whose polarization forms an angle α with the x axis. The propagation of the circularly polarized detection pulse is parallel to the x axis.

The experimental confirmation of this sequence is accomplished in two steps. In a first simple experiment we verify that we can distinguish atomic populations in the hyperfine ground levels $F=1$ and $F=2$. Then we prepare atomic Zeeman superposition states via CPT. Finally, to read out the phase ϕ of such superpositions we apply a STIRAP technique.

5.3.2 Hyperfine state preparation and detection

The analysis of coherent superposition states requires the ability to discriminate in a second step atomic population in $F=1$ from $F=2$ with high efficiency. This task can be accomplished by scattering atomic fluorescence light from the closed transition

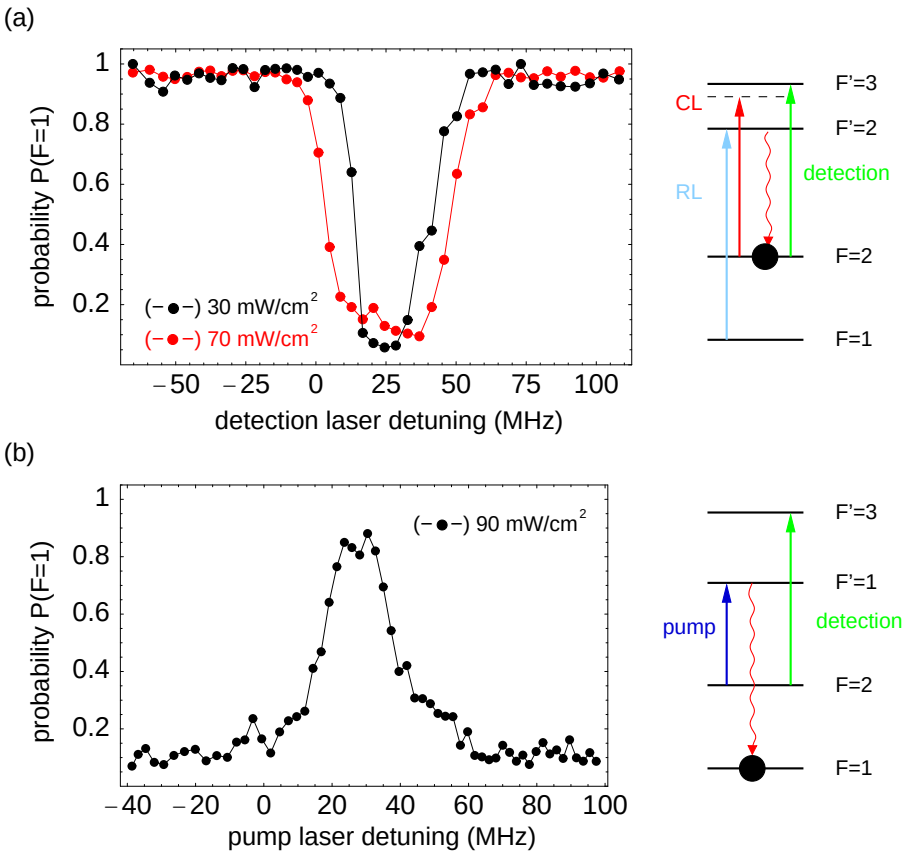

Figure 5.6: Probability to detect the atom in the hyperfine ground state $F = 1$ after application of a hyperfine state selective detection laser pulse as a function of (a) the detection, (b) the pump laser detuning provided the atom is initially prepared in (a) $F = 2$, (b) $F = 1$ respectively. The relative detunings refer to transitions undisturbed by the AC-Stark effect of the dipole laser beam.

$^2S_{1/2}, F = 2 \rightarrow {}^2P_{3/2}, F' = 3$ by applying resonant circularly polarized laser light. Provided the atom is prepared in $F = 1$, then the atomic population is shelved in this "dark" state because the incident laser field does not couple to this level and the atom scatters no light. In contrast, if the atom is prepared in any Zeeman sub-level of $F = 2$ it will be pumped within a few scattering cycles to the outer Zeeman sub-level $m_F = \pm 2$ and will scatter many photons from the ideal two-level transition $^2S_{1/2}, F = 2, m_F = \pm 2 \rightarrow {}^2P_{3/2}, F' = 3, m'_F = \pm 3$ whereby off-resonant excitation to $^2P_{3/2}, F' = 2$ is suppressed by atomic selection rules. The presence or absence of atomic fluorescence light indicates in which hyperfine ground state the atom is.

In contrast to electromagnetically trapped ions, shelving can not be applied in the usual way to optically trapped atoms. The main reason for this is, that atoms are removed from a dipole trap by the transfer of few photon recoil-momentum kicks $\hbar\vec{k}$.

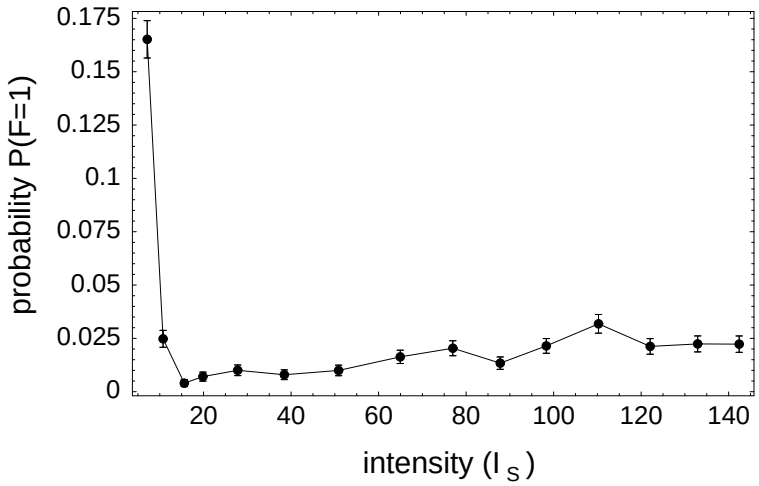

Figure 5.7: Probability to detect a single atom in the hyperfine ground state $F = 1$ as a function of the detection laser intensity in units of the saturation intensity I_S after the atom was pumped to the hyperfine ground state $F = 2$. Optimal hyperfine state detection is achieved for 20..40 saturation intensities I_S and a pulse duration of 10 μs.

Therefore, it is not possible to scatter atomic fluorescence light for at least 10 ms, which is the minimum integration time to discriminate "one" atom in the trap from the case where "no" atom is present whereby the detected fluorescence rate is given by the dark count of the single photon detector (see chapter 3). But combining this push-out effect with a redetection sequence of the atom realizes a destructive state detection [77]. Provided that the atom is detected after application of the detection pulse we know that the population was in $F = 1$. However, if the atom is not detected we know that the atom was in $F = 2$.

To demonstrate this property, the atom is prepared in the hyperfine ground state $F = 2$ by optical pumping. For this purpose we switch on the cooling and repump laser of our MOT and wait for a single atom. If the atomic fluorescence exceeds a certain threshold value, the cooling laser is switched off 4 ms before the repump laser. As the repump laser serves to depopulate the $F = 1$ level the whole atomic population is pumped to the "dark" state $F = 2$. Then we apply a 10 μs long circularly polarized detection laser pulse with a variable detuning and finally we switch on again the cooling and repump-laser and collect fluorescence light from the dipole trap region for 55 ms, in order to check whether the atom is still in the trap or not.

In Fig. 5.6 (a) the probability of redetection is plotted as a function of the detection laser detuning for different laser intensities. If the detection pulse is resonant to the light-shifted transition $^2S_{1/2}, F = 2 \rightarrow {}^2P_{3/2}, F' = 3$ the atom is removed from the dipole trap. If the detection pulse is too intense (red data points) the maximum detection efficiency

on resonance will drop due to an increase of nonresonant excitation to ${}^2P_{3/2}, F' = 2$ and subsequent decay to $F = 1$. This effect is directly observed as power broadening of the line shape. In a second experiment (see Fig. 5.6 (b)) the atom is prepared in the hyperfine ground state $F = 1$ by an additional pump laser pulse before applying the push-out and redetection sequence. When the pump laser is on resonance with the light-shifted hyperfine transition ${}^2S_{1/2}, F = 2 \rightarrow {}^2P_{3/2}, F' = 1$ the redetection probability reaches its maximum because the atom is more efficiently pumped into the dark state $F = 1$. Out of resonance the excitation probability to ${}^2P_{3/2}, F' = 1$ decreases, such that the atomic population basically remains in $F = 2$ and the atom is kicked out of the trap.

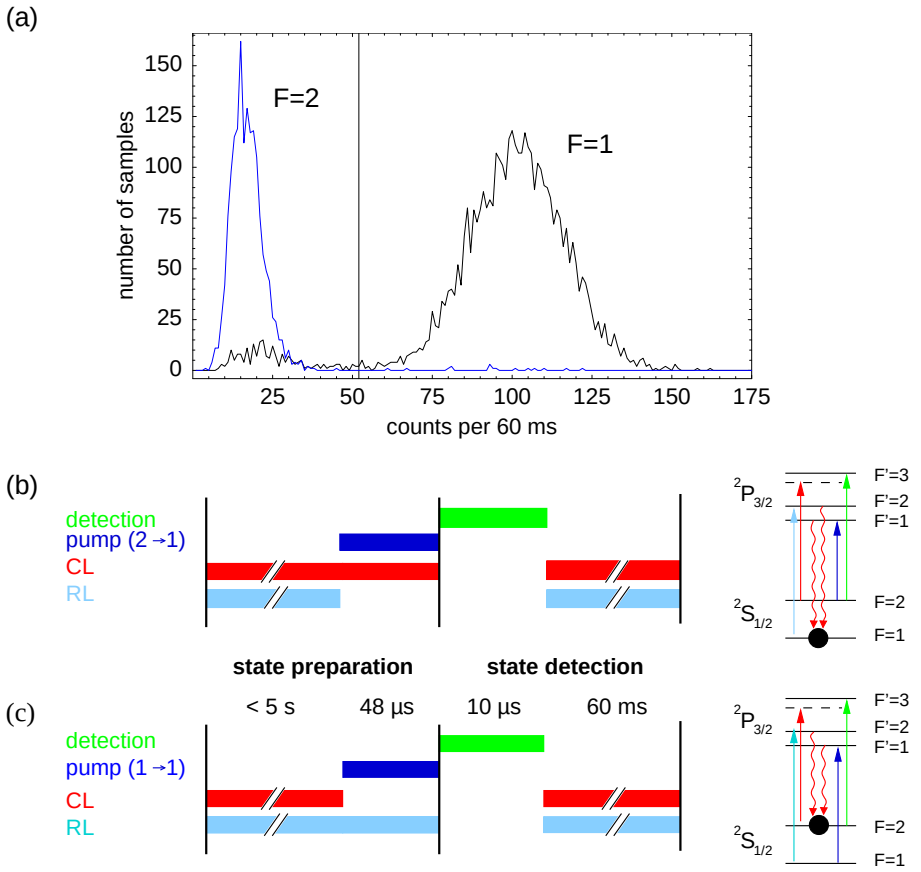

Figure 5.8: (a) Histogramm of photon counts per 60 ms during redetection after application of a hyperfine state selective detection laser pulse. Atoms prepared in $F = 1$ (black line) survive the detection pulse, whereas atoms in $F = 2$ (blue line) are removed from the dipole trap. (b), (c) timing sequence and partial level scheme of ^{87}Rb for state detection in $F = 1$ and $F = 2$, respectively. (Experimental parameters: detection laser intensity = 40 saturation intensities I_S).

In both measurements the duration and intensity of the pump and detection laser pulses were not optimized to achieve efficient state detection within the shortest period of time. In a sequence of adjustment measurements we scanned systematically the power (see fig. 5.7) and duration of the push-out pulse and we find that single atoms prepared in $F = 2$ are removed from the dipole trap with a probability of 0.99 ± 0.01 (see fig. 5.8 (a)), whereas atoms in $F = 1$ survive this pulse and are redetected in the dipole trap with a probability of 0.95 ± 0.01. These numbers are not corrected by accidental loss of the atom during the redetection sequence due to collisions with "hot" atoms from the background gas (see 3.4.1) or with cold atoms from the surrounding optical molasses and they also include incomplete preparation of the atom due to inefficient optical pumping.

Conclusion

The application of a detection laser pulse resonant to the light-shifted cycling transition ${}^2S_{1/2}, F = 2, m_F = 2 \rightarrow {}^2P_{3/2}, F' = 3, m'_F = 3$ and subsequent redetection of the atom in the dipole trap allows to discriminate the hyperfine ground states $F = 1$ and $F = 2$ of Rubidium 87 with a minimum efficiency of 0.95. This value gives the upper bound of the maximum visibility achievable in the two-particle correlation measurements used for the verification of atom-photon entanglement.

5.3.3 Preparation of Zeeman superposition states

The key element for the detection of the atomic qubit in complementary measurement bases is the state-selective adiabatic population transfer from a coherent superposition of Zeeman sublevels $|m_F = -1\rangle$ and $|m_F = +1\rangle$ of the hyperfine ground state $F = 1$ to the hyperfine ground state $F = 2$. To verify this important property of our STIRAP-scheme it is necessary to prepare in a first step a well defined superposition $\frac{1}{\sqrt{2}}(|m_F = -1\rangle + e^{i\phi}|m_F = +1\rangle)$ of the Zeeman sublevels $m_F = -1$ and $m_F = +1$. This task can be realized by two different techniques. One the one hand one could use directly the projective polarization measurement of a spontaneously emitted photon, whereby the polarization state of the photon is initially entangled with the magnetic quantum number $m_F = \pm 1$. Because this task requires a rather complicated control of many experimental parameters including the well defined preparation of the entangled state it seems much more simple to populate directly a coherent superposition $\frac{1}{\sqrt{2}}(|m_F = -1\rangle + e^{i\phi}|m_F = +1\rangle)$ by optical pumping into a coherent dark state. However, also this technique has its difficulties, because coherent population trapping in the Zeeman substructure of a given atomic state is extremely sensitive to residual magnetic fields. The reason for this sensitivity is the time dependence of Zeeman dark-states due to Larmor precession. In order to populate a stable Zeeman dark state by optical pumping it is therefore necessary to reduce the magnetic field below a threshold value.

Because the atom is stored in an optical dipole trap which is located inside a UHV vacuum chamber, it is not possible to measure the magnetic field exactly at the position

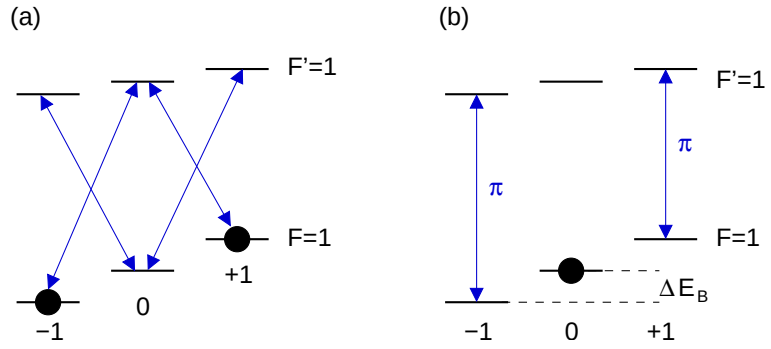

Figure 5.9: Zeeman-splitting of a hyperfine transition $F = 1 \rightarrow F' = 1$. If the linear pump laser polarization is (a) perpendicular to the magnetic field, the dark state $\frac{1}{\sqrt{2}}(|m_F = -1\rangle - e^{i\phi}|m_F = +1\rangle)$ is not stable due to Larmor-precession, (b) parallel to the magnetic field, the dark state $|m_F = 0\rangle$ is an energy eigenstate of the system and stable.

of the atom with usual Hall- or magnetic flux probes. A way to avoid this difficulties is to use the atom itself as a probe. Here I will show, how the Zeeman-splitting of the hyperfine ground state $^2S_{1/2}, F = 1$ allows to minimize the magnetic field and therefore enables the population of coherent Zeeman-superposition states by optical pumping.

Time-dependence of Zeeman superposition states

Consider the simplified case of an atomic transition consisting of a single hyperfine ground-state $F = 1$ and a single excited hyperfine state $F' = 1$. For laser light whose linear polarization direction is orthogonal to the quantization axis z and parallel to y ($\phi = 0$), the state

$$|S_0\rangle = \frac{1}{\sqrt{2}}(|m_F = -1\rangle - |m_F = +1\rangle) \tag{5.15}$$

is dark.

Provided, the level-shift of the bare atomic states $|F = 1, m_F = -1\rangle$ and $|F = 1, m_F = +1\rangle$ due to interaction with a magnetic field is small compared to the hyperfine-splitting, the Zeeman-splitting ΔE_B is given in first order perturbation theory by

$$\hbar\omega_L = \Delta E_B = \mu_B g_F m_F |B_z|, \tag{5.16}$$

where ω_L is the Larmor frequency, μ_B denotes Bohrs magneton, g_F the hyperfine-Lande-factor, m_F the magnetic moment and $|B_z|$ the absolute value of the magnetic field in z-direction. The time-evolution of the state $|S_0\rangle$ is then given by

$$|S(t)\rangle = \frac{1}{\sqrt{2}}(|m_F = -1\rangle - e^{+2i\omega_L t}|m_F = +1\rangle). \tag{5.17}$$

After a characteristic time $T = \pi/2\omega_L$, the atom precessed into the orthogonal quantum state, which is a bright state for the incident linearly polarized laser field and the atom scatters photons until it is pumped again into the dark state $|S_0\rangle$. The magnitude of the magnetic field determines the time-evolution of the dark state and therefore the rate of scattered photons.

Similar considerations are valid for a linearly polarized laser whose polarization direction is parallel to the x-axis. In the case of π-polarized light - the linear polarization direction now is parallel to the magnetic field - the atom is pumped in the energy eigenstate $|F = 1, m_F = 0\rangle$. However, this state is stable in time, independent of the magnitude of the magnetic field pointing along z. Provided the linear polarization direction of a pump laser field - resonant to the hyperfine transition $F = 1 \rightarrow F' = 1$ - is perpendicular to the magnetic field, the rate of scattered photons increases, as the magnitude of the magnetic field increases. For a "zero" field the rate is minimal. This effect, similar to the Hanle-effect, is used in the present experiment to minimize the magnetic field for efficient preparation of atomic superposition states.

Magnetic field compensation

To minimize the magnetic field we shine on the optically trapped ^{87}Rb atom a 1.8 ms linearly polarized dichromatic laser pulse resonant to the hyperfine transitions $^2S_{1/2}, F = 1 \rightarrow {}^2P_{3/2}, F' = 1$ and $^2S_{1/2}, F = 2 \rightarrow {}^2P_{3/2}, F' = 1$ and vary the magnetic field orthogonal to the given linear polarization direction of the pump beams by adjusting the current in the compensation coils. Then we redetect the atom in the dipole trap. If the magnetic field is minimal the atom scatters only few photons during the 1.8 ms and therefore has the highest probability to survive. This procedure is performed for all three componenents B_x, B_y and B_z of the magnetic field vector by rotating the linear polarization of the pump beam and scanning the respective orthogonal magnetic field component. From the measured experimental data in Fig. 5.10 and with the knowledge of the geometry of the compensation coils we can determine an upper bound of the residual magnetic field of 300 mGauss. This value is confirmed by the observation of a Larmor-precession frequency of 370 kHz [81] corresponding to a magnetic field of 132 mGauss.

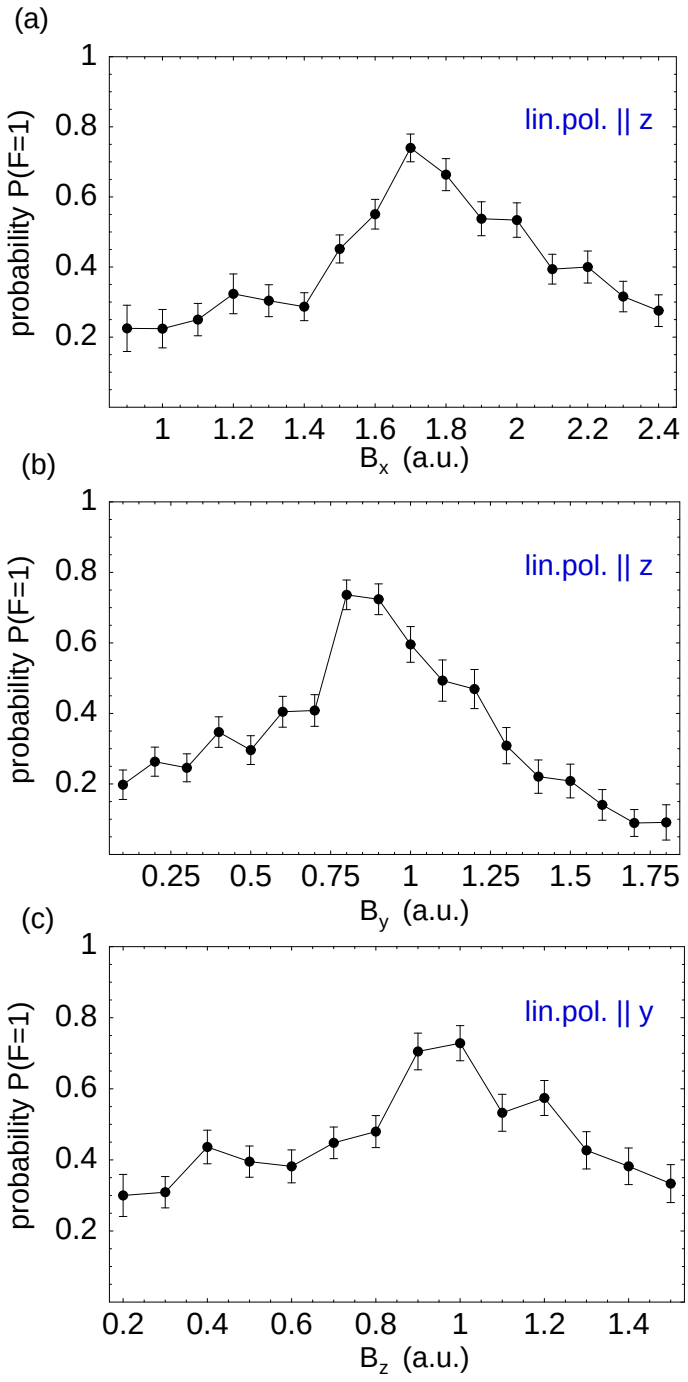

Figure 5.10: Probability to detect the atom in the dipole trap after application of a 1.8 ms pump pulse as a function of the magnetic compensation field in x-,y- and z-direction. If the respective magnetic field component is minimal, the atom is effectivly pumped into the stable Zeeman dark-state $F = 1, m_F = 0$, and scatters no light. Therefore, the atom has a high survival probability.

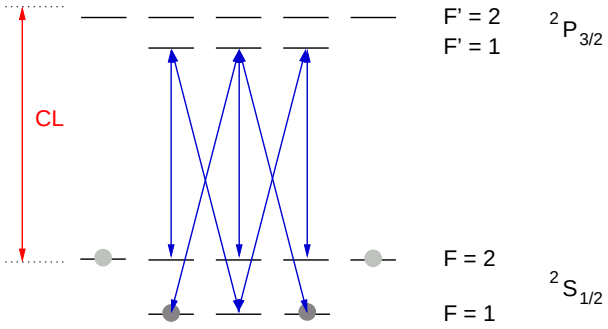

Figure 5.11: Preparation of a Zeeman-superposition state $\frac{1}{\sqrt{2}}(|1,-1\rangle - |1,+1\rangle)$ via coherent population trapping (CPT). To avoid a dark state in $F = 2$ we additionally apply the unpolarized cooling laser (CL) of our MOT.

State preparation

To prepare an atomic superposition state

$$|S_{prep}\rangle = \frac{1}{\sqrt{2}}(|1,-1\rangle - |1,+1\rangle) \tag{5.18}$$

via coherent population trapping (CPT) we apply a 5-μs linearly polarized (parallel to y) laser pulse resonant to the hyperfine transition $^2S_{1/2}, F = 1 \rightarrow {}^2P_{3/2}, F' = 1$. Because this simple light field configuration pumps the atom also to a dark state of the hyperfine ground level $F = 2$ we apply simultaneously two additional laser fields, depopulating $F = 2$ (see Fig. 5.11).

5.3.4 Detection of Zeeman superposition states

Now, the prepared atomic superposition state $|S_{prep}\rangle$ can be analyzed by a state-selective Stimulated-Raman-Adiabatic-Passage (STIRAP) technique. So far, the experimental setup as shown in chapter 3 was only slightly modified by pump beams which have been derived from cooling and repump lasers of the MOT. But for the adiabatic population transfer additional lasers are necessarily operating at 795 nm. Before focussing on the experimental results I will first give a short overview about the extended experimental setup.

Experimental setup

The STIRAP-pulses are generated by two independent laser diodes locked via Doppler-free saturation spectroscopy [77] to the hyperfine transitions $^2S_{1/2}, F = 1 \rightarrow {}^2P_{1/2}, F' = 1$ and $^2S_{1/2}, F = 2 \rightarrow {}^2P_{1/2}, F' = 1$ of the D1-line in Rubidium 87. The shape of each

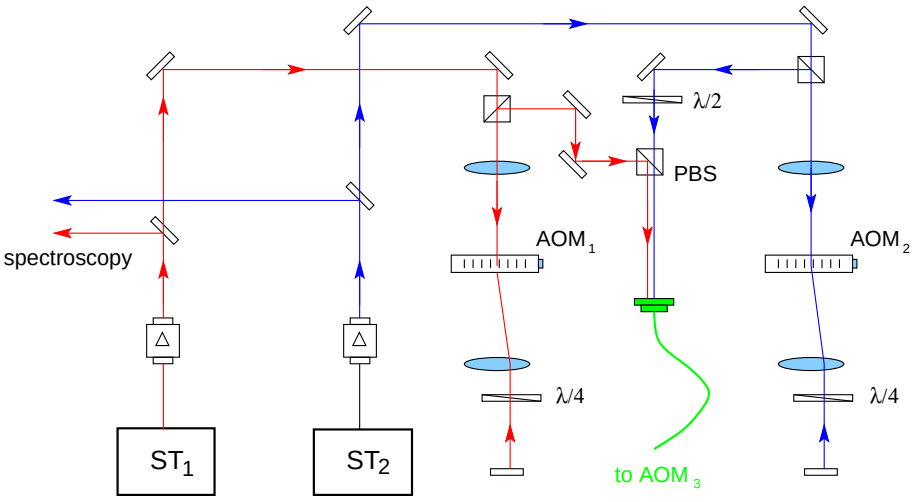

Figure 5.12: Experimentel setup of the STIRAP-lasers. (ST_1 ... STIRAP-laser 1, ST_1 ... STIRAP-laser 2, PBS ... polarizing beam splitter, AOM ... acousto-optical modulator, $\lambda/2$ ... half wave plate, $\lambda/4$ ... quarter wave plate)

pulse (amplitude and duration) is adjusted by an AOM in double-pass configuration down to a minimum pulse length of approximatly 15 ns. The delay of the Stokes pulse with respect to the pump pulse is controlled by a tuneable electric delay line and a programmable pattern generator [124], which allows to switch on and off the AOMs with a time resolution of 20 ns. The pump and Stokes beams are overlapped on a polarizing beam-splitter (PBS) and coupled into a single mode optical fiber. Because the STIRAP-pulses have to be applied to the atom in the observation direction of atomic fluorescence light, a good on/off-switching ratio of the AOMs is necessary to eliminate unwanted background light from the STIRAP-beams. An overall optical isolation of approximately 120 dB is realized by an additional acousto-optical modulator AOM_3 switching both pulses after overlapping.

To connect the preparation part of the STIRAP pulses (see Fig. 5.12) with the trap setup (see Fig. 5.13) the STIRAP beams are coupled again into a single mode optical fiber. At the exit port of the fiber a rotable half-wave plate ($\lambda/2$) is used to adjust the linear polarization angle α of the STIRAP pulses Ω_1 and Ω_2. In addition a tilted birefringent crystall (C) compensates for relative phase shifts between s- and p- polarized components that occur at the reflection on dielectric mirrors. Finally the STIRAP-pulses are focussed with an objective onto the atom to a waist of 5..10 μm.

For the preparation and analysis of atomic superposition states additional pump and detection beams resonant to specific hyperfine transitions within the D2-line of Rubidium 87 are necessary. Therefore different beams are extracted from the cooling and repump lasers and switched independently by AOMs in double-pass configuration. Then each beam is coupled into a single-mode optical fiber and focussed onto the atom.

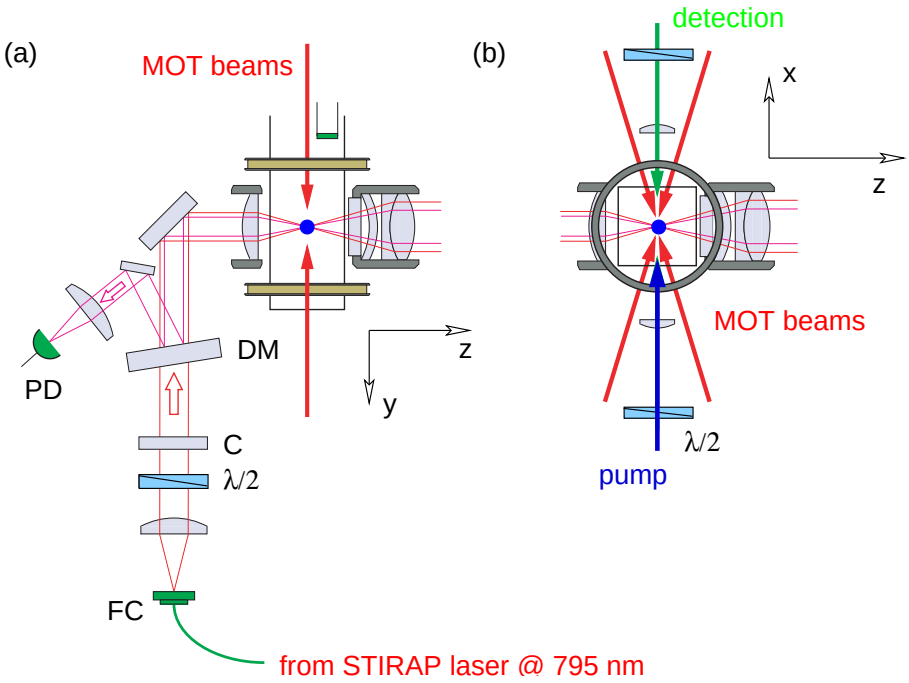

Figure 5.13: Schematic view of the experimental setup to investigate a coherent superposition of the Zeeman states $|F = 1, m_F = -1\rangle$ and $|F = 1, m_F = +1\rangle$. (a) horizontal view; (b) upright view.

Experimental process

To verify the selective detection of Zeeman-superposition states via STIRAP, we first load a single ^{87}Rb atom into the dipole trap. Then a 5-μs optical laser pulse (see preceding section) pumps the atomic population into the dark superposition state

$$|S_{prep}\rangle = \frac{1}{\sqrt{2}}(|1,-1\rangle - |1,+1\rangle) \tag{5.19}$$

of the $^2S_{1/2}, F = 1$ ground level. To analyze this state we apply immediatly after the preparation pulse a 70 ns STIRAP-pulse, transferring a superposition state

$$|S_{trans}\rangle = \frac{1}{\sqrt{2}}(|1,-1\rangle - e^{2i\alpha}|1,+1\rangle) \tag{5.20}$$

adiabatically to the hyperfine ground state $F = 2$. Due to destructive interference of the excitation amplitudes the orthogonal quantum state $|S_{dark}\rangle = \frac{1}{\sqrt{2}}(|1,-1\rangle + e^{2i\alpha}|1,+1\rangle)$ does not couple to the STIRAP laser field Ω_1 and remains in $F = 1$. The relative phase of these states can be controlled by the linear polarisation angle α of the STIRAP laser Ω_1 with respect to the x-axis. After the transfer we apply a hyperfine state selective 40 μs push-out laser pulse to discriminate the hyperfine ground states. Finally the

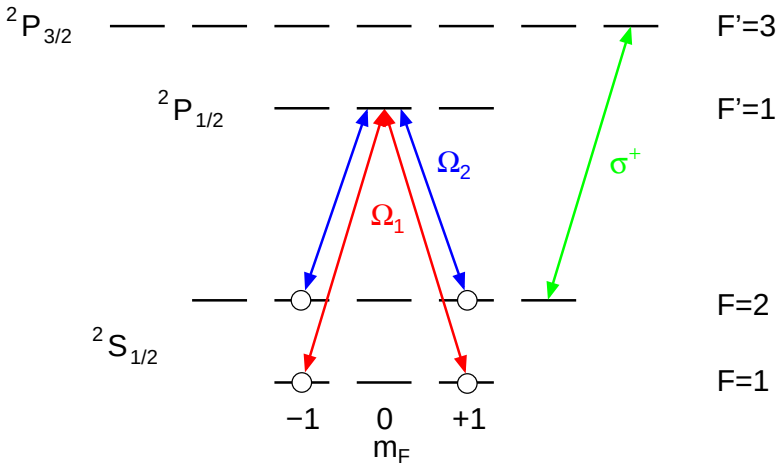

Figure 5.14: Coupling scheme for the analysis of coherent superposition states. The STIRAP process transfers the superposition $\frac{1}{\sqrt{2}}(|1,-1\rangle + e^{i\phi}|1,+1\rangle)$ to the $F = 2$ ground state whereas the orthogonal state $\frac{1}{\sqrt{2}}(|1,-1\rangle - e^{i\phi}|1,+1\rangle)$ remains in $F = 1$. To distinguish the hyperfine ground states, a σ^+ polarized detection laser pulse resonant to the cycling transition $^2S_{1/2}, F = 2 \rightarrow {}^2P_{3/2}, F' = 3$ is used.

cooling and repump laser of the MOT are switched on and the atomic fluorescence light is integrated for 60 ms to decide whether the atom is still in the trap or not. The probability to redetect the atom in the dipole trap is ideally given by

$$P = |\langle S_{prep}|S_{dark}\rangle|^2 = \sin^2\alpha, \tag{5.21}$$

which is the overlap of the prepared atomic state $|S_{prep}\rangle$ with the dark state $|S_{dark}\rangle$.

In Fig. 5.15 we show the measured probability P to detect the atom in the hyperfine ground state $F = 1$ after application of the STIRAP and push-out pulses as a function of the linear polarization angle α of the STIRAP laser. For $\alpha = 0$ the prepared state $\frac{1}{\sqrt{2}}(|1,-1\rangle - |1,+1\rangle)$ is transferred to $F = 2$ because it is a bright state of the vertically polarized STIRAP-laser field Ω_1. In this case the atom does not survive the detection pulse and is not redetected. For $\alpha = \pi/2$ the state $|S_{prep}\rangle$ is dark and therefore not transferred to $F = 2$. Consequently it is not influenced by the detection laser and redetected with a probability of 0.75.

The measured experimental data points in Fig. 5.15 are fitted with a modified function $a + V/2\sin^2(\alpha + \alpha_0)$ yielding a visibility V (defined as peak to peak amplitude) of 0.57 ± 0.01. The reduction of the observed visibility can be explained by two effects. First, the state preparation via optical pumping is not perfect. 20 percent of the atomic population are pumped to a Zeeman dark state of the $F = 2$ hyperfine ground state.

This situation effects the Zeeman state analysis in the following way. Suppose that 20 percent of the atomic population are in $F = 2$ and 80 percent are ideally in the prepared dark state $\frac{1}{\sqrt{2}}(|1,-1\rangle - |1,+1\rangle)$. Then, if the polarization of the STIRAP laser is chosen such that it couples maximally to the prepared superposition in $F = 1$ and maximally to the population in $F = 2$, the fraction in $F = 1$ will be transferred to $F = 2$, whereas population initially in $F = 2$ is partially transferred to $F = 1$. Suppose the STIRAP laser does not couple to the superposition in $F = 1$ because the prepared Zeeman superposition state is a dark state with respect to the chosen polarisation, then population in $F = 2$ will be partially transferred to $F = 1$. To get an estimation about the impact of this process on the measured data we numerically solved a master equation of the STIRAP-process on the basis of a simplified three-level model including spontaneous emission from the intermediate level. We get the result that after the STIRAP-pulse maximally 84 percent of the atomic population will be in $F = 1$ provided the STIRAP polarization is chosen such that the STIRAP does not couple to the prepared Zeeman state in $F = 1$, whereas if the STIRAP couples initially to population in $F = 1$ and $F = 2$, after the pulse 5 percent will remain in $F = 1$. On the basis of this estimation we calculate a corrected visibility of 0.71 ± 0.01.

A second important source of errors is the imperfect state transfer via the STIRAP pulses. For further optimization of the process, it is useful to decouple the inefficient state preparation from the state detection. After all, the preparation of a "clean" initial atomic state can be best realized by the polarization measurement of a spontaneously emitted photon, provided the photon was initially entangled with the Zeeman state $m_F = \pm 1$ of the atom.

5.4 Conclusion and discussion

We have set up a laser system which allows to read out a Zeeman superposition state of a single atom. Depending on the polarisation of the STIRAP pulses a superposition $\frac{1}{\sqrt{2}}(|F = 1, m_F = -1\rangle + e^{i\phi}|F = 1, m_F = +1\rangle)$ of the ${}^2S_{1/2}, F = 1, m_F = \pm 1$ hyperfine ground state is adiabatically transferred to the $F = 2$ state. Due to destructive interference of the excitation amplitudes the orthogonal quantum state $\frac{1}{\sqrt{2}}(|F = 1, m_F = -1\rangle - e^{i\phi}|F = 1, m_F = +1\rangle)$ does not couple to the STIRAP pulse and remains in $F = 1$. To discriminate these states we apply a detection laser pulse resonant to the cycling transition ${}^2S_{1/2}, F = 2 \rightarrow {}^2P_{3/2}, F' = 3$. Provided the atom is in $F = 2$ it scatters photons from this laser beam, and with each scattering event the atom acquires an additional photon momentum $\hbar\vec{k}$. After approximately 40 to 50 scattering events the atom is pushed out of the dipole trap. Finally, to read out the atomic state the cooling and repump beams of the MOT are switched on and the atomic fluorescence light is integrated for 60 ms to decide if the atom is still in the trap or not.

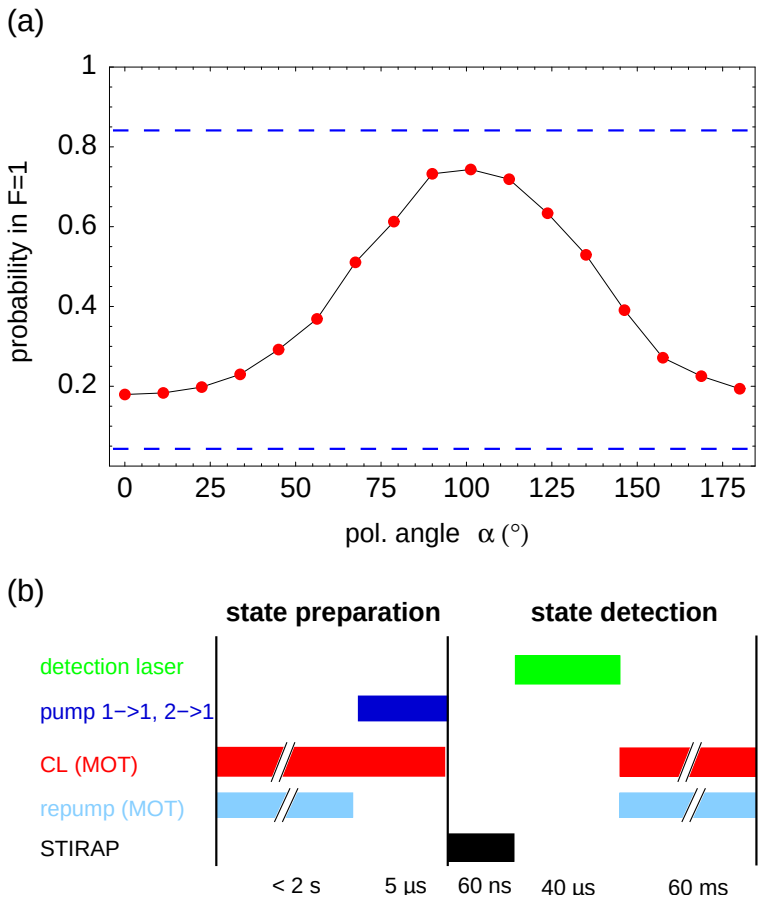

Figure 5.15: **(a)** Probability to detect the atom in the hyperfine ground state $F = 1$ after application of a state-selective STIRAP and detection laser pulse as a function of the linear polarization angle α of the STIRAP laser. Initially the atom was prepared by a 5-μs pump pulse in the superposition state $\frac{1}{\sqrt{2}}(|1,-1\rangle + |1,+1\rangle)$. For $\alpha = 0$ the prepared state is adiabatically transferred to $F = 2$, whereas for $\alpha = 90°$ it is a dark state with respect to the polarization of the STIRAP laser and remains in $F = 1$. Atoms in $F = 1$ survive the detection pulse and are redetected, while atoms in $F = 2$ are removed from the trap. **(b)** Timing sequence for the preparation and the analysis of a coherent Zeeman superposition state.

6 Observation of atom-photon entanglement

6.1 Introduction

Atom-photon entanglement has been implicit in many previous experimental systems, from early measurements of Bell's inequality violations in atomic cascade systems [4, 6] to fluorescence studies in trapped atomic ions [28, 29] and atomic beam experiments [30]. However, it has not been directly observed until quite recently [35], as the individual atoms and photons have not been under sufficient control.

In our experiment a single photon is spontaneously emitted from a single optically trapped ^{87}Rb atom, which is initially excited to a state which has multiple decay channels. Along a certain emission direction two decay channels are selected and the photon polarization is maximally entangled with two particular Zeeman sublevels of the hyperfine ground states of the atom.

To verify entanglement of the generated atom-photon state one has to disprove the possibility that the two-particle quantum system can be a statistical mixture of seperable states. This task is closly connected to a violation of Bell's inequality and requiress correlated local state measurements of the atom and the photon in complementary bases.

In this chapter I will report in detail on the generation and analysis of atom-photon entanglement. The experimental process is described and first experimental results are discussed confirming spin-entanglement between the atom and the photon.

6.2 Experimental process

First, we load a single ^{87}Rb atom from a magneto-optical trap - operated in a pulsed mode - into the optical dipole trap. Then a 5.5-μs linearly polarized optical pulse pumps the atom into the $^2S_{1/2}, |1,0\rangle$ dark state (for details see preceding chapter), from where the atom is excited by a 30-ns π-polarized optical π-pulse to the $^2P_{3/2}, |0,0\rangle$ state. Here $|F, m_F\rangle$ denotes the internal atomic quantum numbers of the total angular momentum and its projection along the quantization axis z.

In the following spontaneous emission the atom decays either to the $|1,-1\rangle$ ground state while emitting a photon in the polarization state $|\sigma^+\rangle$, or to the $|1,0\rangle$ state while emitting a $|\pi\rangle$-polarized photon or it decays to the $|1,+1\rangle$ ground state and emits a $|\sigma^-\rangle$-polarized photon. Because the residual magnetic field is smaller than 100 mGauss,

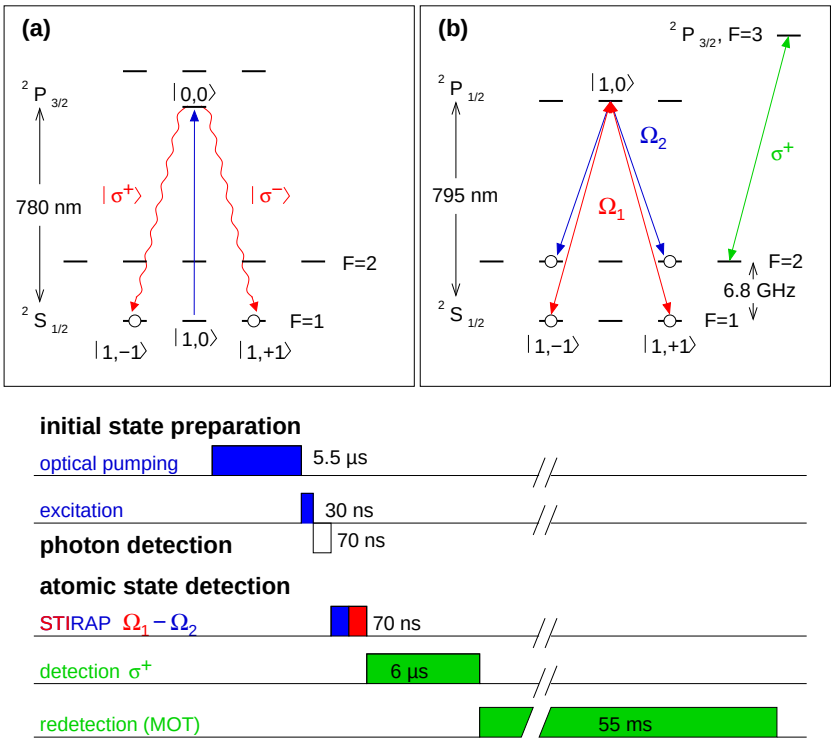

Figure 6.1: The experimental process (time not to scale). **(a)** The atom is initialized to the $|1,0\rangle$ hyperfine ground state by optical pumping (not shown) and excited by a 30-ns π-polarized π-pulse to the $|0,0\rangle$ excited state. In the following spontaneous decay the polarization state of the photon is entangled with magnetic hyperfine state of the atom. **(b)** After the polarization measurement of the photon the internal state of the atom is measured by a 70-ns STIRAP and a 6-μs detection pulse, before atomic fluorescence light is accumulated for 55 ms.

the Zeeman-splitting of these states is two orders of magnitude smaller than the natural linewidth of the transition. Therefore these decay channels are spectrally indistiguishable and a coherent superposition of separable atom-photon states is formed, entangling the magnetic quantum number m_F of the atom with the polarization state of the emitted photon. Along the observation direction, defined by the aperture of the microscope objective, π-polarized photons are not emitted. Thus, the resulting atom-photon state is maximally entangled:

$$|\Psi^+\rangle = \frac{1}{\sqrt{2}}(|1,-1\rangle|\sigma^+\rangle + |1,+1\rangle|\sigma^-\rangle). \tag{6.1}$$

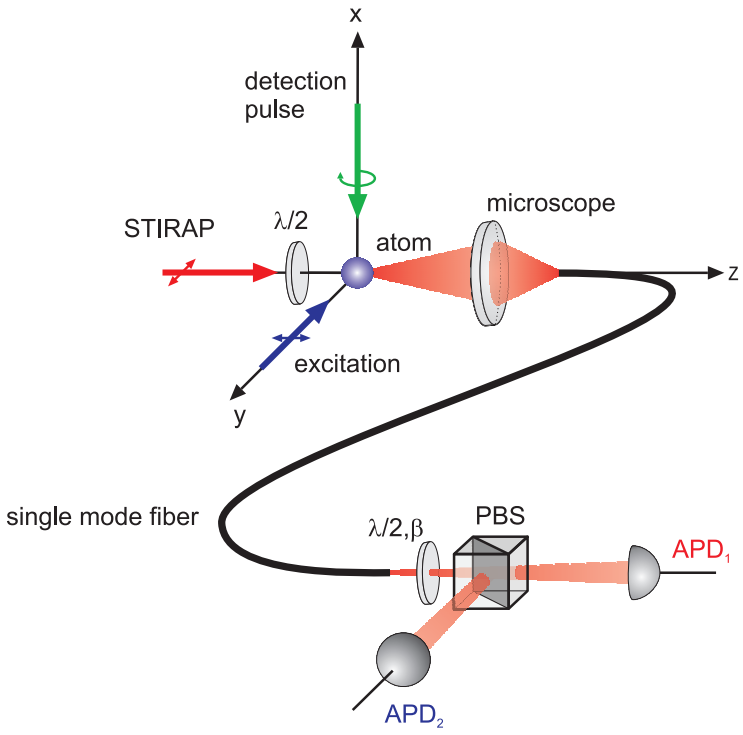

Figure 6.2: Simplified setup of the experimental apparatus. The π-polarized excitation beam propagates perpendicular to the quantization axis z defined by the optical axis of the detection optics. The scattered photons are collected by a microscope objective, coupled to a single mode optical fiber and directed to a polarizing beam splitter (PBS). Two single photon detectors APD_1 and APD_2 register the H- and V-polarized photons, respectively. The $\lambda/2$-waveplate is used to rotate the photon polarization for photonic qubit measurements in different bases. The atomic state is analysed by a STIRAP-pulse driving coherent two-photon transitions between the hyperfine levels of the atomic ground state. The atomic measurement basis is defined by the angle α of the linearly polarized STIRAP laser field Ω_1 with respect to the y-axis.

To investigate the nonclassical correlation properties of this state, the single photon from the spontaneous decay is collected with a microscope objective (see Fig. 6.2) and coupled into a single-mode optical fiber guiding it to a polarization analyzer consisting of a rotable $\lambda/2$-halfwave plate, a polarizing beam splitter (PBS) and two avalanche photo-diodes APD_1 and APD_2 for single photon detection. Triggered by the detection of a photon, the internal quantum state of the atom is analyzed by a state-selective Stimulated-Raman-Adiabatic-Passage (STIRAP) technique transferring the superposition $\frac{1}{\sqrt{2}}(|1,-1\rangle + e^{2i\alpha}|1,+1\rangle)$ to the hyperfine ground state $F = 2$ (see chapter 5). Due to destructive interference of the excitation amplitudes the orthogonal quantum

state $\frac{1}{\sqrt{2}}(|1,-1\rangle - e^{2i\alpha}|1,+1\rangle)$ does not couple to the STIRAP laser field Ω_1 (see Fig. 6.1(a)) and remains in $F = 1$. Here the relative phase 2α is defined by the linear polarization angle α of the STIRAP laser Ω_1 with respect to the y-axis. The phase settings $\alpha = 0, \pi/2$ and $\alpha = \pi/4, 3\pi/4$ define two sets of complementary basis-states $\{\frac{1}{\sqrt{2}}(|1,-1\rangle + |1,+1\rangle), \frac{1}{\sqrt{2}}(|1,-1\rangle - |1,+1\rangle)\}$ and $\{\frac{1}{\sqrt{2}}(|1,-1\rangle + i|1,+1\rangle), \frac{1}{\sqrt{2}}(|1,-1\rangle - i|1,+1\rangle)\}$, which allow to measure the atomic qubit in the σ_x- and σ_y-basis, whereby $|1,\pm1\rangle$ are eigenstates of σ_z.

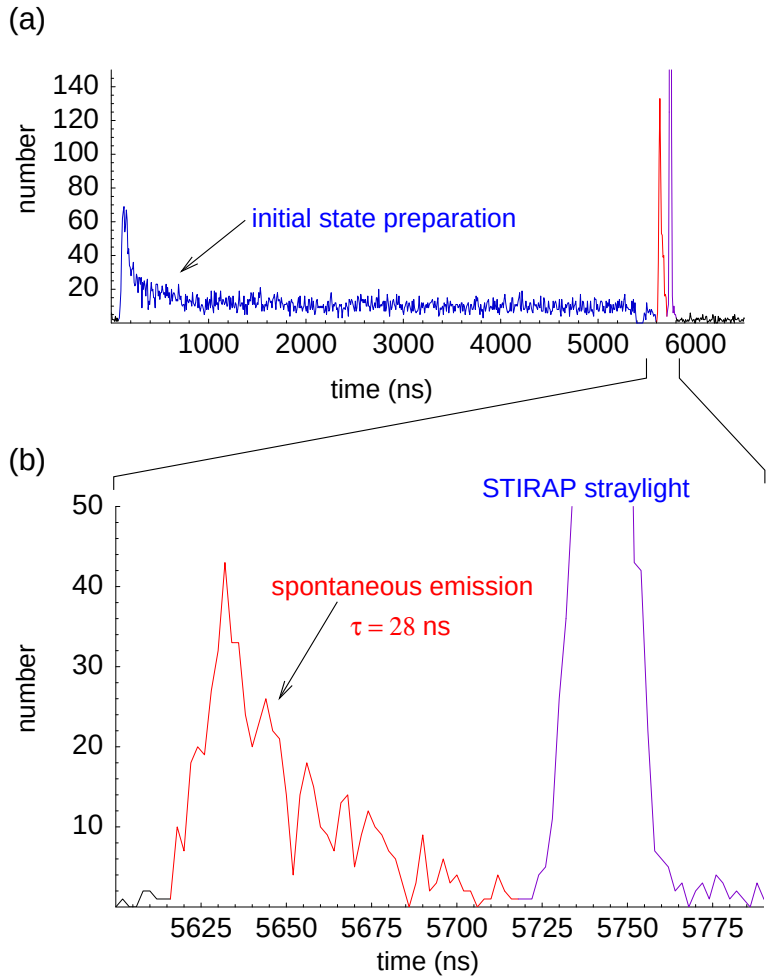

Figure 6.3: Number of scattered photons as a function of time during **(a)** preparation of the initial state via optical pumping into the dark state $^2S_{1/2}, |1,0\rangle$ (integration time bin $\Delta t = 8$ns), **(b)** excitation to $^2P_{3/2}, |0,0\rangle$ and subsequent spontaneous decay to $^2S_{1/2}, |1,\pm1\rangle$ (integration time bin $\Delta t = 2$ns).

After the state-selective population transfer the atom is in a superposition of the hyperfine ground states $F = 1$ and $F = 2$. To discriminate these states we apply a 6-μs detection laser pulse resonant to the cycling transition $5^2S_{1/2}, F = 2 \rightarrow 5^2P_{3/2}, F = 3$. If the atom is in the hyperfine ground state $F = 2$, it is removed from the dipole trap due to photon recoil heating. If the atom was in state $F = 1$, fluorescence is observed after the cooling and repump lasers of the MOT are switched on. Counts are integrated for 55 ms to decide whether the atom is still in the trap or not.

In Fig. 6.3 the number of scattered photons during the preparation of the initial state $^2P_{3/2}, |0, 0\rangle$ is shown as a function of time. When the pump pulse is switched on, the number of scattered photons decreases after few 100 ns as the atomic population is pumped to the Zeeman dark state $^2S_{1/2}, |1, 0\rangle$. The intensity of the following 30-ns optical π-pulse is chosen such, that at the end of the pulse the maximum atomic population is in the $^2P_{3/2}, |0, 0\rangle$ state. In the following spontaneous decay - indicated by the red data trace in Fig. 6.3(b) - the number of scattered photons drops exponentially with a measured time constant of 28 ns. To correlate the atomic state detection with the internal state of a spontaneously emitted photon we restrict the detection of photons to a well defined time window of 70 ns following the optical excitation pulse (see Fig. 6.1).

The generation of entangled atom-photon pairs is probabilistic because a spontaneously emitted photon is detected with a probability of $\eta = 5 \times 10^{-4}$. This means, that the atom has to be excited approximately 2000 times until a photon is detected. To achieve the best rate of detected atom-photon pairs, the excitation cycle - consisting of optical pumping to $5^2S_{1/2}, |1, 0\rangle$ and following excitation to $5^2P_{3/2}, |0, 0\rangle$ - is repeated as long until a photon is detected. Once a photon is detected the atom is measured with almost perfect efficiency, limited only by loss from the dipole trap during the fluorescence detection.

6.3 Experimental results

To verify atom-photon entanglement we measure the conditional probability of detecting the atomic qubit in the complementary bases σ_x and σ_y as a function of the polarization state of the detected photon.

In Fig. 6.4(a) the polarisation of the STIRAP-lasers is set to $\alpha = 0$ defining the σ_x measurement basis for the atom and the polarization of the photon is rotated on the Poincare-sphere by a variable angle 2β. We observe strong correlations between the polarization state of the detected photon and the internal quantum state of the atom. As expected, if the photon is detected in the polarization state $\frac{1}{\sqrt{2}}(|\sigma^+\rangle + |\sigma^-\rangle)$ (detection in APD_1) the atom is projected to the corresponding superposition state $\frac{1}{\sqrt{2}}(|1, -1\rangle + |1, +1\rangle)$. This atomic state is a "dark" state for the chosen linear polarization of the STIRAP laser field Ω_1. Hence the atomic population will remain in $F = 1$ after the STIRAP-pulse. If the photonic qubit is rotated by a phase of $\phi = \pi$ before state reduction the single photon detectors exchange their role and a detection at APD_1

projects the atom to $\frac{1}{\sqrt{2}}(|1,-1\rangle - |1,+1\rangle)$. Now, this atomic state can be transferred to the hyperfine ground state $F = 2$, i.e. $P(F = 1)$ goes to a minimum. From a fit of the measured correlations we obtain a visibility (defined as peak to peak amplitude) of 0.81 ± 0.04. To verify entanglement this measurement has to be repeated for an atomic basis conjugate to the first one. Thus the atomic qubit was analyzed in the complementary σ_y basis (see Fig. 6.4(b)). Therefore the STIRAP polarization angle α is set to $\pi/4$. Again, strong correlations are observed with a visibility of 0.70 ± 0.04. But now the measured atom-photon correlations are shifted by $\beta = \pi/4$, as we expect from an entangled state.

To quantify the amount of entanglement we determine the entanglement fidelity $F = \langle\Psi^+|\rho|\Psi^+\rangle$, which is defined as the overlap of the measured state - characterized by the density matrix ρ - with the maximally entangled state $|\Psi^+\rangle$ we expect to generate. Because the atomic state detection is imperfect, we model these errors by a quantum channel which is subjected to white noise. Therefore, the density matrix of the detected state can be expressed as $\rho = V|\Psi^+\rangle\langle\Psi^+| + \frac{1-V}{4}\hat{1}$, where V is the mean visibility of the observed correlations in the two complementary bases. From this we derive an entanglement fidelity of 0.82 ± 0.04.

6.4 Conclusion and discussion

In the current experiment we excite a single optically trapped ^{87}Rb atom by a short optical pulse to a state which has multiple decay channels and detect the subsequent spontaneously emitted single photon. Along a certain emission direction - defined by the optical axis of the detection optics - two decay channels are selected and the photon polarization is maximally entangled with two particular Zeeman sublevels of the hyperfine ground states of the atom. The entanglement is directly verified by appropriate polarization analysis of the photon and Zeeman state detection of the trapped atom. We observe strong atom-photon correlations in complementary measurement bases yielding an entanglement fildelity of 0.82 ± 0.04.

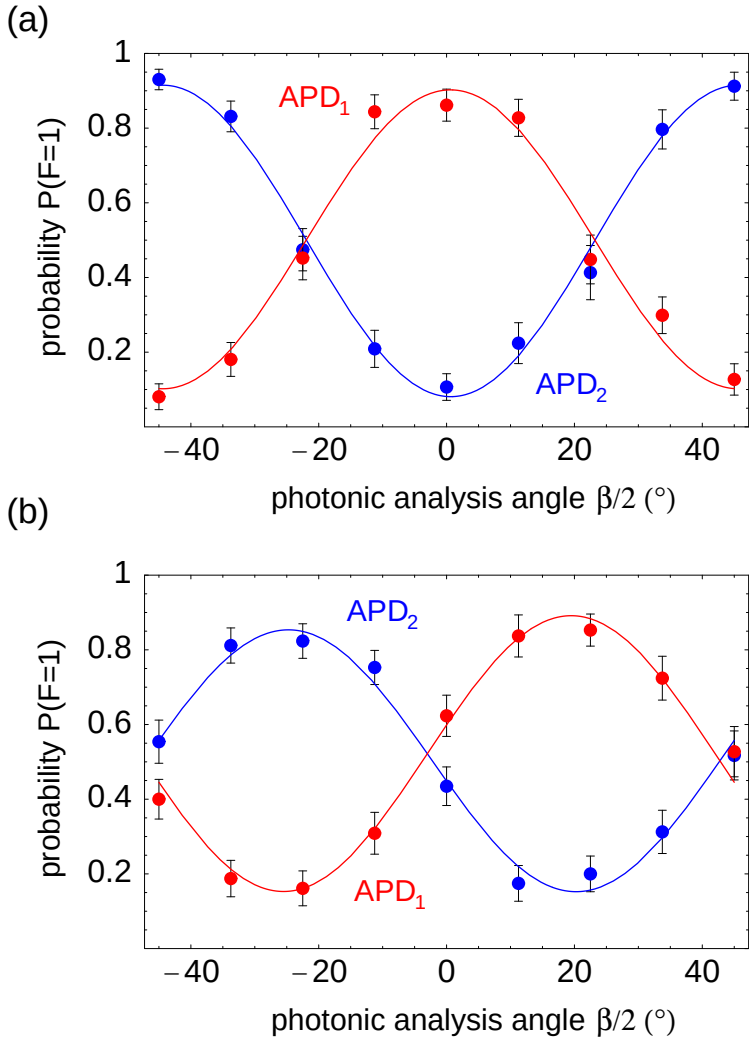

Figure 6.4: Probability of detecting the atom in the ground state $F = 1$ (after the STIRAP pulse) conditioned on the detection of the photon in detector APD_1 (red data points) or detector APD_2 (blue data points) as the phase $\phi = 2\beta$ of the photonic rotation is varied. The atomic qubit is projected **(a)** to the states $1/\sqrt{2}(|1,-1\rangle \pm |1,+1\rangle)$, **(b)** to the states $1/\sqrt{2}(|1,-1\rangle \pm i|1,+1\rangle)$ corresponding to a spin measurement in σ_x and σ_y, respectively, whereas the photonic qubit is projected onto the states $\frac{1}{\sqrt{2}}(|\sigma^+\rangle \pm e^{i\phi}|\sigma^-\rangle)$.

7 Conclusion and Outlook

The goal of this thesis was the experimental generation and analysis of entanglement between the spin state of a single neutral ^{87}Rb atom and the polarization state of a single spontaneously emitted photon suitable for long-distance transport in optical fibers and air. This task required in a first step the efficient detection and manipulation of a single ^{87}Rb atom. For this purpose a far-off-resonance optical dipole trap was set up. Because of the small trap volume and due to light-induced two-body collisions, which are present during the loading stage within the light fields of a magneto-optical trap, only single atoms are captured. This blockade effect was confirmed by the observation of photon antibunching in the detected fluorescence light. To generate the entangled atom-photon state the atom is excited to a state which has two decay channels. Due to conservation of angular momentum in the following spontaneous emission the polarization state of the photon is maximally entangled with two particular Zeeman sub-levels of the atomic ground state. To detect entanglement of this atom-photon state we performed correlated local measurements of the polarization state of the photon and the internal quantum state of the atom. The atomic spin state was analyzed by means of a Stimulated-Raman-Adiabatic-Passage (STIRAP) process, where the polarization of the analyzing laser light defined the atomic measurement basis. Strong nonclassical atom-photon correlations in complementary measurement bases were observed yielding an entanglement fidelity of 0.82 ± 0.04.

The realization of entanglement between a single optically trapped ^{87}Rb atom and a spontaneously emitted single photon described in this work marks a first successful step towards the remote state preparation of a single atom over large distances and a first loophole-free test of Bell's inequality [13, 14].

Remote state preparation of a single atom

A first step towards entanglement swapping or the closely related quantum teleportation is the so-called remote state preparation [125, 126]. In this protocoll generic, state independent unitary transformations U on the atom are sufficient to prepare it in the arbitrary quantum state $|\Psi_B\rangle = \cos\alpha|\uparrow\rangle - \sin\alpha e^{i\beta}|\downarrow\rangle$. This process works as follows: Suppose a single atom is entangled with a single photon. Then the photon propagates to Alice who performs a unitary operation $U(\alpha, \beta)$ with two free parameters α, β in an extended four-dimensional Hilbert space, before she projects the photon onto a generalized Bell-basis [127]. Depending on her measurement result, Bob now has to perform a unitary spin rotation U in order to prepare the required quantum state of the atom.

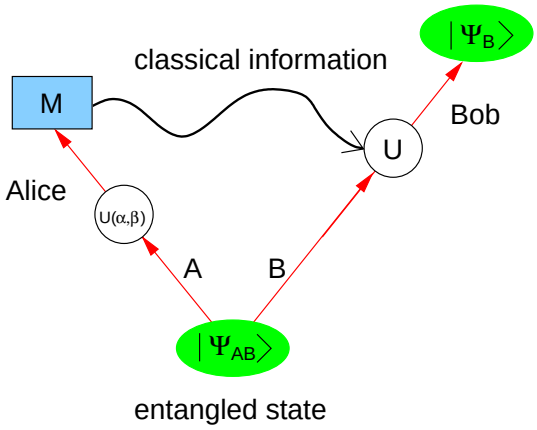

Figure 7.1: Principle of Remote State Preparation.

This scheme generalizes to teleportation, if one introduces yet another photon, allowing a direct transfer of a photonic qubit to an atom which can be used for robust long-term storage of quantum information. To reconvert the stored information onto a single photon one can reexcite the atom on a so-called V-type transition [128]. Furthermore, if one puts the atom into a high Q cavity, it is possible to force the atom to emit the photon into one selected spatial mode. These properties fulfill all requirements for efficient quantum networking. But teleportation or entanglement swapping is the key for a loophole free Bell experiment.

Loophole-free test of Bell's inequality

For a loophole-free test of Bell's inequality one needs two entangled quantum systems which can be detected with high efficiency and which are separated far enough that local observations of each system are space-like separated. This task can be accomplished by two entangled atoms. First, atoms have the important property that they can be detected with almost perfect efficiency. Second, entanglement between two distant atoms can be generated in a robust way by an entanglement swapping [15] process between two independently created entangled atom-photon pairs [13, 14]. Suppose one starts with two atoms in two distant traps, where in each trap only one atom is stored. Then each atom is entangled with one spontaneously emitted photon. The independently generated photons then propagate to an intermediate location where a partial Bell-state analysis is performed, projecting the atoms onto an entangled state.

In the present experiment verifying atom-photon entanglement the atomic state detection is performed with an efficiency of one because every state measurement gives a result. Hence, the measured entanglement fidelity already includes all experimental errors of the atomic state detection and no additional fair-sampling assumption has to be made for a Bell test with entangled atoms. To close at the same time the locality loophole, the atoms have to be space-like separated with respect to the duration of the

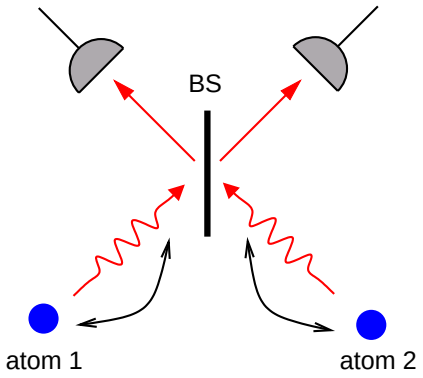

Figure 7.2: Atom-atom entanglement by two-photon interference.

atomic state detection. That is, in our experiment the minimum distance of the atoms is determined by the duration of the detection laser pulse. In detail the reduction of the atomic state is performed by scattering photons from a closed atomic transition. After approximately 10 lifetimes ($\tau = 26$ ns) of the $5^2P_{3/2}$ excited state, the state reduction is completed with a probability of more then 99%. Together with the STIRAP-process this yields an overall measurement time of less than 0.5 μs corresponding to a minimum distance between the two atoms of 150 m. This requirement can easily be achieved since the transmission losses of single photons at a wavelength of 780 nm passing through an optical fiber or air are very low.

The observation of entangled atom-photon pairs is probabilistic with a success probability given by the total detection efficiency $\eta = 5 \times 10^{-4}$ of a single photon. This argument holds also for the generation of entanglement between two distant atoms. But, given the case of a coincident detection of the two photons in the two output ports of the beamsplitter (BS) in Fig. 7.2, the atoms are projected with certainty onto a maximally entangled Bell state. The total success probability for this entanglement swapping process is given by $\frac{1}{4}\eta^2 T^2$, where the factor 1/4 accounts for the fact that only one of four photon Bell-states is detected and $T = \sqrt{0.95}$ corresponds to the transmission probability of the photonic qubit through 75 m (halfway distance) optical fiber. The maximum repetition rate of this experiment is determined by the time it takes for the photon to travel from the locations where the atoms are trapped to the intermediate location where the photons are detected. For a halfway distance of 75 m, a minimum cycle time of 1 μs for the experimental generation of entangled atoms is possible. This corresponds to a maximum repetition rate of 1×10^6 s^{-1}. From this estimation one can calculate an expected generation rate of entangled atom-atom pairs of 0.8 per minute, including the limited lifetime of the atoms in the dipole traps.

For a violation of Bell's inequality a minimum entanglement fidelity of 0.78 is necessary. This threshold yields a minimum entanglement fidelity of the generated atom-photon pairs of 0.88. Recently we performed new measurements verifying atom-photon entanglement with an overall fidelity of $(89.4 \pm 0.7)\%$ [129]. Hence we expect an ent-

anglement fidelity of 80 % for the entangled atom-atom state. The loophole-free violation of a CHSH-type Bell's inequality [40] by three standard deviations would require approximately 7000 atom pairs. On the basis of the above estimations a total measurement time of 12 days should be feasible, starting with the performance of the setup developed in this work.

A Appendix

Table A.1: Physical properties of ^{87}Rb [61].

Atomic Number	Z	37
Total Nucleons	$Z+N$	87
Relative Natural Abundance	η	27.83(2) %
Nuclear Spin	I	3/2
Atomic Mass	m	86.9092 u
Vacuum Wavelength D_1-Transition	λ_{D1}	794.979 nm
Vacuum Wavelength D_2-Transition	λ_{D2}	780.246 nm
Lifetime 5 $^2P_{1/2}$		27.70 ns
Lifetime 5 $^2P_{3/2}$		26.24 ns
Natural Line Width D_1-Transition	Γ_{D1}	$2\pi \times 5.746(8)$ MHz
Natural Line Width D_2-Transition	Γ_{D2}	$2\pi \times 6.065(9)$ MHz
Ground State Hyperfine Splitting	ν_{HFS}	6834.68 MHz
Recoil Velocity D_2-Transition	v_r	5.8845 mm/s
Recoil Temperature D_2-Transition	T_r	361.95 nK
Doppler Temperature D_2-Transition	T_D	146 μK
Dipole Matrix Element D_2-Transition	$\langle J\|\|er\|\|J'\rangle$	$3.584(4) \times 10^{-29}$ C m
Saturation Intensity $5^2S_{1/2}, F=2, m_F=\pm 2 \rightarrow 5^2P_{3/2}, F=3, m_F=\pm 3$ Transition	I_S	1.67 mW/cm^2

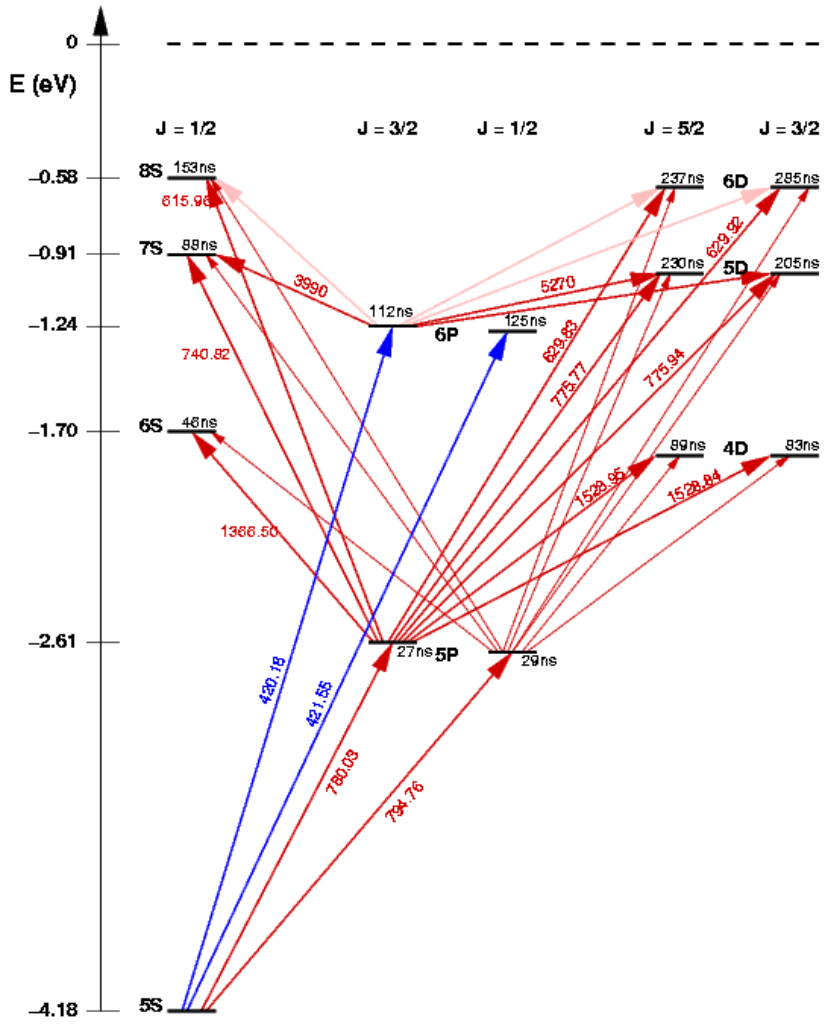

Figure A.1: Combined partial energy-level - Grotrian diagramm for ^{87}Rb with lifetimes of atomic levels and transition wavelengths in air [130].

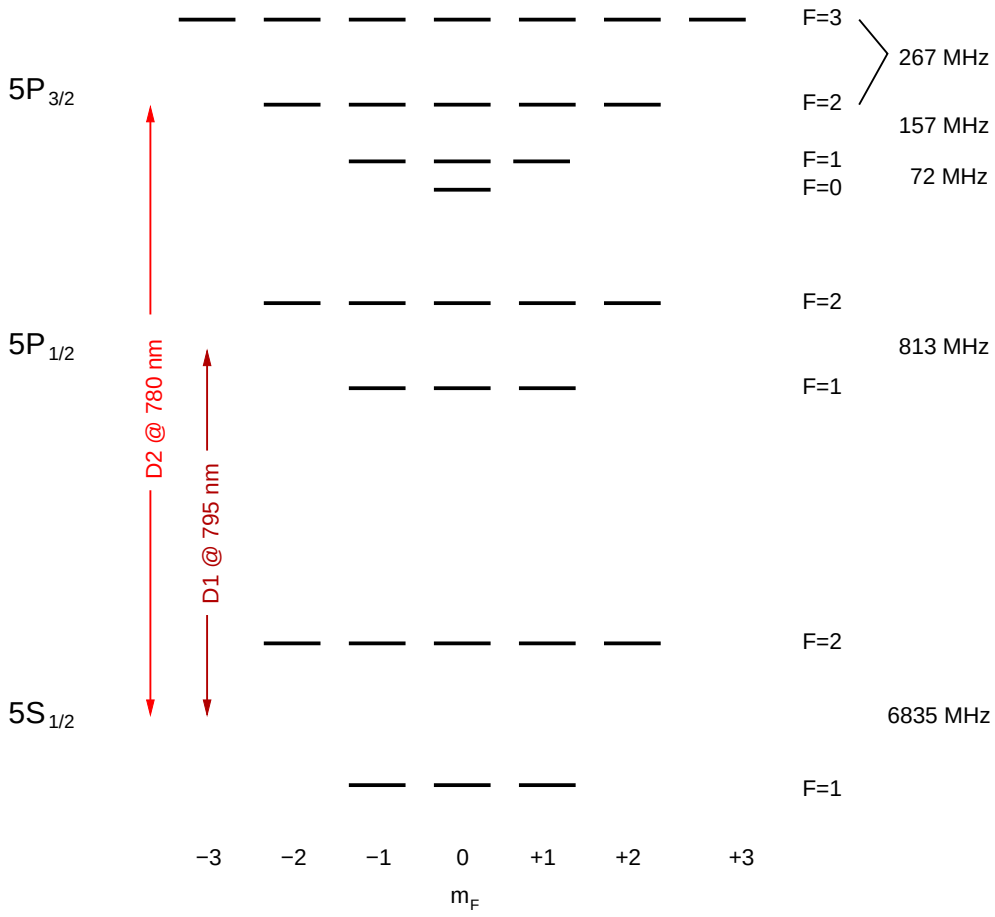

Figure A.2: Level scheme of ^{87}Rb with nuclear spin $I = 3/2$.

Bibliography

[1] E. Schrödinger. Die gegenwärtige Situtation in der Quantenmechanik. *Naturwissenschaften*, **23**:807–812, 823–828, 844–849, 1935.

[2] A. Einstein, B. Podolsky, and N. Rosen. Can quantum-mechanical description of reality be considered complete ? *Phys. Rev.*, **47**:777–780, 1935.

[3] J. S. Bell. On the Einstein-Podolsky-Rosen Paradox. *Physics*, **1**:195–200, 1964.

[4] S. J. Freedman and J. F. Clauser. Experimental test of Local Hidden-Variable Theories. *Phys. Rev. Lett.*, **28**:938, 1972.

[5] A. Aspect, P. Grangier, and G. Roger. Experimental Test of Realistic Local Theories via Bell's theorem. *Phys. Rev. Lett.*, **47**:460, 1981.

[6] A. Aspect, P. Grangier, and G. Roger. Experimental Realization of Einstein-Podolsky-Rosen-Bohm Gedankenexperiment. *Phys. Rev. Lett.*, **49**:91, 1982.

[7] G. Weihs, T. Jennewein, C. Simon, H. Weinfurter, and A. Zeilinger. Violation of Bell's Inequality under Strict Einstein Locality Conditions. *Phys. Rev. Lett.*, **81**:5039, 1998.

[8] M. A. Rowe, D. Kielpinsky, V. Meyer, C. A. Sacket, W. M. Itano, C. Monroe, and D. J. Wineland. Experimental violation of a Bell's inequality with efficient detection. *Nature*, **409**:791, 2001.

[9] J. S. Bell. *Speakable and Unspeakable in Quantum Mechanics.* Cambridge University Press, Cambridge, 1988.

[10] E. Santos. Critical analysis of the empirical tests of local hidden-variable theories. *Phys. Rev. A*, **46**:3646, 1992.

[11] P. Pearle. Hidden variable example based upon data rejection. *Phys. Rev. D*, **2**:1418, 1970.

[12] E. Santos. Constraints for the violation of the Bell inequality in Einstein-Podolsky-Rosen-Bohm experiments. *Phys. Lett. A*, **200**:1, 1995.

[13] K. Saucke. Optische Dipolfalle für Einzelatome. Master's thesis, Ludwig-Maximilians-Universität München, 2002.

[14] C. Simon and T. M. Irvine. Robust Long-Distance Entanglement and a Loophole-Free Test with Ions and Photons. *Phys. Rev. Lett.*, **91**:110405, 2003.

[15] M. Zukowski, A. Zeilinger, M. A. Horne, and A. K. Ekert. "Event-ready-detectors" Bell experiment via entanglement swapping. *Phys. Rev. Lett.*, **71**:4287, 1993.

[16] D. Bouwmeester, A. Ekert, and A. Zeilinger. *The Physics of Quantum Information.* Springer-Verlag, Berlin, Heidelberg, 2000.

[17] I. Chuang and M. Nielsen. *Quantum Computation and Quantum Information.* Cambridge University Press, Cambridge, 2000.

[18] Z. Y. Ou and L. Mandel. Violation of Bell's Inequality and Classical Probability in a Two-Photon Correlation Experiment. *Phys. Rev. Lett.*, **61**:50, 1988.

[19] E. Hagley, X. Maitre, G. Nogues, C. Wunderlich, M. Brune, J. M. Raimond, and S. Haroche. Generation of Einstein-Podolsky-Rosen Pairs of Atoms. *Phys. Rev. Lett.*, **79**:1–5, 1997.

[20] C. A. Sackett, D. Kielpinski, B. E. King, C. Langer, V. Meyer, C. J. Myatt, M. Rowe, Q. A. Turchette, W. M. Itano, D. J. Wineland, and C. Monroe. Experimental entanglement of four particles. *Nature*, **404**:256, 2000.

[21] M. D. Barrett, J. Chiaverini, T. Schaetz, J. Britton, W. M. Itano, J. D. Jost, E. Knill, C. Langer, D. Leibfried, R. Ozeri, and D. J. Wineland. Deterministic quantum teleportation of atomic qubits. *Nature*, **429**:737, 2004.

[22] M. Riebe, H. Häffer, C. F. Roos, W. Hänsel, J. Benhelm, G. P. T. Lancaster, T. W. Körber, C. Becher, F. Schmidt-Kaler, D. F. V. James, and R. Blatt. Deterministic quantum teleportation with atoms. *Nature*, **429**:734, 2004.

[23] A. Kuzmich and E. S. Polzik. Quantum information with continous variables. Dordrecht, 2003. Kluwer.

[24] M. D. Lukin. Trapping and manipulating photon states in atomic ensembles. *Rev. Mod. Phys.*, **75**:457, 2003.

[25] L.-M. Duan, M. Lukin, J. I. Cirac, and P. Zoller. Long-distance quantum communication with atomic ensembles and linear optics. *Nature*, **414**:413, 2001.

[26] L.-M. Duan and H. J. Kimble. Efficient Engineering of Multiatom Entanglement through Single-Photon Detections. *Phys. Rev. Lett.*, **90**:253601, 2003.

[27] X. L. Feng, Z. M. Zhang, X. D. Li, S. Q. Gong, and Z. Z. Xu. Entangling Distant Atoms by Interference of Polarized Photons. *Phys. Rev. Lett.*, **90**:217902, 2003.

[28] U. Eichmann, J. C. Bergquist, J. J. Bollinger, J. M. Gilligan, W. M. Itano, and D. J. Wineland. Young's interference experiment with light scattered from two atoms. *Phys. Rev. Lett.*, **70**:2359, 1993.

[29] R. G. DeVoe and R. G. Brewer. Observation of superradiant and subradiant spontaneous emission of two trapped ions. *Phys. Rev. Lett.*, **76**:2049, 1996.

[30] C. Kurtsiefer. *Atomoptische Experimente zu nichtklassischen Zuständen der Bewegung von metastabilen Edelgasatomen und Atom-Photon-Paaren*. PhD thesis, Universität Konstanz, 1997.

[31] X. Maitre, E. Hagley, G. Nogues, C. Wunderlich, P. Goy, M. Brune, J. M. Raimond, and S. Haroche. Quantum Memory with a Single Photon in a Cavity. *Phys. Rev. Lett.*, **79**:769–772, 1997.

[32] S. Haroche, J. M. Raimond, and M. Brune. Experimental Quantum Computation and Information. pages pp. 37–66, Amsterdam, 2002. Proceedings of the International School of Physics Enrico Fermi, course CXLVIII, IOS Press.

[33] A. Auffeves, P. Maioli, T. Meunier, S. Gleyzes, G. Nogues, M. Brune, J. M. Raimond, and S. Haroche. Entanglement of a Mesoscopic Field with an Atom Induced by Photon Graininess in a Cavity. *Phys. Rev. Lett.*, **91**:230405, 2003.

[34] Matsukevich D. N. and A. Kuzmich. Quantum State Transfer Between Matter and Light. *Science*, **306**:663, 2004.

[35] B. B. Blinov, D. L. Moehring, L.-M. Duan, and C. Monroe. Observation of entanglement between a single trapped atom and a single photon. *Nature*, **428**:153, 2004.

[36] N. Bohr. The quantum postulate and the recent development of atomic theory. *Nature*, **121**:580, 1928.

[37] D. Bohm. *Quantum Theory*. Prentice-Hall, Englewood Cliffs, New York, 1951.

[38] N. Bohr. Can Quantum-Mechanical Description of Physical Reality be Considered Complete ? *Phys. Rev.*, **48**:696, 1936.

[39] A. Afriat and F. Selleri. *The Einstein, Podolsky, and Rosen Paradox in Atomic, Nuclear, and Particle Physics*. Plenum Press, New York and London, 1999.

[40] J. F. Clauser, M. A. Horne, A. Shimony, and R. A. Holt. Proposed Experiment to Test Local Hidden-Variable Theories. *Phys. Rev. Lett.*, **23**:880, 1969.

[41] J. F. Clauser and M. A. Horne. Experimental consequences of objective local theories. *Phys. Rev. D*, **10**:526, 1974.

[42] W. Tittel, J. Brendel, H. Zbinden, and N. Gisin. Violation of Bells inequalities by photons more than 10 km apart. *Phys. Rev. Lett.*, **81**:3563, 1998.

[43] G. Vidal. Entanglement monotones. *J. Mod. Opt.*, **47**:355, 2000.

[44] C. H. Bennet, D. P. DiVincenco, J. A. Smolin, and W. K. Wootters. Mixed-state entanglement and quantum error correction. *Phys. Rev. A*, **54**:3824, 1996.

[45] A. Ekert. Quantum Cryptography based on Bell's theorem. *Phys. Rev. Lett.*, **67**:661, 1991.

[46] C. H. Bennett, G. Brassard, G. Crepeau, R. Jozsa, A. Peres, and W. K. Wootters. Teleporting an unknown quantum state via dual classical and Einstein-Podolsky-Rosen channels. *Phys. Rev. Lett.*, **70**:1895, 1993.

[47] C. Cohen-Tannoudji, J. Dupont-Roc, and G. Grynberg. *Atom-Photon Interactions, Basic Processes and Applications*. Wiley, New York, 1998.

[48] Weisskopf V. and E. Wigner. Berechnung der naturlichen Linienbreite auf Grund der Diracschen Lichttheorie. *ZS. f. Phys.*, **63**:54, 1930.

[49] M. O. Scully and M. Zubairy. *Quantum Optics*. Cambridge University Press, Cambridge, 1997.

[50] A. L. Migdall, J. V. Prodan, W. D. Phillips, T. H. Bergemann, and H. J. Metcalf. First Observation of Magnetically Trapped Neutral Atoms. *Phys. Rev. Lett.*, **54**:2596, 1985.

[51] T. H. Bergeman, G. Erez, and H. J. Metcalf. Magnetostatic trapping fields for neutral atoms. *Phys. Rev. A*, **35**:1535, 1987.

[52] D. E. Pritchard, E. L. Raab, V. S. Bagnato, C. E. Wieman, and R. N. Watts. Light Traps Using Spontaneous Forces. *Phys. Rev. Lett.*, **57**:310, 1986.

[53] E. L. Raab, E. L. Prentiss, A. Cable, S. Chu, and D. E. Pritchard. Trapping of neutral sodium atoms with radiation pressure. *Phys. Rev. Lett.*, **59**:2631, 1987.

[54] G. A. Askar'yan. Effects of the gradient of a strong electromagnetic beam on electrons and atoms. *Sov. Phys. JETP*, **15**:1088, 1962.

[55] V. S. Letokhov. *JETP Lett.*, **7**:272, 1968.

[56] D. Frese, B. Überholz, S. Kuhr, W. Alt, D. Schrader, V. Gomer, and D. Meschede. Single atoms in an optical dipole trap: Towards a deterministic source of cold atoms. *Phys. Rev. Lett.*, **85**:3777, 2000.

[57] R. Grimm, M. Weidemüller, and Y. B. Ovchinnikov. Optical dipole traps for neutral atoms. *Adv. At. Mol. Opt. Phys.*, **42**:95, 2000.

[58] J. D. Jackson. *Classical electrodynamics*. Wiley, New York, 1962.

[59] B. W. Shore. *The theory of coherent atomic excitation*. Wiley, New York, 1990.

[60] I. I. Sobelman. *Atomic Spectra and Radiative Transitions*. Springer, Berlin, Heidelberg, New-York, 1991.

[61] D. A. Steck. Rubidium 87 D Line Data. *http://steck.us/alkalidata*.

[62] C. Monroe, W. Swann, H. Robinson, and C. Wieman. Very cold trapped atoms in a vapor cell. *Phys. Rev. Lett.*, **65**:1571, 1990.

[63] T. W. Hänsch and A. L. Schawlow. Cooling of gases by laser radiation. *Opt. Comm.*, **13**:68, 1975.

[64] V. G. Minogin and V. S. Letokhov. *Laser light pressure on atoms*. Gordon and Breach, New York, 1987.

[65] S. Chu, J. E. Bjorkholm, A. Ashkin, and A. Cable. Experimental observation of optically trapped atoms. *Phys. Rev. Lett.*, **57**:314, 1986.

[66] P. D. Lett, W. D. Phillips, S. L. Rolston, C. E. Tanner, R. N. Watts, and C. Westbrook. Observation of Atoms Laser Cooled below the Doppler Limit. *Phys. Rev. Lett.*, **61**:169, 1988.

[67] J. Dalibard and C. Cohen-Tannoudji. Laser cooling below the doppler limit by polarization gradients: simple theoretical models. *J. Opt. Soc. Am. B*, **6**:2023, 1989.

[68] A. M. Steane and C. J. Foot. Laser cooling below the Doppler limit in a magneto-optical trap. *Europhys. Lett.*, **14**:231, 1991.

[69] D. Boiron, A. Michaud, Fournier J. M., L. Simard, M. Sprenger, G. Grynberg, and C. Salomon. Cold and dense cesium clouds in far-detuned dipole traps. *Phys. Rev. A*, **57**:R4106, 1998.

[70] B. M. Garraway and V. G. Minogin. Theory of an optical dipole trap for cold atoms. *Phys. Rev. A*, **62**:043406, 2000.

[71] S. J. M. Kuppens, K. L. Corwin, K. L. Miller, T. E. Chupp, and C. E. Wieman. Loading an optical dipole trap. *Phys. Rev. A*, **62**:013406, 2000.

[72] N. Schlosser, G. Reymond, I. Protsenko, and P. Grangier. Sub-poissonian loading of single atoms in a microscopic dipole trap. *Nature*, **411**:1024, 2001.

[73] N. Schlosser, G. Reymond, and P. Grangier. Collisional blockade in microscopic optical dipole traps. *Phys. Rev. Lett.*, **89**:023005, 2002.

[74] T. W. Hänsch, M. D. Levenson, and A. L. Schawlow. Hyperfine Structure of a Molecular Iodine Line. *Phys. Rev. Lett.*, **26**:946, 1971.

[75] J. C. Camparo. The Diode Laser in Atomic Physics. *Contemp. Phys.*, **26**:443, 1985.

[76] L. Ricci, M. Weidemüller, T. Esslinger, A. Hemmerich, C. Zimmermann, V. Vuletic, W. König, and T. W. Hänsch. A compact Grating-Stabilized Diode Laser System for Atomic Physics. *Opt. Commun.*, **117**:541, 1995.

[77] J. Vrana. State selective Detection of a Single Atom. Master's thesis, Ludwig-Maximilians-Universität München, 2004.

[78] M. Greiner. Magnetischer Transfer von Atomen - Ein Weg zur einfachen Bose-Einstein-Kondensation. Master's thesis, Ludwig-Maximilians-Universität München, 2000.

[79] U. Schünemann, H. Engler, R. Grimm, M. Weidemüller, and M. Zielonkovski. Simple scheme for tunable frequency offset locking of two lasers. *Rev. Sci. Instrum.*, **70**:242, 1999.

[80] H. J. Metcalf and P. van Straten. *Laser Cooling and Trapping*. Springer, New York, Berlin, Heidelberg, 1999.

[81] Volz, Jürgen. private communication.

[82] M. Weber. Wie man die Werte von σ_x, σ_y und σ_z eines Spin-$\frac{1}{2}$ Teilchens bestimmt. Master's thesis, Ludwig-Maximilians-Universität München, 2000.

[83] B. R. Mollow. Power spectrum of Light Scattered by Two-level Systems. *Phys. Rev.*, **188**:1969, 1969.

[84] F. Schuda, C. Stroud Jr, and M. Hercher. Nonclassical effects in optical spectra. *J. Phys. B*, **1**:L198, 1974.

[85] F. Y. Wu, R. E. Grove, and S. Ezekiel. Investigation of the Spectrum of Resonance Fluorescence Induced by a Monochromatic Field. *Phys. Rev. Lett.*, **35**:1426, 1975.

[86] W. Hartig, W. Rasmussen, R. Schieder, and H. Walther. *Z. Phys. A*, **278**:205, 1976.

[87] Y. Stalgies, I. Siemers, B. Appasamy, T. Altevogt, and P. E. Toschek. The spectrum of single-atom resonance fluorescence. *Europhys. Lett.*, **35**:259, 1996.

[88] H. M. Gibbs and T. N. C. Ventkatesan. Direct observation of fluorescence narrower than the natural linewidth. *Opt. Commun.*, **17**:87, 1976.

[89] C. I. Westbrook, R. N. Watts, C. E. Tanner, S. L. Rolston, W. D. Phillips, P. D. Lett, and P. L. Gould. Localization of atoms in a three-dimensional standing wave. *Phys. Rev. Lett.*, **65**:33, 1990.

[90] P. S. Jessen, C. Gerz, P. D. Lett, W. D. Phillips, S. L. Rolston, R. J. C. Spreeuw, and C. I. Westbrook. Observation of quantized motion of Rb atoms in an optical field. *Phys. Rev. Lett.*, **69**:49, 1992.

[91] J. T. Höffges, H. W. Baldauf, W. Lange, and H. Walther. Heterodyne measurement of the resonance fluorescence of a single ion. *J. Mod. Opt.*, **44**:1999, 1997.

[92] J. T. Höffges, H. W. Baldauf, T. Eichler, S. R. Helmfrid, and H. Walther. Heterodyne measurement of the fluorescent radiation of a single trapped ion. *Opt. Commun.*, **133**:170, 1997.

[93] This procedure is justified because the statistical error on the data points of the reference laser spectrum is much smaller than the error on the fluorescence data.

[94] R. Hanbury Brown and R. Q. Twiss. Correlations between photons in two coherent beams of light. *Nature*, **177**:27, 1956.

[95] R. Hanbury Brown and R. Q. Twiss. A Test of a New Type of Stellar Interferometer on Sirius. *Nature*, **178**:1046, 1956.

[96] R. J. Glauber. Coherent and Incoherent States of the Radiation Field. *Phys. Rev.*, **131**:2766, 1963.

[97] R. Loudon. *The Quantum Theory of Light*. Oxford Univ. Press, Oxford, 2001.

[98] M. Lax. Quantum Noise. IV. Quantum Theory of Noise Sources. *Phys. Rev.*, **145**:110, 1966.

[99] H. J. Carmichael and D. F. Walls. A quantum-mechanical master equation treatment of the dynamical stark effect. *J. Phys. B*, **9**:1199, 1976.

[100] H. J. Kimble, M. Dagenais, and L. Mandel. Photon Antibunching in Resonance Fluorescence. *Phys. Rev. Lett.*, **39**:691, 1977.

[101] R. Short and L. Mandel. Observation of Sub-Poissonian Photon Statistics. *Phys. Rev. Lett.*, **51**:384, 1983.

[102] F. Diedrich and H. Walther. Nonclassical radiation of a single stored ion. *Phys. Rev. Lett.*, **58**:203, 1987.

[103] M. Schubert, I. Siemers, R. Blatt, W. Neuhauser, and P. E. Toschek. Photon antibunching and non-Poissonian fluorescence of a single three-level ion. *Phys. Rev. Lett.*, **68**:3016, 1992.

[104] M. Schubert, I. Siemers, R. Blatt, W. Neuhauser, and P. E. Toschek. Transient internal dynamics of a multilevel ion. *Phys. Rev. A*, **52**:2994, 1995.

[105] R. K. Wangsness and F. Bloch. The Dynamical Theory of Nuclear Induction. *Phys. Rev.*, **89**:728, 1953.

[106] W. H. Press, S. A. Teukolsky, W. T. Vetterling, and B. P. Flannery. *Numerical Recipes in C - The Art of Scientific Computing*. Cambridge University Press, Cambridge, 1995.

[107] D. T. Pegg, R. Loudon, and P. L. Knight. Correlations in light emitted by three-level atoms. *Phys. Rev. A*, **33**:4085, 1986.

[108] V. Gomer, B. Ueberholz, S. Knappe, F. Strauch, D. Frese, and D. Meschede. Decoding the dynamics of a single trapped atom from photon correlations. *Appl. Phys. B*, **67**:689, 1998.

[109] T. W. Hodapp, C. Gerz, Furtlehner C., C. I. Westbrook, W. D. Phillips, and J. Dalibard. Three dimensional spatial diffusion in optical molasses. *Appl. Phys. B*, **60**:135, 1995.

[110] S. Marksteiner, K. Ellinger, and P. Zoller. Anomalous diffusion and Levy walks in optical lattices. *Phys. Rev. A*, **53**:3409, 1996.

[111] C. Kurtsiefer, P. Zarda, S. Mayer, and H. Weinfurter. The breakdown flash of Silicon Avalanche diodes - backdoor for eavesdropper attacks. *J. of Mod. Opt.*, **48**:2039, 2001.

[112] S. Reynaud. *Ann. Phys. (Paris)*, **8**:351, 1983.

[113] H. Dehmelt. Proposed 1014 $\Delta\nu > \nu$ Laser Fluorescence Spectroscopy ? n Tl+ Mono-Ion Oscillator, II ? *Bull. Am. Phys. Soc.*, **20**:60, 1975.

[114] J. R. Kuklinski, U. Gaubatz, F. T. Hioe, and K. Bergmann. Adiabatic population transfer in a three-level system driven by delayed laser pulses. *Phys. Rev. A*, **40**:6741, 1989.

[115] J. Oreg, F. T. Hioe, and J. H. Eberly. Adiabatic following in multilevel systems. *Phys. Rev. A*, **29**:690, 1984.

[116] G. W. Coulston and K. Bergmann. Population transfer by stimulated Raman scattering with delayed pulses: Analytic results for multilevel systems. *J. Chem. Phys.*, **96**:3467, 1991.

[117] T. A. Laine and S. Stenholm. Adiabatic processes in three-level systems. *Phys. Rev. A*, **53**:2501, 1996.

[118] N. V. Vitanov and S. Stenholm. Population transfer via a decaying state. *Phys. Rev. A*, **56**:1463, 1997.

[119] N. V. Vitanov and S. Stenholm. Analytic properties and effective two-level problems in stimulated Raman adiabatic passage. *Phys. Rev. A*, **55**:648, 1997.

[120] R. G. Unanyan, M. Fleischhauer, B. W. Shore, and K. Bergmann. Robust creation and phase-sensitive probing of superposition states via stimulated Raman adiabatic passage (STIRAP) with degenerate dark states. *Opt. Commun.*, **155**:144, 1998.

[121] H. Theuer, R. G. Unanyan, C. Habscheid, K. Klein, and K. Bergmann. Novel laser controlled variable matter wave beamsplitter. *Opt. Exp.*, **4**:78, 1999.

[122] R. G. Unanyan, B. W. Shore, and K. Bergmann. Laser-driven population transfer in four-level atoms: Consequences of non-Abelian geometrical adiabatic phase factors. *Phys. Rev. A*, **59**:2910, 1999.

[123] F. Vewinger, M. Heinz, R. G. Fernandez, V. Vitanov, and K. Bergmann. Creation and Measurement of a Coherent Superposition of Quantum States. *Phys. Rev. Lett.*, **91**:213001, 2003.

[124] C. Kurtsiefer. *A programmable pattern generator.*, 2002. unpublished.

[125] D. Boschi, S. Branca, F. De Martini, L. Hardy, and S. Popescu. Experimental Realization of Teleporting an Unknown Pure Quantum State via Dual Classical and Einstein-Podolsky-Rosen Channels. *Phys. Rev. Lett.*, **80**:1121, 1998.

[126] A. K. Pati. Remote state preparation and measurement of a single photon. *arXiv:quant-ph/0212164*, 2002.

[127] M. Michler, K. Mattle, H. Weinfurter, and A. Zeilinger. Interferometric Bell-state analysis. *Phys. Rev. A*, **53**:R1209, 1996.

[128] Y. L. Lim and A. Beige. Photon polarisation entanglement from distant dipole sources. *arXiv:quant-ph/0308095*, 2003.

[129] J. Volz, M. Weber, D. Schlenk, W. Rosenfeld, J. Vrana, K. Saucke, C. Kurtsiefer, and H. Weinfurter. Atom-photon entanglement: towards a loophole-free test of Bell's inequality. *to be published*, 2005.

[130] M. Schulz. *Tightly confined atoms in optical dipole traps.* PhD thesis, Universität Innsbruck, 2002.